The role of *Leishmania major* proliferation for the interaction between the parasite and its tissue environment *in vivo*

Dissertation

zur Erlangung des akademischen Grades

doctor rerum naturalium

(Dr. rer. nat.)

Fakultät für Naturwissenschaften

Otto-von-Guericke-Universität Magdeburg

von M. Sc. Sandrina Heyde

geb. am 07.10.1988 in Berlin

eingereicht am: 20.07.2018
verteidigt am: 26.02.2019

1. Gutachter: Prof. Dr. Andreas Müller
2. Gutachter: Prof. Dr. Ger van Zandbergen

Eigenständigkeitserklärung

Hiermit erkläre ich, dass ich die von mir eingereichte Dissertation zum dem Thema:

“The role of *Leishmania major* proliferation for the interaction between the parasite and its tissue environment *in vivo*”

selbständig verfasst, nicht schon als Dissertation verwendet habe und die benutzten Hilfsmittel und Quellen vollständig angegeben wurden.

Weiterhin erkläre ich, dass ich weder diese noch eine andere Arbeit zur Erlangung des akademischen Grades doctor rerum naturalium (Dr. rer. nat.) an anderen Einrichtungen eingereicht habe.

Magdeburg, den 20.07.2018

M. Sc. Sandrina Heyde

Abstract

Leishmania major (*L. major*) survives within a variety of host phagocytes and undergoes cycles of replication, release from, and uptake into new cells. It is unclear whether distinct phases and host cell types within these cycles are permissive or inhibitory for pathogen proliferation. Therefore, a novel photoconversion-based proliferation reporter (mKikumeGR) was used in the presented thesis to determine *L. major* proliferation in relation to distinct phagocyte subpopulations in the ongoing infection. The thesis is divided into three main parts:

(1) In the first part, the mKikumeGR reporter system, constitutively expressed in *L. major* (*Lm*^{SWITCH}), was improved for more efficient application of the system. Photoconversion of *Lm*^{SWITCH} with a LED diode array *in vitro* and *in vivo* as well as compatibility with flow cytometry analysis and immunohistochemical methods was successfully established.

(2) In the second part of the thesis, the tissue niche of high and low proliferating *L. major* was defined, and a cell-intrinsic control mechanism for *Leishmania* proliferation was determined. Cells positive for the markers CD11c^{+} and Ly6C^{+} were defined as main cell type harboring rapidly proliferating *L. major* in the ongoing infection, irrespective of the activation state of the cells. Furthermore, high proliferating parasites were defined to represent the main *L. major* subpopulation capable of successful transfer to new host cells. Newly recruited host cells were infected irrespectively of their cell type, however among these newly infected cells, only cells positive for CD11c and Ly6C were permissive for efficient proliferation.

(3) The third part provides perspectives for future analysis, like the analysis of antigen presenting cell (APC) – T cell interactions in the context of the proliferative state of the parasites. To this end, an approach including a specific transgenic T cell receptor and ovalbumin expressing *Lm*^{SWITCH} was successfully established for intravital 2-photon microscopy. Therefore, the interactions between APCs containing *L. major* of different proliferation states with specific Th1 CD4^{+} cells in the living host organism can be analyzed reliably and quantitatively.

Taken together, this work provides for the first time a quantification of *L. major* proliferation rates with respect to different host cell types, and to different phases in the cell-to-cell transfer cycle, in an unperturbed infection setting. It is established that, besides their well-described function for priming and activating T cell effector functions against *L. major*, CD11c^{+} cells provide a reservoir for rapidly proliferating parasites that disseminate at the site of infection.

Zusammenfassung

Leishmanien sind eukaryotische, einzellige Parasiten, die im Darm von Sandmücken persistieren und ihren Lebenszyklus im Säugetier vollenden. Dort leben und proliferieren die Parasiten in einer Vielzahl von professionellen Phagozyten. Sie durchlaufen Zyklen von Replikation, Freisetzung und erneuter Aufnahme in andere Phagozyten des Wirtsorganismus. Bis jetzt war es weitgehend unklar, ob die verschiedenen Phasen und Wirtszellen innerhalb dieser Zyklen die Pathogenproliferation begünstigen oder inhibieren. Dieses Thema hat eine hohe Relevanz, um einerseits das Überleben der Parasiten im Wirtsorganismus, und andererseits die erfolgreiche Induktion einer Immunantwort bei einer Infektion zu verstehen. Um diese Fragestellung auf Zellebene zu adressieren, wurde in der vorliegenden Arbeit ein neuartiger Fluoreszenzprotein-basierter Proliferationsreporter (mKikumeGR) angewendet. *Leishmania major* (*L. major*), die diesen photokonvertierbaren Reporter konstitutiv exprimieren, zeigen eine grüne Fluoreszenz, die durch Bestrahlung mit UV – Licht irreversibel zu roter Fluoreszenz konvertiert werden kann. Es wurde gezeigt, dass die Neuexpression von nicht konvertiertem, grün fluoreszierendem Protein, nach der Photokonversion, sowie die Verdünnung des rot fluoreszierenden Proteins, an die Zellteilung gekoppelt ist. Somit kann dieses System als Reporter für die Parasitenproliferation genutzt werden. Mit Hilfe dieses Reporters wurde in der vorliegenden Arbeit die *L. major* Proliferation während der aktiven Infektion in verschiedenen infizierten Zellpopulationen und deren Transmission in neue Wirtszellen gemessen.

Die Ergebnisse der vorliegenden Arbeit lassen sich in drei Hauptteile untergliedern:

(1) Im ersten Teil der Arbeit wurde das mKikumeGR Proliferationsreportersystem in *L. major* (*Lm*^{SWITCH}) detaillierter charakterisiert, um ein breiteres Anwendungsspektrum zu erreichen und somit eine effektivere Analyse zu ermöglichen. Die erfolgreiche Anwendung eines LED Dioden Arrays zur Photokonversion konnte sowohl *in vitro* als auch *in vivo* etabliert werden, wodurch es möglich wurde, größere Flächen, zum Beispiel eine komplette Infektion im Mausohr, zu photokonvertieren. Des Weiteren konnte die Kompatibilität von *Lm*^{SWITCH} mit der Analyse von Proben im Durchflusszytometer und immunhistochemischen Methoden gezeigt werden.

(2) Im zweiten Teil der Arbeit wurde die Nische von stark und gering proliferierenden Leishmanien im infizierten Gewebe, mittels Durchflusszytometrie, *Multi-epitope ligand cartography* (MELC) und intravitaler 2-Photonenmikroskpie, definiert. Dabei wurden Hinweise auf einen zell-intrinsischen Kontrollmechanismus für die Proliferation von *L. major* beobachtet, da die Mehrheit der Wirtszellen entweder stark proliferierende oder gering proliferierende

Leishmanien beinhalteten, jedoch nur sehr selten verschiedene Subpopulationen unterschiedlich proliferierender Parasiten. Weiterhin konnten Zellen, die positiv für die Oberflächenmarker CD11c und Ly6C sind, als Hauptzelltyp für stark proliferierende Leishmanien definiert werden, unabhängig vom Aktivierungsgrad der Zellen. Dementsprechend sind gering proliferierende Leishmanien vorrangig in $CD11c^-$ Zellen lokalisiert, ebenfalls unabhängig von der Expression von Aktivierungsmarkern wie CD86 und MHC-Klasse-II. Des Weiteren wurden strak proliferierende Leishmanien als wichtigste Subpopulation für einen erfolgreichen Transfer von einer Wirtszelle in eine neue Wirtszelle definiert, wobei ein direkter Transfer von einer Zelle in die nächste Zelle sowohl *in vitro* als auch *in vivo* gezeigt werden konnte. Neu rekrutierte Wirtszellen werden dabei unabhängig von ihrem Zelltyp infiziert, wobei jedoch nur Zellen, die positiv für CD11c und Ly6C sind, eine effiziente Parasitenproliferation zulassen.

(3) Im dritten Teil der Arbeit wurden Ansätze für zukünftige Analysen etabliert. Um mögliche molekulare Mechanismen hinter den im zweiten Teil gewonnenen Erkenntnissen zu identifizieren, wurden Experimente zu eventuellen zell-intrinsischen Effekten von iNOS beziehungsweise der NADPH Oxidase etabliert. In ersten Experimenten konnte gezeigt werden, dass die Leishmanienproliferation in $iNOS^{-/-}$-Zellen signifikant erhöht ist im Vergleich zu benachbarten Wildtyp-Zellen. Das deutet auf einen zell-intrinsischen Kontrollmechanismus von iNOS hin. Für die NADPH Oxidase hingegen, konnten solche Unterschiede nicht detektiert werden.

Des Weiteren wurden Methoden etabliert, die die Analyse von Interaktionen zwischen *L. major* infizierten Antigen-präsentierenden Zellen (APCs) und T-Helferzellen in Abhängigkeit vom Proliferationsstatus der Parasiten ermöglichen. Dazu wurde im Rahmen dieser Arbeit ein OT II-Ovalbumin basiertes System für die Analyse mittels intravitaler 2-Photonenmikroskopie aufgesetzt. Hierfür wurde ein Ovalbumin exprimierender Lm^{SWITCH} Stamm (Lm^{SWITCH_OVA}) generiert. Mit diesem experimentellen Ansatz können Interaktionen zwischen APCs, die Lm^{SWITCH_OVA} mit unterschiedlichen Proliferationsstadien enthalten, mit antigenspezifischen $CD4^+$ Zellen im lebenden Organismus quantitativ analysiert werden.

Zusammengefasst liefert die hier präsentierte Arbeit zum ersten Mal eine Quantifizierung der Leishmanienproliferation innerhalb verschiedener Wirtszelltypen mit Betrachtung der unterschiedlichen Phasen des Zell-zu-Zell Transfers in einer Infektion. Demzufolge haben $CD11c^+$ Zellen in der Haut, neben ihrer gut charakterisierten Rolle zur Aktivierung von Effektor-T-Zellen, eine Funktion als Reservoir für stark proliferierende Parasiten, die sich an der Infektionsseite ausbreiten. Diese Erkenntnisse sind von großer Relevanz für das Verständnis darüber, wie der Aufenthalt in einer spezifischen zellulären Nische Leishmanien dazu befähigt, sich effizient zu multiplizieren und an der Infektionsseite langfristig zu persistieren. Dieses

Wissen könnte dabei helfen die Entwicklung von verlässlichen Impfstoffen voranzutreiben und effiziente Therapien zu entwickeln.

Table of contents

Abbreviations

°C	degree Celsius
α	alpha
β	beta
γ	gamma
δ	delta
κ	kappa
μ	mu
µg	microgram
µL	microlitre
µm	micrometre
µM	micromolar
Ab	antibody
APC	antigen-presenting cell, or when used in conjunction with antibody labelling
APS	ammoniumpersulfat
BamHI	restriction endonuclease enzyme isolated from *Bacillus amyloliquefaciens* strain H
bp	base pair
BglII	restriction endonuclease enzyme isolated from *Bacillus globigii*
BM	bone marrow
BMMDC	bone marrow-derived macrophages and dendritic cell mixtures
BrdU	5-Bromo-2′-deoxyuridine
BSA	bovine serum albumin
BV	brilliant violet
Ca^{2+}	calcium ion
CCR7	C-C-motif chemokine receptor 7
CCR2	C-C-motif chemokine receptor 2
CD	cluster of differentiation
cDC	conventional dendritic cell
CFP	cyan fluorescent protein
CLSM	confocal laser-scanning microscopy
cm	centimetre
CX_3CR1	fractalkine receptor

Da	Dalton
DC	dendritic cell
DMSO	dimethyl sulfoxide
DNA	deoxyribonucleic acid
DTR	diphtheria toxin receptor
DTX	diphtheria toxin
dNTP	deoxyribonucleoside triphosphate
ddH_2O	double distilled water
E. coli	*Escherichia coli*
EDTA	ethylenediaminetetraacetic acid
em	emission
ex	excitation
F	Farad
FACS	fluorescence-activated cell sorting
FCS	fetal calf serum
FITC	fluorescein isothiocyanate conjugate
g	gram, or “multiplied by gravity (9.81 m/s^2)” when used in conjunction with centrifugation
GFP	green fluorescent protein
GM-CSF	granulocyte/macrophage colony-stimulating factor
GPI	glycosylphosphatidylinositol
Gy	Gray
h	hours
HASPB	hydrophilic acylated surface protein B
iNOS	inducible nitric oxide synthase
IFN	interferon
IGF1	insulin growth factor
IL	interleukin
Ig	immunoglobulin
l	litre
KBMA	killed but metabolic active
k.o.	knock out
LACK	*Leishmania* homologue of receptors for activated C kinase
L-NIL	N6-(1-iminoethyl)-L-lysine hydrochloride
LED	light-emitting diode

L. amazonensis	*Leishmania amazonensis*
L. major	*Leishmania major*
L. mexicana	*Leishmania mexicana*
L.m.	*Leishmania major*
LN	lymph node
LPG	lipophosphoglycan
LPS	lipopolysaccharide
mAb	monoclonal antibody
MELC	multi-epitope ligand cartography
MHC	major histocompatibility complex
mg	milligram
Mg^{2+}	magnesium ion
min	minute
ml	millilitre
mRNA	messenger ribonucleic acid
mW	milliwatt
MyD88	myeloid differentiation primary response gene 88
NADPH	nicotinamide adenine dinucleotide phosphate hydrogen
NET	neutrophil extracellular trap
NF-κB	nuclear factor kappa B
ng	nanogram
nm	nanometre
NO	nitric oxide
NotI	restriction endonuclease enzyme isolated from *Nocardia otitidis-caviarum*
NK	natural killer (cell)
OVA	ovalbumin
PAMPs	pathogen-associated molecular pattern
PBS	phosphate-buffered saline
PCR	polymerase chain reaction
pDC	plasmacytoid dendritic cell
PE	phycoerythrin
PerCP	peridinin chlorophyll protein
PFA	paraformaldehyde
PPG	proteophosphoglycan

PRRs	pattern-recognition receptors
PSG	promastigote secretory gel
RACE	real-time accurate cell-shape extractor
RNA	ribonucleic acid
ROS	reactive oxygen species
RT	room temperature
SD	standard deviation
SDS-PAGE	sodium dodecyl sulfate polyacrylamide gel electrophoresis
SNARF	1 carboxylic acid, acetate, succinimidyl ester
SpeI	restriction endonuclease enzyme isolated from *Sphaerotilus species*
Spp	species pluralis
SwaI	restriction endonuclease enzyme isolated from *Staphylococcus warneri*
Taq	*Thermus aquaticus*
TCR	T cell receptor
TEMED	tetramethylethylenediamine
TGF-β1	transforming growth factor beta 1
Th	helper T cell
TLR	toll-like receptor
TNF	tumor necrosis factor
T_{regs}	regulatory T cells
TRIF	TIR-domain-containing adapter-inducing interferon-β
V	volt
v/v	volume per volume
wt	wildtype
w/v	weight per volume

List of figures and tables

List of figures

List of tables

1 Introduction

1.1 How to deal with intracellular pathogens

The main task of the immune system is to protect the body from pathogens, toxins, and malignant cells, which must be recognized and eliminated. To prevent the invasion of pathogens into the host, first lines of defence are mechanical barriers like the skin, sudor, and mucous membranes. In case this first barrier is overcome by pathogens, the humoral and cellular defences of the immune system come into play. These are grouped into two main parts: the innate and the adaptive immune system.

The evolutionary older innate immune system is not specifically distinguishing self from foreign, but is able to recognize conserved molecular structures of pathogens and toxins via so called pathogen-associated molecular patterns (PAMPs), which are often integral components of the pathogen's physiology and lifestyle. Receptors interacting with these molecular structures are called pattern recognition receptors (PRRs) and recognize structures like oligosaccharides, proteoglycans and lipopolysaccharides as well as CpG-DNA. Recognition of PAMPs results in the recruitment of a variety of cells of the immune system. Among them are different phagocytes, cells specialized in ingesting and degrading the infectious organisms. Being part of the innate immune system, phagocytes have the same myeloid precursor cells which can differentiate into monocytes, mast cells, granulocytes (neutrophils, basophils, eosinophils) and dendritic cells (DCs). To successfully fight diseases, the recruitment and proper function of these cells is orchestrated by soluble factors like cytokines, chemokines and the complement system.

In contrast, the adaptive immune response can recognize the differences between self and foreign. One mechanism by which this is achieved is also the main link between the innate and the adaptive immune system, the presentation of antigen: Peptide fragments of proteins, presented on the surface of macrophages and DCs, enable T lymphocytes to recognize these antigens originating from other sources than the host via highly specific cell surface receptors. Besides the main cellular constituents of the adaptive immune system, i.e. T cells and antibody-producing B cells, cytokines and chemokines represent the main soluble factors responsible for proper function of the adaptive immune system. Furthermore, the adaptive immune system develops an immunological memory, therefore, once T and B cells have fought an infection, some of these cells differentiate into memory cells, which can be activated immediately upon recognition of antigen in a secondary infection, leading to a very fast immune response.

Many mechanisms of both the innate and the adaptive immune response cooperate for an efficient recruitment of phagocytes, activation of these phagocytes by T cell-derived cytokines, and ingestion and intracellular degradation of incoming microbes. However, many pathogens

are able to evade these defence mechanisms, to survive within their host cells and even undergo replication within phagocytes. This can result in prolonged infection with such intracellular pathogens, proliferating within and breaking out of infected phagocytes and invading newly recruited phagocytes in the course of a chronic infection. Parasites of the *Leishmania* genus represent an example for such pathogens which can survive and replicate within the endocytic compartment of phagocytes [1].

1.2 *Leishmania*

1.2.1 Leishmaniasis: Different immune response-different disease?

Leishmania spp. are eukaryotic protozoan parasites which reside within the gut of phlebotomine sandflies and accomplish their life cycle in a mammalian host. Leishmaniasis is a serious disease widespread in tropical and subtropical regions of the world like Central and South America, Northern Africa, South Europe, parts of Asia and the Middle East. Over 150 million people are infected worldwide, leading to about 70.000 deaths per year. Different species of *Leishmania* are causing a variety of different diseases (reviewed in [2]): Species like *Leishmania donovani* and *Leishmania infantum* cause visceral leishmaniasis, in which the inner organs like the spleen, the liver or the bone marrow are invaded. This invasion can ultimately lead to the death of the host. Other species like *Leishmania brasiliensis* and *Leishmania panamensis* trigger mucocutaneous leishmaniasis by severely affecting the mouth and the throat. The third, widely distributed form of the disease, is the cutaneous leishmaniasis initiated by species such as *Leishmania mexicana, Leishmania tropica, Leishmania amazonensis* or *L. major* (Table 1). In contrast to visceral leishmaniasis, cutaneous forms of leishmaniasis are often self-limiting, but very slow-healing or even chronic, and represent by far the largest proportion of leishmaniasis.

Table 1: Main species of *Leishmania* that affect humans (modified from [2]).

Main disease manifestation	Species
visceral leishmaniasis	*Leishmania donovani, Leishmania infantum*
cutaneous leishmaniasis	*Leishmania major, Leishmania tropica, Leishmania mexicana, Leishmania aethiopica, Leishmania pifanol, Leishmania amazonensis*
diffuse cutaneous leishmaniasis	*Leishmania mexicana, Leishmania amazonensis, Leishmania aethiopica*
mucocutaneous leishmaniasis	*Leishmania panamensis, Leishmania braziliensis*

Mouse infection models are an important tool to understand the immune mechanisms that help controlling infection with *Leishmania* spp. For example, the use of defined inbred mouse strains which are either resistant to *Leishmania* (e.g. C57BL/6) or susceptible (e.g. BALB/C) have been very instructive to understand differences between self-controlled versus exacerbating

immunopathological courses of the infection [3]. In particular, the mouse model showed that, depending on the host, *Leishmania* infection can induce two fundamentally different types of immune responses mediated by $CD4^+$ T helper cells: While T helper 1 (Th1) responses mediated mainly by the cytokine interferon gamma (IFNγ) are protective, T helper 2 (Th2) responses, marked mainly by Interleukin-4 (IL4), result in non-control of the parasite and severe immunopathologies [4,5]. Different *Leishmania* species and inbred mouse strains function as distinct model systems for Th1 or Th2 responses, at least partially covering the variety of disease outcomes observed in patients (Table *2*).

In conclusion, the outcome of the disease is strongly dependent on the immune response of the host and the *Leishmania* species [2]. Therefore, in humans the course of disease can vary from a mild progression of infection to life-threatening disease, with immunocompromised individuals being especially at risk. As for now there is no vaccination available against leishmaniasis and drug therapy is often ineffective [2,4,6,5].

Table 2: Different *Leishmania* species and disease outcome in mouse models (modified from [6]).

***Leishmania* species**	**disease outcome**	
	C57BL/6 mice	**BALB/c mice**
Leishmania major	self-healing; Th1	chronic; Th2 [3]
Leishmania mexicana	chronic, Th1 and Th2 [7]	chronic; Th2 [7]
Leishmania braziliensis	self-healing; Th1	self-healing; Th1 [8]
Leishmania amazonensis	chronic, Th1 and Th2	chronic; Th2 [9,10]

1.2.2 The life cycle of *Leishmania* spp.

Through the bite by the sandfly vector from the genera *Phlebotomus* and *Lutzomyia*, the flagellated parasite is transmitted into the dermis of the host vertebrate. Therein, the *Leishmania* are phagocytosed (see chapter 1.2.5) and develop from their infectious flagellated metacyclic promastigote state into a non-flagellated amastigote state [2]. These amastigotes are able to replicate within their host cells. The number of parasites increases by several orders of magnitude, thus, a successful infection also requires the parasite to be released from infected host cells and to reinvade new phagocytes [6]. Closing the life cycle between insect vector and mammalian host, amastigote *Leishmania* are transmitted again when macrophages

are ingested by a female sandfly during its blood meal and transported to its midgut wherein the parasites differentiate again into procyclic promastigotes and furthermore into infectious metacyclic promastigotes [2,4,6,5,11] (Figure 1). Within the midgut of the vector, parasites secrete the promastigote secretory gel (PSG) which can obstruct the gut and therefore promote regurgitation of infectious *Leishmania*. Within the mammalian host, PSG promotes wound healing, cell proliferation, fibrosis, and inflammation. Advanced wound healing is mainly triggered by insulin growth factor-1 (IGF1), activated by PSG, leading to the alternative activation of macrophages [12]. This induces the upregulation of the macrophage arginine levels and therefore promotes intracellular survival and growth of *Leishmania* [13]. Thus, it was concluded, that alternatively activated macrophages can reduce the proinflammatory immune response in wounds [12].

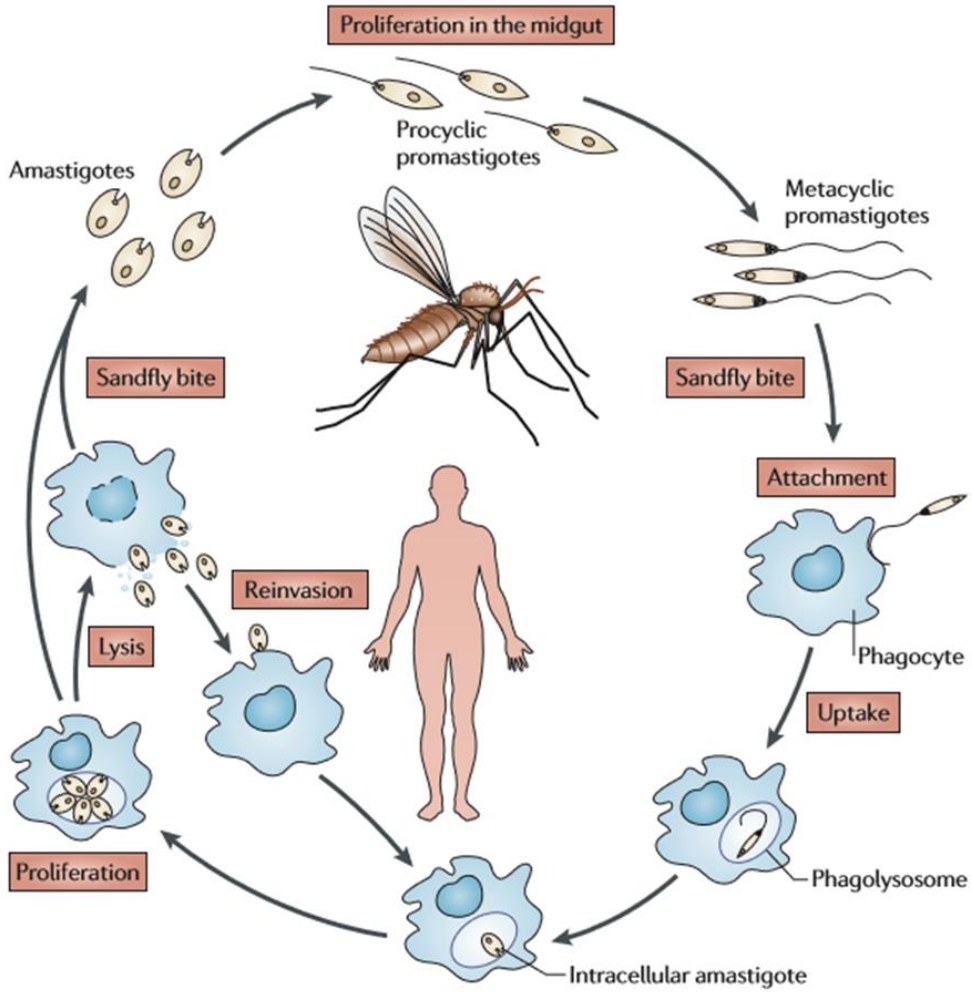

Figure 1: Life cycle of *Leishmania* [2].

1.2.3 *Leishmania* spp. virulence factors and mechanisms

The major niches of *Leishmania* within the mammalian host are professional phagocytes like neutrophils, macrophages and dendritic cells (DCs) (see chapter 1.2.5). Within these cells, *Leishmania* have to evade respectively, inhibit degradation mechanisms of the host, which is reflected by profound morphological and physiological changes of the parasite after inoculation of the mammalian host: Upon injection as promastigotes, they begin to differentiate into non-flagellated amastigotes, which are able to replicate inside acidified parasitophorus vacuoles or lysosome-like compartments and to withstand reactive oxygen and nitrogen species better than the promastigotes [14,15]. Important virulence factors of promastigotes are lipophosphoglycan (LPG) and proteophosphoglycans (PPG), leading for example to delayed maturation of the parasite-containing phagosome by inhibiting the lysosomal fusion [16,17]. Besides this, it was shown that the assembly of the NADPH oxidase complex is inhibited by LPG [18]. Other studies show that although peptide/MHC complexes are expressed at the phagosome membrane of monocytes and macrophages, they are not displayed at the plasma membrane of these cells. This indicates that the parasite inhibits translocation of the peptide/MHC complex to the plasma membrane [19]. This enables amastigotes to evade the immune response for long periods of time, which results in parasite numbers increasing dramatically within the first weeks after the infection [16]. Amastigotes are unable to produce LPG but maintain the ability to synthesize PPG which can be transported to the lumen of lysosomes and furthermore to the cytoplasm of the host cell [14,20–22]. Pharmacological disruption of the Golgi apparatus, which leads to the loss of phosphoglycans, decreases the virulence of parasites severely [20]. Furthermore, glycosylation reactions taking place in the Golgi apparatus seem to be important for the virulence of amastigotes [20]. As an additional virulence factor, *Leishmania* amastigotes produce glycosylphosphatidylinositol (GPI) protein gp63 and the cysteine protease CBP which can trigger tyrosine-specific phosphatases within the host cell leading therefore to the degradation of transcription factors that are responsible for IFNγ responsiveness and production of IL-12 [23,24]. *Leishmania* also reduce the secretion of IL-12 via decreasing the cholesterol level in the membrane of macrophages [25].

1.2.4 The course of the immune response against *Leishmania* spp.

Neutrophil recruitment

Among the most rapid constituents of the innate immune response against *Leishmania* are neutrophils, which is the first cell type that is recruited to the site of infection upon *Leishmania* inoculation. Thus, neutrophils also act as the major infected host cell type in the early phase of the infection. Their role is controversially discussed and differs between different *Leishmania*

species. Within the infection with some species e.g. *L. amazonensis*, neutrophils can kill parasites via neutrophil extracellular trap (NET) formation [26,27] or via the interaction with infected macrophages, which can lead to increased TNF secretion and therefore triggering a respiratory burst, inhibiting the parasite via superoxide [28]. On the other hand, the activation of DCs and macrophages can be reduced after the uptake of apoptotic neutrophils, e.g. in *L. major* infection [29]. Furthermore, neutrophil uptake during early post infection response, prevents efficient priming of a protective T cell response in infections with *Leishmania mexicana* [30]. Therefore, in conclusion, the function of neutrophils seems to rely at least in part on the *Leishmania* species and the genetical background of the host organism [6,2].

Antigen-presenting cells

Within the established infection, relative neutrophil numbers decrease while other phagocytic cell types such as monocytes and macrophages, as well as immature and mature DCs become the main habitat for *Leishmania* parasites, wherein they reside and replicate. While pathogen entry and intracellular survival has been intensely studied, the fact that the intracellularly proliferating pathogens also need a strategy to exit infected cells in order to be transmitted into a new cellular niche has been neglected for a long time [31]. However, this process might have profound implications for the cell tropism of the pathogens and the immune activation. Real et al. published that in macrophage cell culture infections with *L. amazonensis*, amastigotes are transmitted within extrusions from apoptotic macrophages to other macrophages which are in the close proximity. Thus *Leishmania* might avoid full contact with the extracellular milieu and therefore show another strategy to escape the host´s immune response [32]. However, little more is known about how *Leishmania* transmission from one host cell to the next is taking place.

An important function of *Leishmania* infected antigen-presenting cells (APCs) (such as macrophages and DCs) is the activation of the adaptive immune response by antigen presentation. Specifically, monocyte-derived DCs which are activated by the inflammatory signals at the site of infection, are mainly responsible to transport the parasite material to the draining lymph nodes [33]. There, naive T cells, carrying a clonotypic T cell receptor specific for *Leishmania*-derived antigen peptides, which are presented on MHC molecules on the surface of the DCs, are activated. The naive T cells differentiate into effector T cells upon recognition of their cognate antigens and can be activated at the site of infection to deliver their effector functions also by antigen presenting cells different from DCs [34,6,33].

Mast cells can also be activated directly after infection with *Leishmania* parasites, leading to the release of mast cell derived TNF [35], hence promoting the recruitment of neutrophils to the infection site and furthermore promoting proper DC activation [36–39]. In some cases mast

cells can function themselves as antigen presenting cells and therefore they also have a possible role in the induction of antigen-dependent T cell effector functions [40].

Lymphocyte activation

Depending on the genetic background of the host, either a Th1 or a Th2 response is established, leading to a self-healing or chronic infection. In a Th1 response, IL-12 produced upon activation of DCs and macrophages after uptake of the parasite, leads to the differentiation of $CD4^+$ T cells into Th1 cells, which are marked by the production of IFNγ and TNF [4,41,42]. While IFNγ, in combination with PAMPs, can induce iNOS efficiently *in vitro*, TNF is additionally necessary to resolve the infection *in vivo*. Particularly, it was shown that upon *L. major* infection within C57BL/6 mice lacking TNF signalling, IFNγ production was increased systemically, but the animals were unable to control the infection [43]. At the site of infection, both IFNγ and TNF trigger production of iNOS within the APCs [2,6]. iNOS mediates the production of nitric oxide which is necessary to control the *Leishmania* parasites [2,6,44]. It was shown that nitric oxide can diffuse across cell membranes, thus providing an antimicrobial environment produced by a large number of phagocytes. Cells that produce nitric oxide were shown to have the same effectivity to control *Leishmania* as non-nitric oxide producing bystander cells. Therefore, control of *Leishmania* via nitric oxide is a cell-extrinsic mechanism [44]. Another important mechanism to fight the infection is the production of reactive oxygen species (ROS) via activation of the NADPH complex (Figure 2) [6,45]. The particular importance of these two defence mechanisms depends on the organ. It was shown, for example, that ROS is relevant but not completely essential to control the infection in the skin and the draining lymph nodes, but is indispensable for the infection control in the spleen [45]. Furthermore, the production of IL-12 by DCs activates cytotoxicity, as well as the production and release of IFNγ by natural killer (NK) cells [46,47]. This leads therefore to an additional triggering of the Th1 response [46].

While Th1 T cells and NK cells drive the IFNγ dominated, protective immune response, establishment of the IL-4 and IL-10 mediated $CD4^+$ Th2 response leads to susceptibility in mice [48,49]. *Leishmania* homologue of receptors for activated C kinase (LACK) antigen is recognized by $CD4^+$ T cells that express the specific T cell receptor Vβ4Vα8, driving IL-4 production and therefore promoting a Th2 response which leads to IL-4, IL-10, IL-13 as well as transforming growth factor-β (TGF-β) production and susceptibility to *L. major* [50,51]. T cells expressing the Vβ4Vα8 receptor expand in the lymph nodes of infected mice. Interestingly, it was shown that an early Th2 response is also activated in *L. major* resistant mouse strains such as C57BL/6 [52,53]. In these mice the early Th2 response is redirected into a Th1 response by IL-12 [51,54]. It was shown that the production of IL-12 is delayed upon

L. major infection, thus explaining the early Th2 response. The inability of some susceptible mouse strains to redirect the early Th2 response, is based on a few genetic differences between susceptible and resistant mouse strains. One of the most important ones is the inability of a stable IL-12 signalling in susceptible strains which might be due to downregulation of the IL-12 receptor β2-chain [55]. Furthermore, the inability of sufficiently downregulating the cytokines IL-4, IL-10, IL-13 and TGF-β has been proposed to be an important factor for susceptibility, since these cytokines are known to prevent the production of nitric oxide species via the inhibition of IFNγ-activated macrophages [56,57]. Finally, also non-T cell related factors have been shown to contribute to susceptibility against *Leishmania*, such as the differential expression of costimulatory molecules on APCs of different mouse strains [4,58].

The role of cytotoxic $CD8^+$ T cells during *Leishmania* infection was discussed controversially during the last years. It was observed that the activation of $CD8^+$ T cells in the skin led to increased disease severity in some models, on the other hand, a protective role by $CD8^+$ T cells in other organs has been shown. This difference in anti-*Leishmania* activity of $CD8^+$ T cells might be due to the properties of the T cells, depending whether they are cytolytic or if they produce IFNγ [2,36,59–61].

Effector function delivery

After expansion and differentiation in the lymph node, Th1 cells enter the site of infection as effector cells and release their cytokines after the recognition of their cognate antigen. Intravital 2-photon microscopy experiments can be used to directly observe the physical interaction of the Th1 cells with infected APCs [62]. Such experiments showed that both, during priming in the lymph node, as well as for delivery of cytokines, antigen recognition results in the arrest of the T cells at the interaction site, which is dependent on antigen specificity, and can be used as a reliable readout for T cell activation [63,64]. Strikingly, not all infected APCs display interactions with Th1 cells at the site of infection. Instead, stable T cell-APC interactions are limited to distinct hot spots in the infected tissue [63]. Moreover, Müller et al. could show that IFNγ is produced by $CD4^+$ T cells only at such hotspots but can induce the production of nitric oxide in bystander APCs within a range of 80 µm. Therefore, next to T cell-APC interactions, it is not mandatory that every APC forms stable contacts with T cells to produce IFNγ and hence control *L. major* infection [65]. The reasons for the heterogenic distribution of T cells and the formation of clusters at the site of infection are not known so far and have to be investigated to better understand T cell immunity during infections with protozoan intracellular parasites.

Concomitant immunity and chronic infection

Cure of primary *Leishmania* infection leads to life-long immunity to reinfection, caused mainly by $CD4^+$ T cells. However, even in the setting of resistant mouse strains which are controlling *Leishmania* infection, there is always a small number of parasites which reside inside the host, even after the pathology is resolved. This persistence has been shown to be necessary to retain resistance upon reinfection, referred to as concomitant immunity [66,67]. Consequently, mice which achieved sterile control of *L. major*, lose immunity against reinfection. For persistence of the parasite, IL-10 seems to play an important role [68,66,67], as it was shown that infection was cleared completely in the skin, as well as in the draining lymph nodes, in IL-10 knock out mice, leading to sterile control. This might be due to the development of a stronger Th1 response. In contrast, parasite numbers did not decrease after 9.5 weeks of infection (when chronic infections have been shown to be established in wt mice) in IL-4 deficient mice, indicating that IL-4 does not exhibit any influence for the parasite persistence in resistant mice [66]. DCs and macrophages have shown to be responsive to IFNγ as well as to IL-10 [66]. IL-10 has an important function in the regulation of the immune response and is mainly produced by $CD4^+CD25^+$ regulatory T cells (T_{regs}). T_{regs} enrich in the skin where they are responsible for suppression of the $CD4^+$ effector cells, that are competent to clear the infection [67]. In susceptible mouse strains $CD4^+CD25^-Foxp3^-$ IFNγ producing Th1 cells also display an important source of IL-10, thus mediating immune suppression [69]. More recently, the constant presence of short-lived $CD4^+Ly6C^+Tbet^{high}$ effector T cells has been shown to be crucial for an effective memory response. These cells circulate in the blood and migrate immediately to the infection site after re-challenge to drive parasite killing [70]. Additionally, tissue resident memory T cells were identified, mediating protection during the first days of re-infection via the activation and recruitment of monocytes to the site of infection [71,6].

The mode of action by which the cellular defences impact on the pathogen's physiology in order to contain the pathogen at low numbers, without completely eradicating the infection, and thus permitting concomitant immunity, is unclear. Interestingly, it has been shown that there are high and low proliferating pathogens among the persister populations residing in different cell types, mainly DCs and macrophages [72], which suggests that not only pathogen killing, but also adaptations of pathogen proliferation contribute to the low numbers of parasites during the chronic infection [73]. Besides professional phagocytes which are downregulated in their antimicrobial activity, fibroblasts, which also are expected to have lower competence in controlling parasites, have been shown to harbor *Leishmania* during chronic infection [74] (see also chapter 1.2.5).

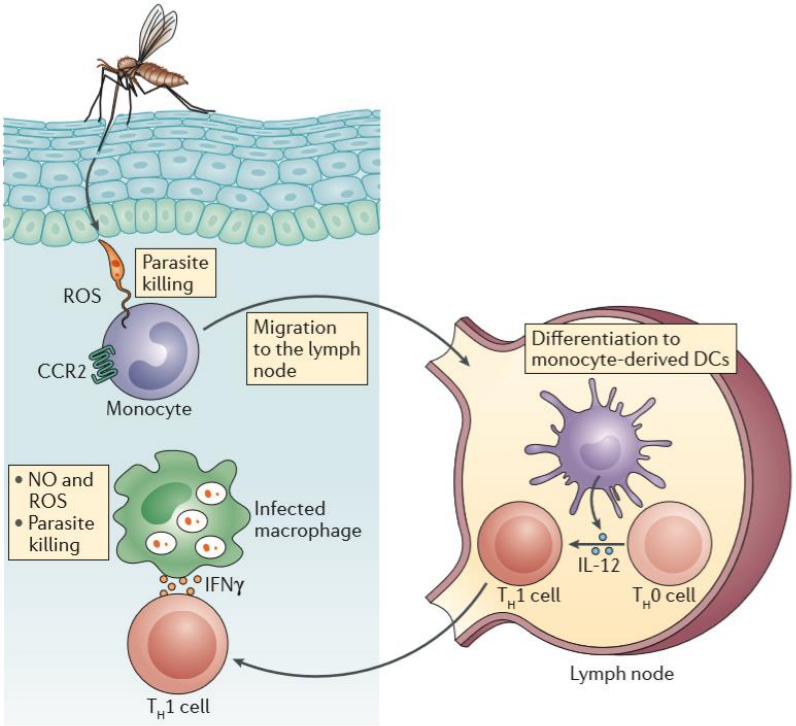

Figure 2: Schematic immune response upon *Leishmania* infection [6].

1.2.5 The spectrum of different cellular niches for *Leishmania* spp.

Macrophages and DCs are the two major host cell types harboring parasites during the established *L. major* infection. But other cells have been shown to play an important role as cellular niches, as well. As the ability of *Leishmania* to invade host cells is relatively weak, compared to other pathogens like *Plasmodium [75]*, they mainly depend on the uptake by phagocytic cells. This explains, that with few exceptions, the habitat observed for *Leishmania* within the mammalian host mainly consists of cells with phagocytic activity.

Neutrophils

Neutrophils are one of the first cell types that are infected upon *Leishmania* inoculation of the skin. Their function is controversially discussed since they can play a role in promoting the infection, as well as killing the parasites (see also chapter 1.2.4). Upon the sandfly bite, neutrophils are immediately recruited to the site of infection and phagocytose *Leishmania* [76]. For example, neutrophils have been proposed to control the parasite via the formation of NETs. NETs are DNA structures that are covered by antimicrobial molecules, therefore they bind microorganisms to immobilize and, in some cases, kill them. Depending on the *Leishmania* species, NETs can lead to the killing of the parasite [26,27] whereas in chronic lesions, like infection of C57BL/6 mice with *L. mexicana*, parasites are able to survive within NETs,

indicating that the escape of NET killing by promastigotes is an essential survival strategy [30]. Phagocytosis of infected neutrophils by macrophages can lead to increased TNF secretion; therefore triggering a respiratory burst causing superoxide production [28]. Contrary to the above, activation of DCs and macrophages can be reduced after uptake of apoptotic neutrophils, which has been shown to occur in *L. major* infections [29]. Although $CD11b^+Ly6C^+CD24^+Ly6G^+$ neutrophils play a major role during the beginning of the infection [77,33] and the uptake of promastigotes, Leon et al. could prove that $CD11b^+Ly6C^+$ neutrophils are also present at the peak of infection at week 3 and 4, where the majority of them is infected by *Leishmania* [33]. According to this, it was recently demonstrated that during the chronic phase of *L. mexicana* infection, acidified vesicles of neutrophils can serve as niche for parasite replication [78].

B cells

B cells represent another cell type that can phagocytose *Leishmania* parasites, and different roles for B cells are described within the infection: On the one hand, B cells were shown to be a niche for *L. major* amastigote proliferation. This furthermore triggers the release of IL-10. Thus, B cells represent an additional cell type responsible for the production of IL-10 [79]. The contribution of B cells to susceptibility of *Leishmania* infection was moreover shown by Gonzaga et al. in *L. chagasi* infection [80]. On the other hand, B cells also have been shown to contribute to successful control of *L. major* infections [2][81]. For example, the uptake of parasites by DCs at the site of infection is linked to the opsonization of *Leishmania* by parasite-reactive IgG and therefore turned out to play a crucial role for T cell priming and IFNγ production [36,82].

Fibroblasts

Fibroblasts are believed to play a role within the early phase of *Leishmania* infection since different subtypes of fibroblasts were found in the early phase upon human cutaneous leishmaniasis infection [83]. It has been demonstrated *in vitro* that *Leishmania* can reside within a parasitophorus vacuole of fibroblasts [84,85]. Bogdan et al. could prove *in vivo* that many parasites reside within fibroblasts during the latent phase of the infection, which might be due to the lower ability of fibroblasts to control the parasites via the activation of iNOS [74].

Macrophages

Leishmania promastigotes can be taken up by macrophages in a receptor-mediated way, for example via complement receptors 1 and 3 (C1 and C3), mannose-fucose receptors and fibronectin receptor. LPG and PPG on the surface of *L. major* promastigotes (see

chapter 1.2.3) are important factors to trigger a successful phagocytosis. The uptake of amastigote *L. major* is facilitated by parasites coated with host IgG which is able to interact with Fc receptors on macrophages. The opsonisation of parasites is also relevant for the efficient uptake via C1 and C3 [86,17]. On the one hand, this induces downstream signalling pathways that support pathogen growth and further inhibit parasite killing [17,87]. Furthermore, phagocytosis together with inflammatory cytokines like TNF [28], IL-1, IFNγ and IFNα/β lead to the activation of iNOS and thus the production of nitric oxide via the oxidation of L-arginine. On the other hand, hydrolysis of L-arginine via host arginase leads to the supply of polyamines and inhibits the production of nitric oxide, therefore driving pathogen proliferation [14,88]. *Leishmania* arginase leads to augmentation of the arginase function of the host and therefore to enhanced parasite survival, particularly via alternative macrophage activation (see chapter 1.2.2) [17,14,88]. In contrast, an additional defence mechanism is displayed by phagocyte NADPH oxidase which induces the production of reactive oxygen species, representing together with iNOS the two main mechanisms in *Leishmania* control. Nevertheless, it was shown that ROS production is important, but not completely indispensable, to control infection in the ear and the draining lymph nodes, in contrast to nitric oxide [89,6,45].

Macrophage subtypes and immune activation at the site of infection

Different subtypes of macrophages are involved as host niche in *Leishmania* infection. One of the first infected macrophage subtypes, within the first hours of infection, are resident dermal macrophages. In mice, these macrophages are $F4/80^{+}$ but show a low expression for GP (also known as CD29) [76], which is important for differentiation of monocytes to macrophages [90]. Furthermore, dermal macrophages are characterized as $Ly6C^{-}CCR2^{-}CX3CR1^{-}$ [77]. In the ongoing infection, monocyte-derived macrophages are recruited to the infection site, where they can be infected by the parasites and represent the main macrophage population in the ongoing infection. These macrophages are, among other markers, characterized by the expression of CD11b and F4/80 [76,33,91,92]. Monocytes are recruited from the blood stream and can differentiate into monocyte-derived macrophages and monocyte-derived DCs. Goncalves et al. show that monocytes can be divided into two main subpopulations which are equally distributed in the blood but differ in the expression of surface proteins and morphology. In particular, the two subpopulations vary in the expression of the surface proteins Ly6C and the CC-chemokine receptor 2 (CCR2) in one population and high expression of fractalkine receptor (CX_3CR1) in the other population, which exhibits lower expression of Ly6C and CCR2. It was proven that a monocyte subpopulation which is rapidly recruited to the site of primary infection within the first hours is able to control the parasites. This subpopulation is characterized by high expression of Ly6C and CCR2 [92]. The monocytes at the site of infection were further analyzed by Romano et al. They defined rapidly recruited inflammatory

monocytes as CD11b^{+}Ly6C^{+}CCR2^{+}CD24^{-}class II MHC^{-}CD11c^{-}. The number of these monocytes (which are efficiently infected) raises fast within the first hours of infection. Additionally, two other cell populations, defined as putative inflammatory monocyte derived cells, were described to play a role in the first days of infection. They were defined as Ly6C^{+}CCR2$^{low/-}$CX3CR1^{+}, respectively Ly6C^{-}CCR2^{+}CX3CR1^{+} [77].

Leon et al. could show that in C57BL/6 mice the number of monocyte derived macrophages increases dramatically by week 3, at which timepoint the largest proportion of infected cells is observed, before it decreases again. These phagocytes are defined by expression of the surface markers CD11b^{high}class II MHC^{high}CD86^{low}CD205^{low}Ly6C^{high}F4/80^{high}. Macrophages as well as infected macrophages can also be found in the draining lymph nodes where they might be able to present antigen and therefore take part in the activation of the adaptive immune response [33]. Nevertheless, the number of macrophages recruited to the lymph nodes appears to be distinctly less than the number of DCs [33], which are described to be the major cell type being responsible for activation of an efficient T cell response upon *Leishmania* infection.

Dendritic cells

As in macrophages, there are also several different subtypes of DCs differing between the distinct organs and even within one organ. In the uninfected skin the following main APC subpopulations are located: dermal DCs (dDCs) (mainly characterized by CD11c, CD11b, class II MHC, DEC-205a and CD103), Langerhans cells (mainly characterized by the expression of langerin, CD11b, dectin-1^{intermediate}, and class II MHC ^{intermediate}) and Langerin^{+} dermal DCs (mainly characterized by the expression of langerin, CD11c, CD86^{intermedaite}, dectin-1^{intermediate}, CD103, and class II MHC^{high}) [93,94].

Upon infection these pre-existing cells are rapidly recruited to the lymph nodes [95–97,94], whereby priming of CD4^{+} T cells is induced by Langerin^{-} dDCs and early priming of CD8^{+} T cells is mediated by Langerin^{+} dermal DCs [94]. Subsequently, CD11b^{+}Ly6C^{+}CCR2^{+} inflammatory monocytes start to enter the dermis and some of them develop into monocyte-derived skin DCs [77]. Therefore, the DC populations of the steady state become outnumbered by newly recruited inflammatory monocytes and monocyte-derived DCs, respectively [77]. The phenotype of the recruited monocyte-derived dermal DCs is similar to that of dDCs thus, it is likely that some important functions of dDCs are taken over during infection by monocyte-derived dDCs, like antigen capturing and transport into the lymph nodes [33]. Within the lymph nodes, other subtypes of DCs, originating from precursor cells that are recruited directly to the lymph node from the blood stream, are located. Among these cells are resident CD8^{+} and CD8^{-} DCs which can activate CD8^{+} T cells via cross-presentation, but also initiate CD4^{+} T cell

responses. These DCs mature upon the presence of DC-activating cues like e.g. inflammatory cytokines and Toll-like receptor ligands (Figure 3) [95]. It was shown that TLR9 and its signalling via the adapter molecule MyD88 plays a crucial role for the induction of *L. major* mediated IL-12 production [47]. Upon skin infection dDCs are recruited into the lymph nodes where they can present antigen, transfer it to $CD8^+$ DCs and activate $CD4^+$ T cells [95]. Therefore, several C-type lectin receptors for efficient antigen internalization are expressed on the surface of dDCs [95,98]. Since monocyte-derived dDCs show a very similar phenotype to dDCs it is very likely that after migration to the draining lymph node they also transfer antigens to $CD8^+$DCs [95] or achieve the direct activation of a $CD4^+$ T cell response via direct priming. This phenomenon has been shown by Leon et al. during *L. major* infection where monocyte-derived dermal DCs migrated from the skin´s infection site to the draining lymph node and subsequently became fully maturated, leading therefore to the induction of a $CD4^+$ Th1 response [33]. The occurrence of monocyte-derived DCs being mainly responsible for $CD4^+$ T cell responses is not limited to *Leishmania* infection: For example, also in *Salmonella* infection, it was observed that monocyte-derived DCs activated $CD4^+$ T cells [99].

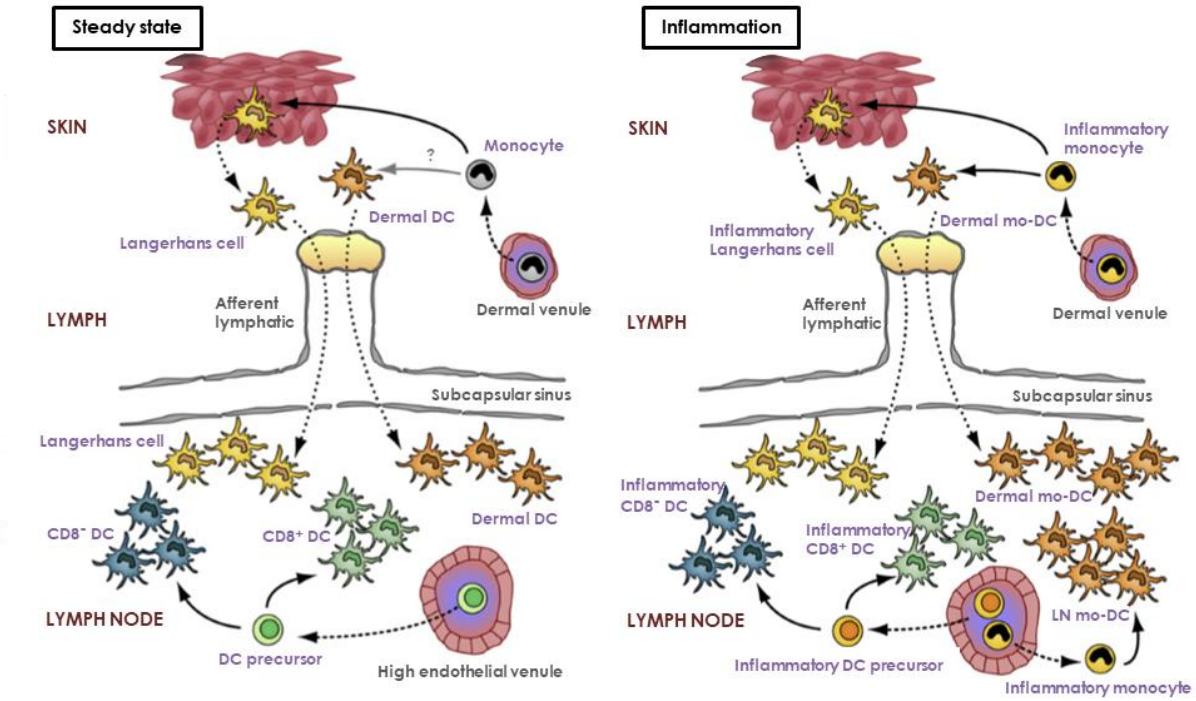

Figure 3: DC subsets in steady state and during inflammation (modified from [95]).

Plasmacytoid DCs (pDCs) constitute another type of DCs, which is characterized by the production of type I interferons like IFNα and β. They are known to respond mainly to bacterial and viral DNA and RNA via TLR 9 and 7 [100–102,103]. pDCs seem to play a role for controlling the *Leishmania* infection although they are not efficiently invaded by the parasite [33,47,96]. They can be activated by leishmanial DNA and are characterized by the expression

of CD40, CD80, CD86, CD11c, CD62L and CD123 [47,103]. Their activation leads to the production of IL-12 and IFNα/β via MyD88 dependent TLR9 signalling, which makes them the main producer of IFNα/β during *Leishmania* infection [47].

Role of dendritic cells as a niche at the infection site

In C57BL/6 mice, from week 2 to week 3 the amount of monocytes, DCs, macrophages and neutrophils is dramatically increased whereby monocyte derived DCs represent the major fraction, both in absolute numbers as well as among infected cells. [6,98,77,104]. Among the monocyte-derived DCs are different subpopulations, representing differentially maturated and activated states of DCs. Within the skin, recruited monocytes can differentiate into immature DCs which are Ly-6C^{high}CCR2^{+}CD11c^{high}CD11b^{high} class II MHC^{intermediate}CD86^{low}F4/80^{low}. These DCs can mature partially at the site of infection, being then defined via the expression of Ly6C$^{low/intermediate}$ CD11c^{high} CD11b^{high} CCR2^{+} class II MHC^{high} CD86$^{intermediate/high}$ F4/80$^{intermediate/high}$ [77,33]. These partially matured DCs migrate to the draining lymph nodes where they fully mature. Within the lymph nodes they represent the major cell type responsible for activating IFNγ production by CD4^{+} and CD8^{+} T cells and therefore inducing a defensive Th1 response [33]. CD11b^{+}CD11c^{+}Ly6C^{+}class II MHC^{+}CD86^{+} cells were furthermore shown to be the major iNOS-producing cell type as well as at the site of infection and in the draining lymph nodes [104,77]. While in macrophages, either the production of nitric oxide via iNOS and the ROS production by NADPH oxidase, are well-described as mechanisms for controlling *Leishmania* intracellularly [45,89], ROS production by DCs has hardly been reported.

1.3 Pathogen physiology

1.3.1 The role of pathogen physiology for the infectious agent

The physiology of pathogens invading the host plays a crucial role for the outcome of the immune response. For example, for a variety of bacterial infections, it was shown that the immune system can fight proliferating bacteria but is less able to kill non-replicating bacteria, leading to persister populations [105,106]. Furthermore, these non-replicating subpopulations are often resistant to antibiotics. The dormant microbes often have a reduced cell-wall synthesis as well as a downregulation of genes that are involved in energy production [105,106]. Another example for such phenotypic (as opposed to genetic) resistance during infections, is the formation of small colony variants by *S. aureus* which are believed to enable the pathogen to escape the immune response and endure antibiotic treatment [107].

Also for parasites, there is evidence that the physiology of the pathogen is important to induce persistence. For example, it was demonstrated for *L. mexicana* infections in BALB/c mice that a slow proliferation rate of the parasite leads to successful establishment of the infection, indicating that this is a successful method to reduce phagocyte activation [108]. It was described that the tissue environment of pathogens has a great influence on parasite proliferation [108]. In line with these findings, it was shown that different pools of high and low proliferating *L. major* are coexisting at the site of infection [72,73]. Specifically, Mandell et al. could show that within the persistent *L. major* there are two populations: One showing high proliferation rates and the other one containing parasites of rather low proliferation, indicating that heterogenic parasite proliferation might be important for persistence.

1.3.2 The role of pathogen physiology for the host

Pathogen physiology is not only important for phenotypic resistance against antimicrobial defence mechanisms and treatment but does also have an impact on the induction of immune responses. This is of great interest with regard to the fact that application of live vaccines often shows a better immune induction than killed vaccines [109,110]. Furthermore, it was shown by Cheers et al. in 1996 that only living intracellular bacteria like *Mycobacteria*, *Salmonella* or *Listeria* induce waves of IL-12 production, further leading to the release of IFNγ, indicating an ability of macrophages to distinguish between dead and alive bacteria [109]. In consequence, a class of vaccines has been developed, that has properties of live pathogens such as metabolic turnover and protein production, but are unable to divide, providing this way a safe vaccine. Such preparations are called killed but metabolic active (KBMA) microbes [111]. It was proven that the innate immune system is involved in detecting live pathogens: For example, prokaryotic mRNA can be detected in a signaling pathway which involves the innate

adaptor molecule TRIF, and has thus been defined as so-called vita-PAMP [112]. Also, viable pathogenic as well as non-pathogenic bacteria can induce inflammasome activation via pro-caspase-1 cleavage, a process known as pyroptosis [113]. DNA:RNA hybrid molecules, besides being an important PAMP of virus replication, could also represent a signature of bacterial and parasite replication: Detected in a MyD88-dependent fashion [114], these molecules also occur in the course of DNA replication, transcription and bacterial DNA demethylation [115]. However, whether the immune system is able to quantitatively detect pathogen proliferation, and by which mechanism this might occur, are mainly unstudied subjects.

1.4 The mKikumeGR proliferation reporter system

With regard to the very important role for parasite survival and at the same time for the induction of a successful immune response, it is essential to understand the relationship between parasite proliferation and the immune system. This is of highest interest for the efficient treatment of infectious diseases and development of vaccination strategies. Nevertheless, it remained challenging to measure *Leishmania* proliferation under physiological conditions *in vivo*. In the last years, techniques like heavy water labelling of *Leishmania* [108] or incorporation of BrdU (5-Bromo-2′-deoxyuridine) into parasite DNA [72] have been developed to investigate parasite proliferation. Using these techniques, parasite replication was calculated from the DNA, RNA and protein turnover rates indicated from the dilution of $^{2}H_2O$, or via the incorporation of BrdU into newly produced DNA in replicating *Leishmania*. However these approaches have not allowed for a cell-resolved analysis of pathogen proliferation, or the application of immunofluorescence microscopy or cytometry in order to analyze the cellular niches of efficient pathogen proliferation. To overcome this limitation, a system was set out to characterize *L. major* proliferation on a single cell level by using a novel fluorescence protein-based *in vivo* proliferation reporter system [78,73].

In 2008 Habuchi et al. published the construction of the photoconvertible monomeric KikGR protein [116]. The green fluorescent protein KikG was originally isolated in its homotetrameric state from the coral *Favia favus* which bears the Japanese name “Kikume-ishi”. It was furthermore genetically engineered to the photoconvertible protein KikGR [117]. The successful expression, bright fluorescence and photoconvertibility in mammalian cells was proven, as well as the ability to partially photoconvert the protein via 2-photon microscopy at 760 nm. Thus, KikGR was established as a reporter protein being adapted for optical cell labelling, also in thick tissues [117]. This protein was modified to its monomeric form by Habuchi et al. to mKikGR, further termed mKikumeGR, which is very important to enable the uncomplicated construction of fluorescence fusion proteins [116]. The photoswitch from green to red fluorescence is caused by irreversible light induced β-elimination within the mKikumeGR protein (Figure 4 A) [116]. It changes its green fluorescence, showing a fluorescence spectrum with a peak at 515 nm, to red, with a peak of the fluorescence spectrum at 591 nm, upon illumination of the protein with light of 405 nm (Figure 4 A-B) [116]. Furthermore, the monomeric state of mKikumeGR makes it possible to use this protein for super resolution imaging. mKikumeGR exhibits stability, a bright fluorescence, constantly high switching rates, and high photostability [116].

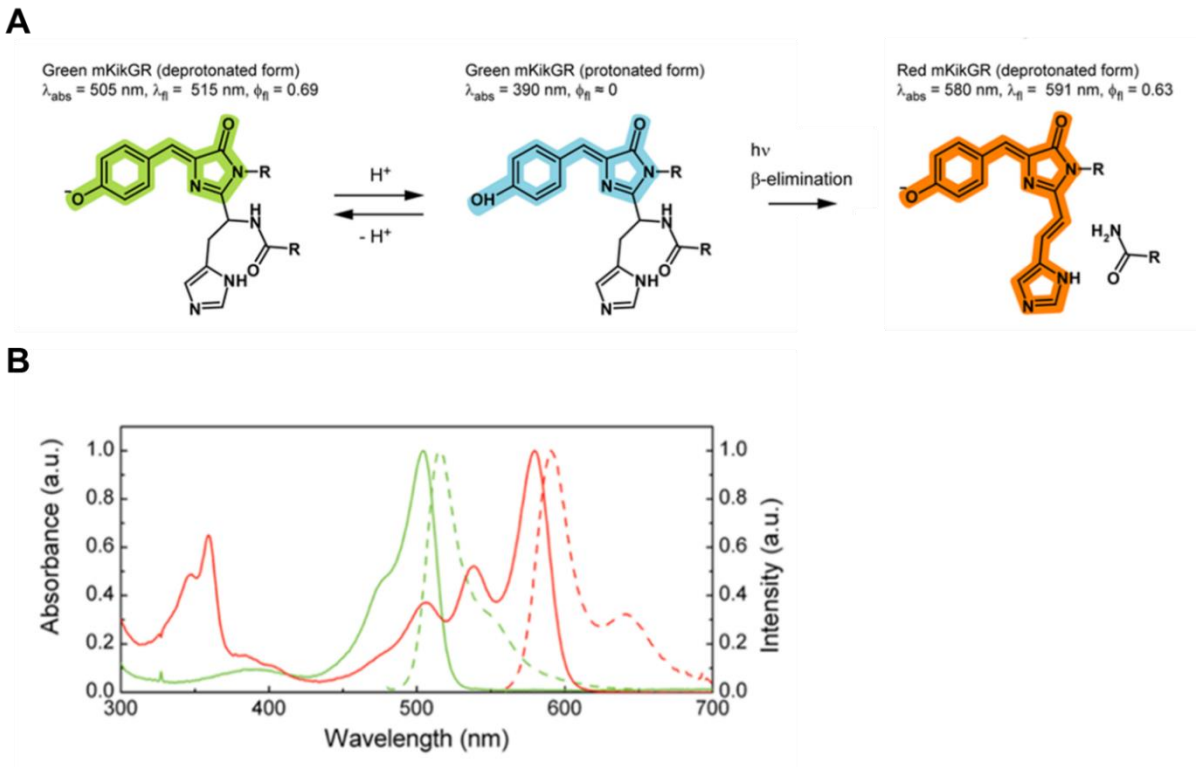

Figure 4: Photoconversion of mKikumeGR (modified from [116]). (A) Molecular mechanism of the photoconversion from green to the red state of mKikGR (mKikumeGR). **(B)** Spectroscopic characteristics of the green and red state of mKikGR (mKikumeGR).

To measure parasite proliferation at the site of infection *in vivo*, *Leishmania* constitutively expressing the mKikumeGR protein were generated [73,78] *L. major* parasites expressing the photoconvertible protein show green fluorescence with 520 nm emission that can be switched to red fluorescence (580 nm emission) after illumination with a 405 nm light pulse, therefore termed as Lm^{SWITCH} [73]. Müller et al. could show the photoconvertibility of Lm^{SWITCH} in the infected dermis (Figure 5). Furthermore, it was demonstrated that the *de novo* expression of non-converted green mKikumeGR protein after photoconversion, as well as dilution of the photoconverted red fluorescent protein, are tightly correlated with cell division (Figure 6, unpublished data from Andreas Müller). Thus, photoconversion of Lm^{SWITCH} and subsequent measurement of the recovery rate from photoconversion can be used as a reporter for parasite proliferation [73,78]. In the presented work, Lm^{SWITCH} were used as a reliable reporter system to measure parasite proliferation *in vivo*.

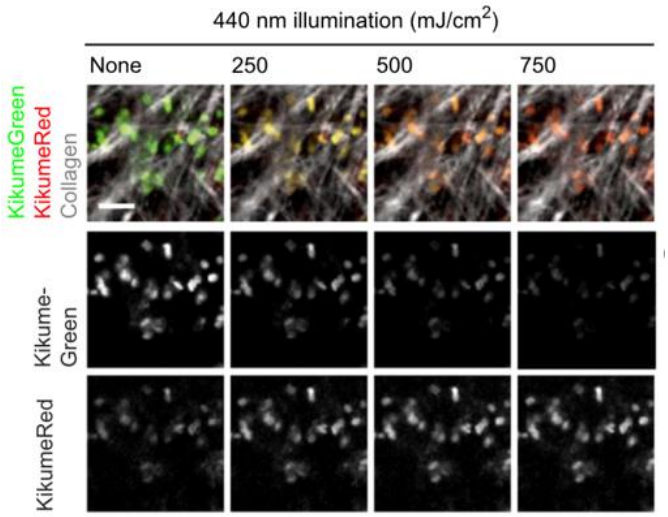

Figure 5: Photoconvertibility of *Lm*^{SWITCH} in the ear dermis of mice with enhancing violet light doses (Müller et al. 2013).

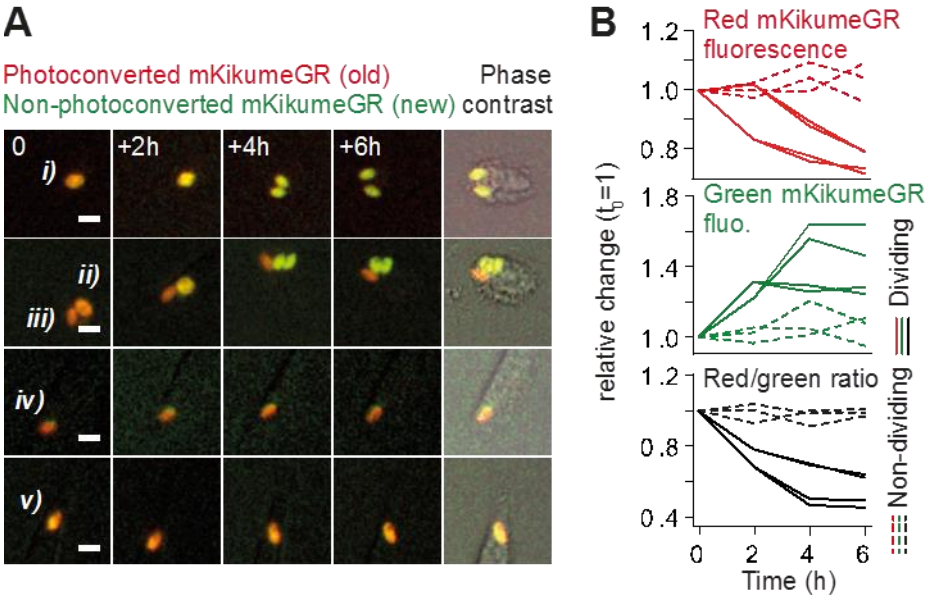

Figure 6: Recovery of the green fluorescence of *Lm*^{SWITCH} after photoconversion is coupled to cell division (unpublished data). (A) Peritoneal macrophages infected with *Lm*^{SWITCH} *in vitro*, photoconverted and imaged over time. i, ii, parasites undergoing cell division in the course of the movie, iii, iv, v, non-dividing parasites. Scale bar, 5 µm. **(B)** Quantification of relative changes of mKikumeGR red and green fluorescence, and red/green ratios from parasites i through v from (A). Each line represents one parasite; solid lines, parasites which undergo division in the course of the movie; dashed line, non-dividing parasites.

1.5 Aims of the study

The pathogen property of being alive and proliferating has a great impact on the course of an infection and the induction of an efficient immune response. Nevertheless, the mechanisms, by which the immune system might distinguish different proliferative states of pathogens are not well understood.

In my study, I analyzed the behavior of immune cells depending on the proliferative state of the intracellular parasite *Leishmania major (L. major)* during the infection.

To investigate this, *Lm*^{SWITCH} (expressing the mKikumeGR proliferation reporter) (see chapter 1.4) were applied. The thesis is subdivided into three main parts:

1) Characterization of *Lm*^{SWITCH} for efficient *in vivo* analysis
   To improve the readout and the capabilities of the mKikumeGR proliferation reporter in *L. major*, the system was further characterized in the first part of this thesis. Therefore, photoconversion of the mKikumeGR protein by the use of LED diodes was established, fixation conditions of *Lm*^{SWITCH} were set up and efficient analysis of *Lm*^{SWITCH} infected tissues by flow cytometry was constituted.
2) *L. major* proliferation in context of the tissue environment
   The virulence of *L. major* relies largely on their ability to undergo cycles of replication within phagocytes, release, and uptake into new host cells. While all these steps are critical for successful establishment of infection, neither the cellular niche of efficient proliferation, nor the spread to new host cells have been characterized *in vivo*. Here, I used the *Lm*^{SWITCH} proliferation reporter to investigate pathogen proliferation in this context by flow cytometry, intravital 2-photon microscopy and immunohistochemical methods in the ongoing infection.
3) Analyzing the dynamics of effector T cells in the context of pathogen proliferation
   L. major triggers a robust protective immune response mediated by T helper cells in immunocompetent individuals. In a series of pilot experiments in the last part of my study, this well-established infection model was used to analyze the dynamics of T helper cells in the context of pathogen proliferation via intravital 2-photon microscopy.

2 Results

2.1 Characterization of the mKikumeGR reporter system

To measure the *L. major* proliferation under physiological conditions *in vivo*, the mKikumeGR fluorescence reporter system was used within this project (see chapter 1.4; [116,78,73]). To improve the readout and the capabilities of the mKikumeGR reporter, the system was further characterized in the first part of the thesis.

2.1.1 Photoconversion of the mKikumeGR protein by the use of LED diodes

So far, the implementation of the photoconversion of the mKikumeGR protein from green to red was performed during microscopy by a laser pulse or epifluorescence illumination under a microscope [73,117]. For facilitating the application of the photoconversion (i.e. to photoconvert larger areas like whole infected ears or cell cultures) a diode array was constructed (Figure 8 A, see chapter 4.1.4). The photoconverted parasites were analyzed after 48 h by flow cytometry, multi-epitope ligand cartography, confocal microscopy or intravital microscopy.

Photoconversion of *Lm*^{SWITCH} (mKikumeGR expressing *L. major*), via the constructed LED diode array was confirmed *in vitro* by flow cytometry and *in vivo* by 2-photon microscopy. To prove photoconversion *in vitro, Leishmania* suspension was transferred into 96-well plates and irradiated by a 2x2 LED diode array for 1 min as described in detail in chapter 4.1.4. *Leishmania* suspension was subsequently analyzed via flow cytometry (Figure 7). It could be shown that there is a complete shift from green to red fluorescence by comparing the non-photoconverted parasites with *Leishmania* that were irradiated and subsequently analyzed (Figure 7, left panel). To quantify efficiency and level of photoconversion the red-to-green ratio is calculated from the mKikumeGR fluorescence (Figure 7, right panel).

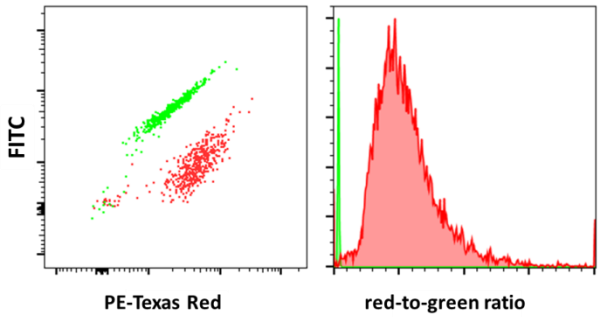

Figure 7: Analysis of photoconversion of *Lm*^{SWITCH} *in vitro* by flow cytometry. An axenic *Leishmania* suspension was irradiated by a 2x2 LED diode array for 1 min. Left: *Leishmania* fluorescence before (green population) and directly after (red population) photoconversion. Green mKikumeGR fluorescence is plotted on the y-axis (FITC channel) and red mKikumeGR fluorescence is

plotted on the x-axis (PE-Texas Red channel). Right: Red mKikumeGR fluorescence divided by green mKikumeGR fluorescence (red-to-green ratio) before (green) and directly after (red) photoconversion.

Successful photoconversion via a diode array and recovery from photoconversion *in vivo* was demonstrated by imaging infected ears of anesthetized mice via 2-photon microscopy (Figure 8 B). To this end, C57BL/6 mice were infected with 200.000 *Lm*^{SWITCH} parasites for 10 days, then anesthetized and analyzed non-invasively using 2-photon microscopy before, 0 h, and 24 h after photoconversion. Following, green and red mKikumeGR fluorescence data were transferred into a FlowJo.fcs format using the DiscIT software [118] and analyzed by plotting the green mKikumeGR fluorescence against the red mKikumeGR fluorescence. As expected, *Lm*^{SWITCH} showed a green fluorescence before photoconversion, which was completely converted to red, when imaged directly after illumination. Recovery from photoconversion was observed by imaging the infection site 24 h after photoconversion. Of note, some parasites displayed complete recovery from photoconversion, while some parasites exhibited an intermediate state, displaying as well fluorescence of newly expressed green mKikumeGR protein as photoconverted red protein. Furthermore, a large population of parasites still exhibited exclusively red fluorescence. Thus, *in vivo*, *L. major* proliferates at heterogenic rates.

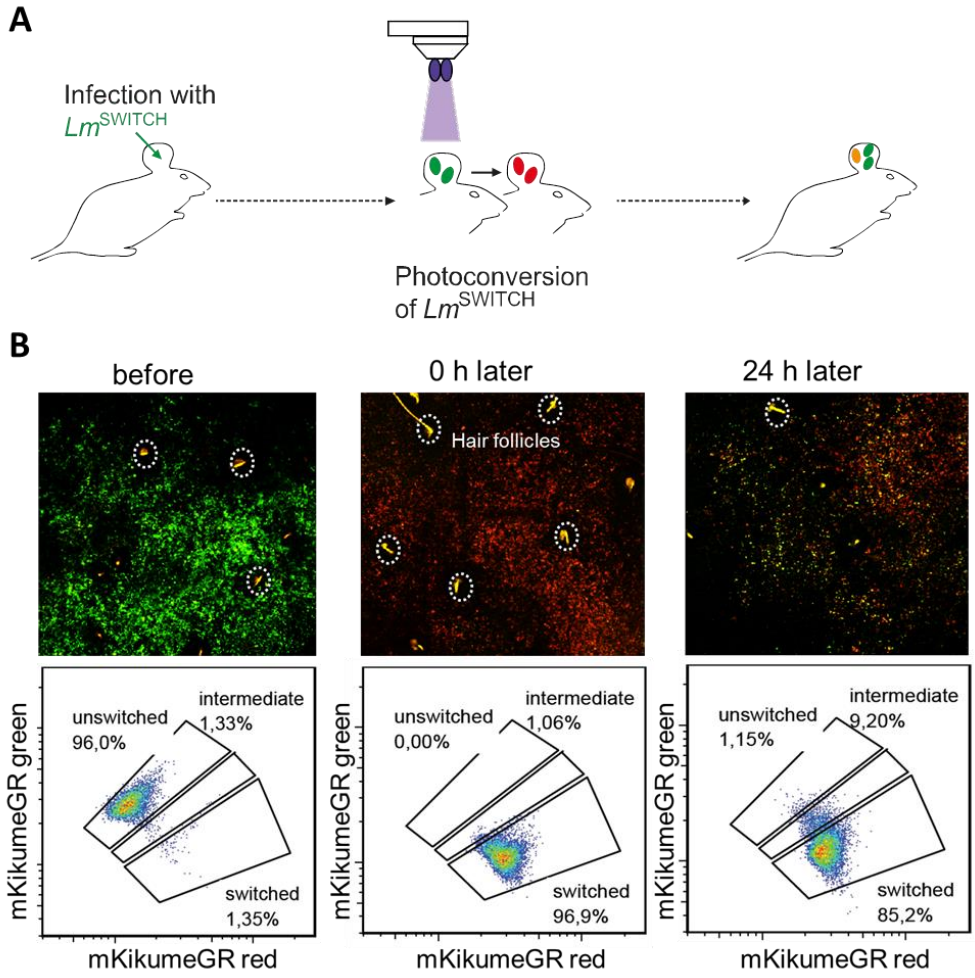

Figure 8: Illumination of *Lm*^{SWITCH} infected mice with a diode array and analysis of photoconversion via intravital 2-photon microscopy. (A) Mice were anesthetized and infected ears were fixed in a defined distance to the diode array, consisting of 2x2 LED diodes. Illumination was implemented for 1 min on each site of the mouse ear with a wavelength of 405 nm to photoconvert green fluorescent *Lm*^{SWITCH} into red. **(B)** (Upper panel) Imaging of non-photoconverted *Lm*^{SWITCH} showed a green fluorescence (left) which was completely photoconverted into red fluorescence (middle), demonstrated by imaging directly after photoconversion. (lower panel) Values of green and red *Leishmania* fluorescence were transferred into flow cytometry data sets. Subsequently mKikumeGR green fluorescence was plotted against mKikumeGR red fluorescence. Flow cytometry plots related to non-photoconverted (before) and just photoconverted (0 h) were compared with the red and green fluorescence of parasites that have been photoconverted for 24 h. Partial rediscovery of green fluorescence was observed 24 h after photoconversion (right).

2.1.2 Establishing fixation conditions for *Lm*^{SWITCH}

For a broader application of the mKikumeGR reporter system, it was tested if mKikumeGR protein expressed by *L. major* (*Lm*^{SWITCH}) is fixable. Therefore, it was tested if the mKikumeGR protein is chemically fixable at conditions that are compatible with immunofluorescence staining. To this end, *Lm*^{SWITCH} infected mouse ears were photoconverted, harvested 48 h later

and incubated in 4% paraformaldehyde (PFA) at 4°C for 2 h. Afterwards, the tissues were transferred into 20% sucrose and incubated over night at 4°C before they were shock-frozen by liquid nitrogen in Tissue-Tek® O.C.T.™ Compound. Histological ear slices were prepared, cells were stained anti-CD54 and successful fixation of the green fluorescence (which was expected to recover 48 h after photoconversion in some parasites) and the red fluorescence of the mKikumeGR protein, within *Leishmania* infected cells, was tested using confocal microscopy (Figure 9 A). Strikingly, as with intravital 2-photon microscopy, both green and red parasites were observed, indicating that the mKikumeGR proliferation reporter system is compatible with PFA fixation and immunofluorescence staining.

2.1.3 *L. major* proliferation is heterogenic on a tissue level but cell-intrinsically homogenous

The mKikumeGR reporter system was employed to determine *L. major* proliferation rates *in vivo* three weeks post infection of the ear dermis. Using anti-CD54 staining to mark cell outlines for confocal immunofluorescence microscopy, it was observed that 48 h after photoconversion *L. major* proliferation rates were very similar among the parasites within individual infected cells (Figure 9 A). However, the pathogen proliferation rates between different host cells varied dramatically (Figure 9). This was quantified by investigating the red and green fluorescence of single parasites infecting individual cells in Figure 9 B (one cell represented in each column and ordered according to the mean red-to-green fluorescence ratio of parasites in the respective column). The distribution of mKikumeGR red and green fluorescence among individual cells suggested that the majority of the cells harbors either red, low proliferating, parasites or green, high proliferating, parasites. As a control, individual parasites were assigned randomly to the same number of cells. By plotting the number of *Lm*^{SWITCH} which are mainly red within a single cell against the number of mainly green *Lm*^{SWITCH} within the same cell, this finding can be validated (Figure 9 C). Intravital 2-photon microscopy of mouse ear tissue, which was infected and photoconverted using the already mentioned conditions, also clearly revealed clusters of high proliferating parasites separated from clusters of low proliferating parasites (Figure 9 D-F). Thus, it could be concluded that distinct pathogen proliferation rates are linked to specific cellular niches.

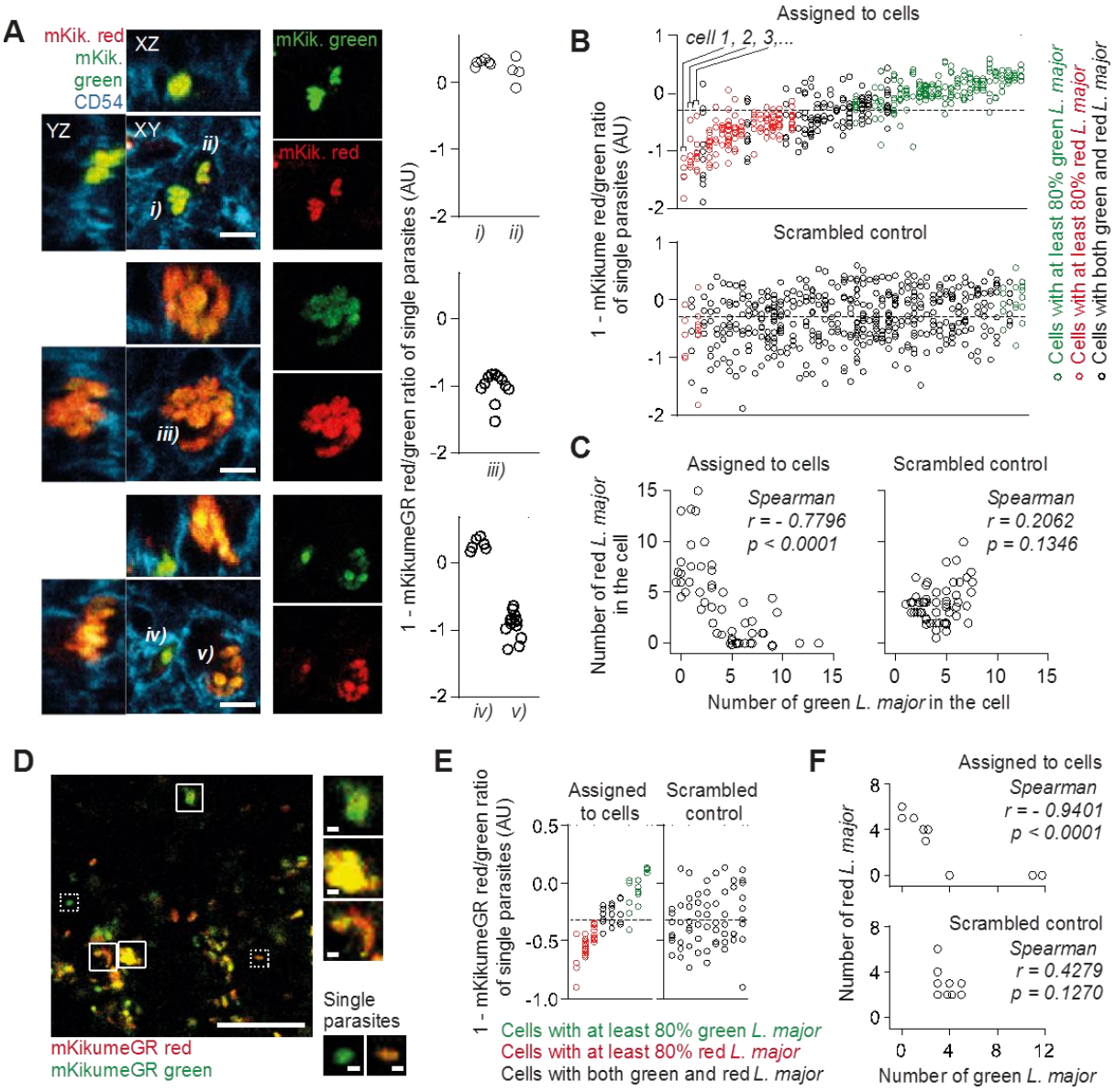

Figure 9: Photoconversion-based proliferation measurements show cell-intrinsic impact on *L. major* proliferation rates *in vivo*. (A) Immunofluorescence analysis of *Lm*^{SWITCH} infected C57BL/6 mouse ears after 48 h of photoconversion. Tissues were stained anti-CD54 to mark cell outlines, and red/green ratios of the individual parasites within the cells (i-v) were determined (graphs, each symbol represents one parasite segmented manually from at least 3 different Z slices of the stack shown on the left). Scale bar, 5 µm. Values represented as 1 – red/green fluorescence ratio. **(B)** Quantification of single parasite red/green ratios (one symbol per parasite) infecting individual cells (one cell is represented in each column), ordered according to the mean red/green fluorescence ratio of parasites in the respective column. (Upper panel) Parasites grouped according to their actual localization in cells. (Lower panel) Scrambled control, individual parasites assigned randomly to the same number of cells. Red symbols, 80% of the parasite within the cell exhibit a red/green ratio above the overall mean (weakly proliferating), green symbols, 80% of the parasite within the cell exhibit a red/green ratio below the overall mean (strongly proliferating). The overall mean is represented by a dotted line. Values represented as 1 – red/green fluorescence ratio. **(C)** (Left panel) Number of *Lm*^{SWITCH} which are mainly

red within a single cell plotted against the number of mainly green *Lm*^{SWITCH} within the same cell. (Right panel) Scrambled control as described in (C). Each symbol represents one infected cell analyzed. **(D)** Intravital 2-photon microscopy analysis of *Lm*^{SWITCH} infected C57BL/6 mouse ears 48 h after photoconversion. Solid boxes, groups of more than 5 parasite-sized signals localized closely enough to be in the same host cell, dotted boxes, individual (less than 3) parasites. Scale bars, 50 µm (large image), 3 µm (insets). **(E-F)** Analysis of mKikumeGR red/green ratio of *Lm*^{SWITCH} within individual parasite clusters as described in (B-C). Examples representative of >5 animals imaged.

2.1.4 Establishing analysis of *Lm*^{SWITCH} infected tissues by flow cytometry

For an efficient and comprehensive analysis of parasite proliferation *in vivo* with the mKikumeGR reporter system the usage of flow cytometry would be of great advantage. Therewith, different surface molecules and intracellular molecules of cells, which are important during *L. major* infection, should be stained via fluorescence labelled antibodies. Thereby their role in relation to high or low *Leishmania* proliferation should be investigated. The application of flow cytometry and the following analysis of collected data was established with *Lm*^{SWITCH} infected ear tissues within this project. One of the greatest obstacles to overcome by flow cytometric analysis of ear tissues is the huge autofluorescence of ear tissue coming up in the red fluorescence channels, thus partially overlapping with red fluorescence of mKikumeGR. Therefore, a strategy to distinguish between tissue autofluorescence and red mKikumeGR fluorescence was developed. As a result, red mKikumeGR fluorescence was read out with 561 nm excitation and 610/20 nm emission; green mKikumeGR fluorescence was read out with 488 nm excitation and 530/30 nm emission. To gate on *Lm*^{SWITCH} infected cells, an autofluorescence channel with 488 excitation and 695/40 nm emission was plotted against a combined channel of red and green mKikumeGR fluorescence (Figure 10 A). Prior to this, infected ears were harvested, enzymatically digested, and stained with fluorescence labelled antibodies against the surface marker CD45 for the identification of leukocytes. In Figure 10 results of a flow cytometry analysis are displayed. After gating for CD45^{+} cells, *Lm*^{SWITCH}-infected cells were gated out by comparing them with a sample infected with a non-fluorescent wt *L. major* strain (*L.m. wt*) (Figure 10 A, lower row, left). Figure 10 B shows that photoconversion as well as recovery from photoconversion within the infected ear is clearly detectable by flow cytometry. After calculating the red-to-green ratios of the parasites, non-photoconverted populations (green population) are apparently distinguishable from completely photoconverted populations (red population) 0 h after photoconversion. The red-to-green ratio of *Leishmania* populations 48 h after photoconversion show an intermediate population displaying some cells which are containing parasites that have already completely recovered their green fluorescence, whereas other cells harbor parasites that still fully show red

fluorescence, while some leukocytes are infected by parasites that have partially recovered their green fluorescence showing an intermediate state (yellow population).

2.2 Defining the niche of high and low proliferating *L. major*

2.2.1 CD11c defines a phagocyte subset harboring highly proliferative *L. major*

Monocyte-derived macrophages and DCs as well as neutrophils constitute the main infected cell types in an ongoing *L. major* infection [104,33,44]. However, it is not known whether any of these cell types preferentially harbors parasites of a distinct proliferation rate [72]. The fact that the mKikumeGR-based proliferation reporter is compatible with immunofluorescence staining allowed the characterization of the cellular niche of proliferating *L. major* via flow cytometry. For this, C57BL/6 mice were infected intradermally in the ear with *Lm*^{SWITCH}. After three weeks, the sites of infection were photoconverted, and ears were harvested 48 h after photoconversion for tissue homogenization and flow cytometry analysis of *Lm*^{SWITCH} proliferation in infected cells. The isolated cells were stained anti-CD45 to identify leukocytes, as well as CD11c and F4/80 to characterize the infected cell subsets (Figure 10). In order to represent proliferation as a normalized value, a proliferation index, which includes a negative term of the mKikumeGR red-to-green ratio, was calculated. Strikingly, *L. major* proliferation was significantly higher in CD11c$^+$F4/80$^+$ and CD11c$^+$F4/80$^-$ cells than in all CD11c-negative cell populations (Figure 10 C-D). To exclude a possible spectral overlap of the antibody staining as an explanation for the different proliferation rates observed in the distinct cell populations, a scrambled control with arbitrary photoconversion right before proliferation measurement was analyzed. To this end, *Lm*^{SWITCH} in the ear were photoconverted at random by using a grid (Figure 11). In these controls, host cell CD11c expression and pathogen proliferation index were no longer correlated (Figure 11 B). Thus, a possible spectral overlap between marker staining and mKikumeGR red and green fluorescence readout was not responsible for the enrichment in parasites exhibiting a high proliferation signal observed in CD11c$^+$ cells (Figure 10 C-D). Taken together, these experiments suggest that CD11c$^+$ cells represent a cellular niche for rapidly proliferating *L. major* at the site of infection.

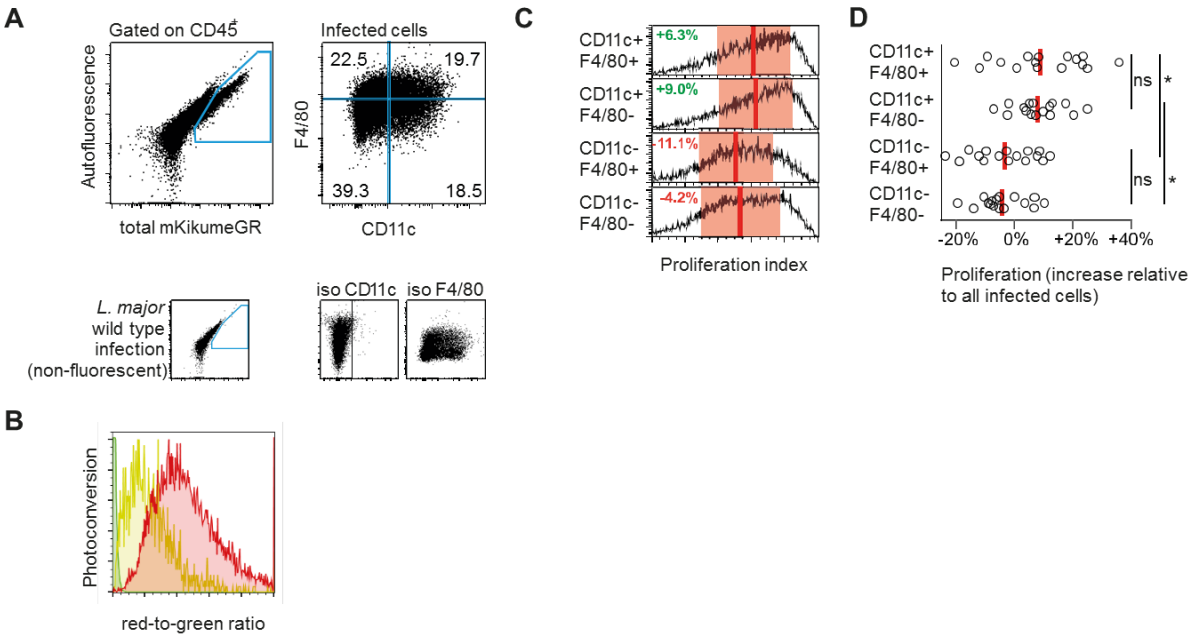

Figure 10: CD11c defines a phagocyte subset harboring highly proliferative *L. major*. (A) C57BL/6 mice ears were infected intradermally with *Lm*^{SWITCH}. 3 weeks post infection, parasites in the mouse ear were photoconverted and 48 h later ears were harvested for flow cytometry analysis of intracellular *L. major* proliferation (upper row). Controls infected with non-fluorescent *L. major* wt parasites were used to define the infected cells by gating on a combined mKikumeGR red and green signal (total mKikumeGR). Isotype controls (iso) were used to define the gating strategy for F4/80 versus CD11c (lower row, small plots). **(B)** Verification of efficiency of flow cytometry analysis for *Lm*^{SWITCH} infected mouse ears. Therein red-to-green ratio of non-photoconverted (green) parasites is compared to 0 h photoconverted parasites (red) and 48 h photoconverted parasites (yellow). **(C)** Relative proliferation rates of *Lm*^{SWITCH} located in the different cell compartments defined by F4/80 and CD11c staining. Data shown are from one sample each, normalized to the overall mean proliferation index within the sample. Vertical bars denote the mean and shaded red boxes the standard deviation. **(D)** Quantitative analysis of the proliferative states of *Lm*^{SWITCH} within the different cell populations. Each dot represents one mouse ear. Relative proliferation indices were obtained by normalization of the subpopulation's proliferation index to the overall mean proliferation index within each sample. Vertical bars represent the mean. *p < 0.05; ns, not significant. Data pooled from three independent experiments.

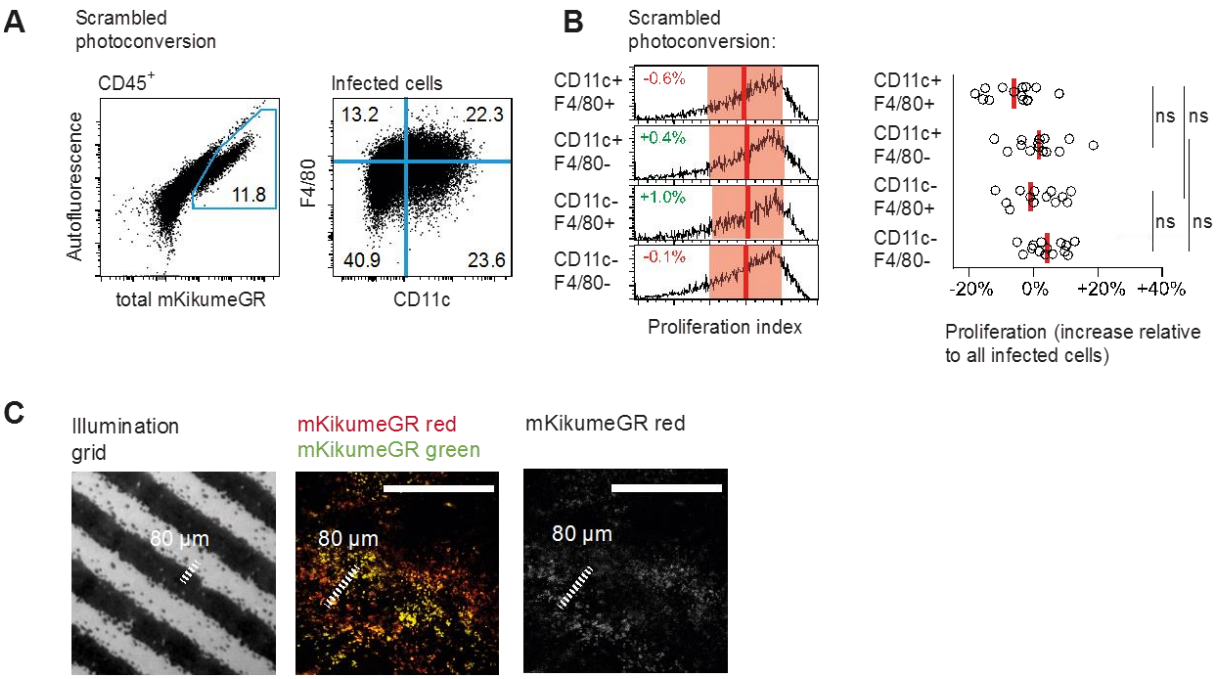

Figure 11: Random photoconversion of *Lm*^{SWITCH} using an illumination grid. (A) C57BL/6 mice ears were infected intradermally with *Lm*^{SWITCH}. 3 weeks post infection, parasites in the mouse ear were photoconverted and 48 h later ears were harvested for flow cytometry analysis of intracellular *L. major* proliferation. To exclude spectral overlap of the antibody staining with the observed results, experiments were performed in which parasites were photoconverted randomly immediately before analysis, thus the red or green fluorescence was independent of the proliferative state. **(B)** (Left panel) Relative proliferation rates of *Lm*^{SWITCH} located in the different cell compartments defined by F4/80 and CD11 staining. Data shown are from one sample each, normalized to the overall mean proliferation index within the sample. Vertical bars denote the mean and shaded red boxes the standard deviation. (Right panel) Quantitative analysis of the proliferative states of *Lm*^{SWITCH} within the different cell populations. Each dot represents one mouse ear. Relative proliferation indices were obtained by normalization of the subpopulation's proliferation index to the overall mean proliferation index within each sample. Vertical bars represent the mean. *$p < 0.05$; ns, not significant. **(C)** (Left panel) Illumination grid (transmitted light image). (Middle panel) Intravital 2-photon microscopy of a scramble-photoconverted *Lm*^{SWITCH}-infected site in the ear, an image aligned to the grid showing photoconverted 80 µm spanning (dotted lines), parasite regions are shown. (Right image) mKikumeGR red channel only. A Z-projection of a 40 µm stack is shown in the middle and lower panel. Scale bars, 200 µm. Data pooled from three independent experiments.

Based on these results, the effect of a temporary lack of CD11c cells, using a DTR-depletion model [119], was investigated. To this end, CD11c-DTR-GFP mice were infected with *L. major* for 21 days. 48 h prior to analysis CD11c$^+$ cells were depleted via the injection of diphtheria toxin (DTX) and parasite burden was analyzed by preparation of limiting dilutions (Figure 12 A). In DTX injected mice, most of the CD11c-GFP cells were successfully depleted (Figure 12 B), which was shown by comparing non-DTX treated CD11c-DTR-GFP with depleted mice.

Limiting dilution analysis of pathogen burden indicated that parasite numbers are significantly reduced in CD11c depleted mice (Figure 12 C). These results confirm the previous findings of CD11c$^+$ cells representing the main niche for parasite proliferation.

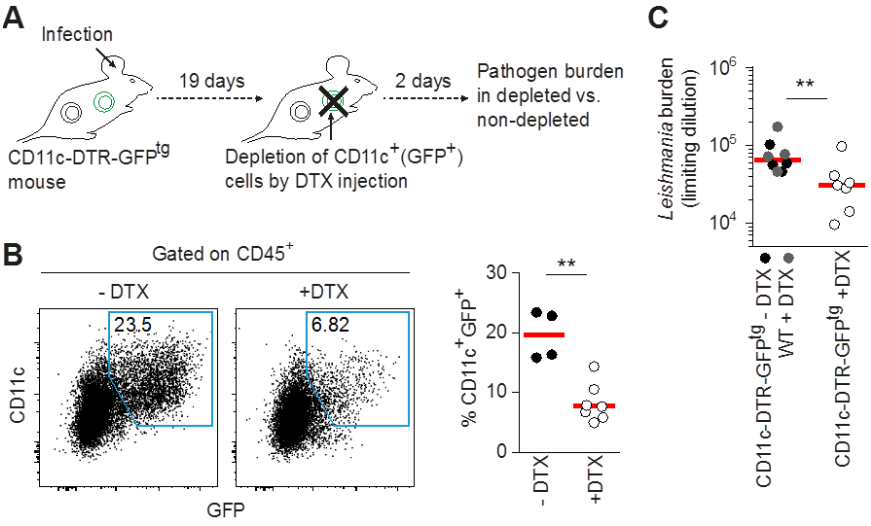

Figure 12: Parasite burden is decreased in CD11c depleted CD11c-DTR-GFP mice. (A) CD11c-DTR-GFP mice were infected with *L. major* for 21 days. 2 days prior to analysis CD11c$^+$ cells were depleted via the injection of diphtheria toxin (DTX). **(B)** Successful depletion of the majority of CD11c-GFP cells in mice which were treated with DTX. **(C)** Result of analysis of pathogen burden by limiting dilution. Non-DTX treated CD11c-DTR-GFP mice and DTX treated wt mice were compared with depleted mice. Horizontal bars represent the mean. **p < 0.01; *p < 0.05.

2.2.2 CD11c$^+$ cells are a main cellular niche of high *L. major* proliferation, irrespective of the expression of activation markers

Monocytes, monocyte derived DCs and macrophages have been described to represent important cell types to be recruited to and residing at the site of the established *Leishmania* infection [33,77,104]. Therefore, monocyte activation markers CD86 and class II MHC were included in addition to CD11c and F4/80 in the analysis in order to characterize the cellular niche of high *L. major* proliferation in more detail. However, for ratiometric analysis of mKikumeGR recovery after photoconversion by flow cytometry, only a limited set of additional fluorophores with both excitation (ex) and emission (em) spectra different from the two forms of mKikumeGR (green, ex/em 488 nm/515 nm and red, ex/em 561 nm/590 nm) can be used in flow cytometry. Therefore, Multi-Epitope Ligand Cartography (MELC), a multiparameter microscopy approach based on consecutive immunofluorescence staining/bleaching cycles, was employed [120]. In brief, fixed cryosections of infected ear tissue were imaged to detect both red and green mKikumeGR in *L. major*, photobleached, and in subsequent individual automated immunofluorescence staining/bleaching cycles, probed for expression of CD45, CD54, CD11b, CD11c, F4/80, CD86, class II MHC, CD45R, and finally stained with propidium

iodide at the same site. With each cycle, a transmitted light image was recorded to which the fluorescence images were aligned. Cell outlines were automatically defined from the CD45, CD11b, and CD54 images, and mean cell body and outline fluorescence values were normalized and converted into cytometry data [118] (Figure 13 A+B, Figure 14 A). For this, image stacks of CD11b, CD45 and CD54 stainings were deconvolved and aligned before they were used separately as membrane input. The corresponding propidium iodide staining served as seed input for the Real-time Accurate Cell-shape Extractor (RACE) program developed by Stegmaier et al. [121] (Figure 13A). Optimization of RACE conditions was performed to detect the largest number of cells and highest percentage of infected cells (see chapter 4.1.3). Regions of interest (ROIs) were generated from the resulting image stacks. To measure the mKikumeGR fluorescence the cellular ROIs were used (Figure 13 B, upper image). Rim masks generated from the ROIs were used for surface marker measurements (Figure 13 B, middle). The mean fluorescence of the cellular and rim ROIs was extracted for each cell and fluorescence channel. To define fluorescence thresholds for gating within the FlowJo software, 30 marker-positive and 30 marker-negative cells were selected from images of three different sites of infection and a cutoff was defined (i.e. no marker-negative cells in the positive gate). Manually selected cells from three different experiments served to define a threshold for CD11c, F4/80, CD86, class II MHC as markers for in-depth characterization of infected phagocytes [33], and CD45R as a marker unrelated to the different monocyte subsets (Figure 13 C).

To detect cells which contained *L. major*, combined red and green mKikumeGR fluorescence (total mKikumeGR) in infected and non-infected cells, manually selected from the propidium iodide DNA staining, were analyzed. This allowed for determination of a total mKikumeGR threshold applicable to images acquired in different experiments and different tissue depths (Figure 14 B-E). Thus, the localization of *Lm*^{SWITCH} in the infected tissue could be reliably and automatically determined in conjunction with multiplex analysis of the parasite's host cell.

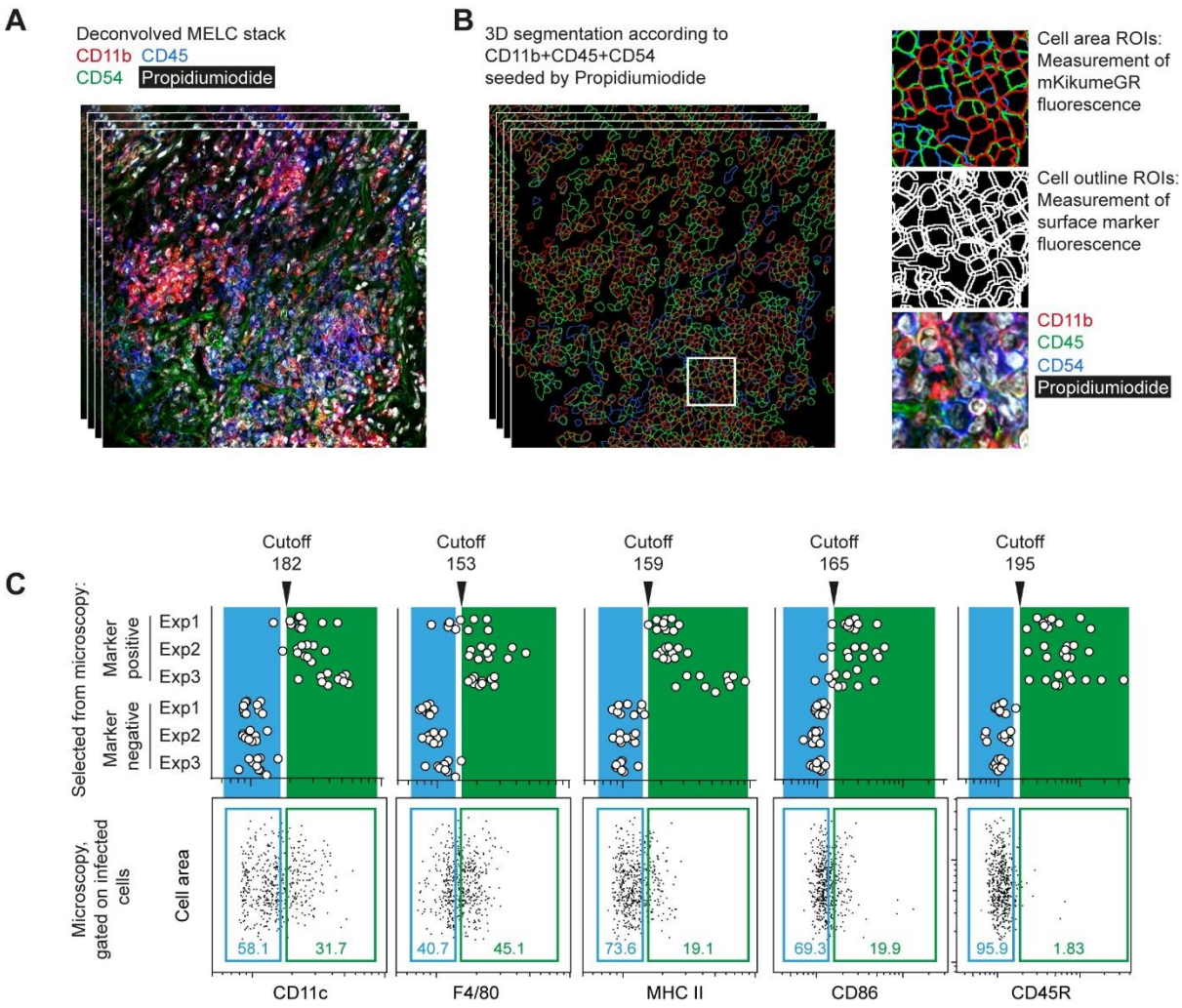

Figure 13: Establishing Multi-Epitope Ligand Cartography (MELC) to analyze the tissue niche of *L. major* referred to the proliferative state of the parasites. (A) Deconvolved and aligned image stacks of CD11b, CD45 and CD54 stainings were used separately as membrane input, the corresponding propidium iodide staining served as seed input for the Real-time Accurate Cell-shape Extractor (RACE) program. **(B)** From the resulting image stacks, regions of interest (ROIs) were generated. The cellular ROIs were used for mKikumeGR fluorescence measurement. Rim masks generated from the ROIs were used for surface marker measurements. The mean fluorescence of the cellular and rim ROIs were extracted for each cell and fluorescence channel. **(C)** (Upper panels) For defining fluorescence thresholds for gating within FlowJo, 30 marker-positive and 30 marker-negative cells were selected from images of three different sites of infection and a cutoff was defined (i.e. no marker-negative cells in the positive gate). (Lower panels) Examples of MELC datasets gated for marker-positive (green) and marker-negative (blue) infected cells.

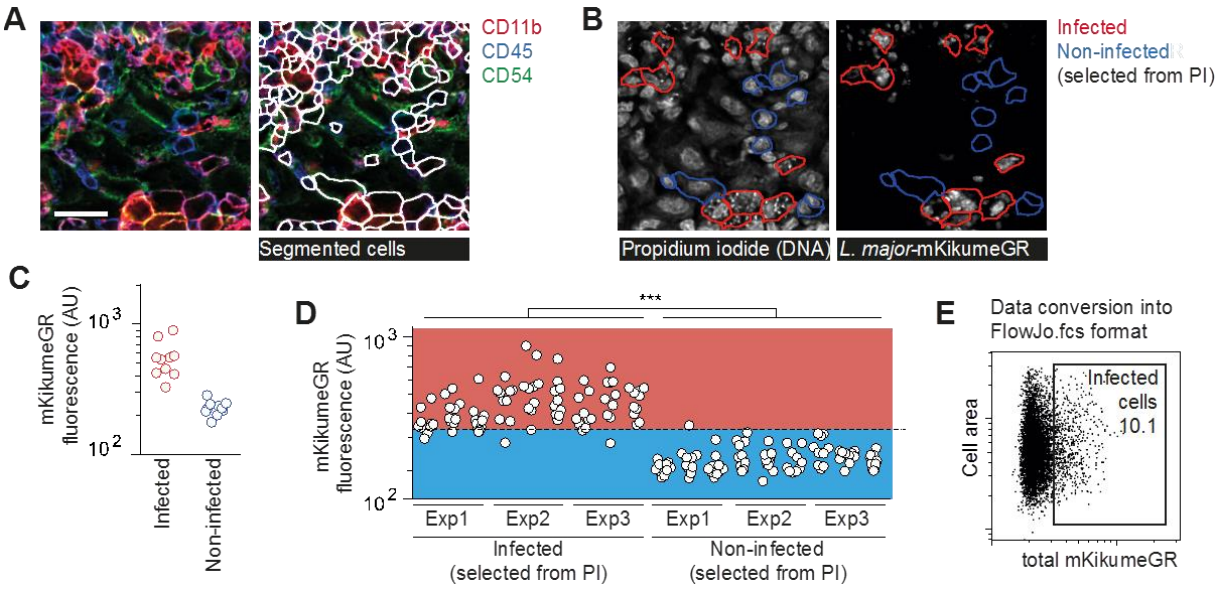

Figure 14: Detecting *L. major* containing cells during application of MELC. *Lm*^{SWITCH}-infected ears were photoconverted 3 weeks post infection and analyzed 48 h later via MELC. **(A)** Automated cell segmentation using the RACE software [121] based on CD45, CD54 and CD11b signals. Scale bar, 20 µm. **(B-C)** Examples (B) and quantification (C) of infected cells (red outlines and symbols) and non-infected cells (blue outlines and symbols) identified manually by propidium iodide staining of the small parasite nuclei. **(D)** Definition of a threshold based on the total mKikumeGR signal from infected and non-infected cells manually identified from three Z-planes in three independent experiments (each symbol represents one cell). **(E)** Conversion to FlowJo.fcs format allowed for gating on infected cells according to the threshold defined in (D).

Subsequently, a positive and a negative population of infected cells was defined for each marker (Figure 15 A, top row), and *L. major* proliferation rates were compared between the respective marker-positive and -negative populations (Figure 15 A, bottom row). Confirming the flow cytometry data, it was observed that infected cells that were positive for the DC marker CD11c^{+} were enriched in high proliferating pathogens, whereas all other markers tested were not per se specific for a distinct pathogen proliferation rate (Figure 15 B). In order to find differences in pathogen proliferation within subsets of CD11c-positive and negative phagocyte subsets, combined marker analysis was performed, in which *L. major* proliferation was assessed in subpopulations of cells differentially expressing CD11c or F4/80 in combination with class II MHC or CD86 (Figure 15 C). Importantly, also when analyzed in combination with CD11c expression, F4/80, class II MHC and CD86 expression were not characteristic of a distinct pathogen proliferation rate (Figure 15 C-D, i-iii). Likewise, analysis of F4/80-positive and negative subpopulations regarding class II MHC and CD86 expression revealed no significant change of pathogen proliferation in any subset analyzed (Figure 15 C-D, iv, v). Thus, among the infected cells in the skin, CD11c^{+} cells, irrespective of their activation state, preferentially harbored high proliferating *L. major*. In contrast, CD11c^{-} cells possibly

representing non-differentiated monocytes, macrophages and neutrophils were less permissive for efficient *L. major* proliferation.

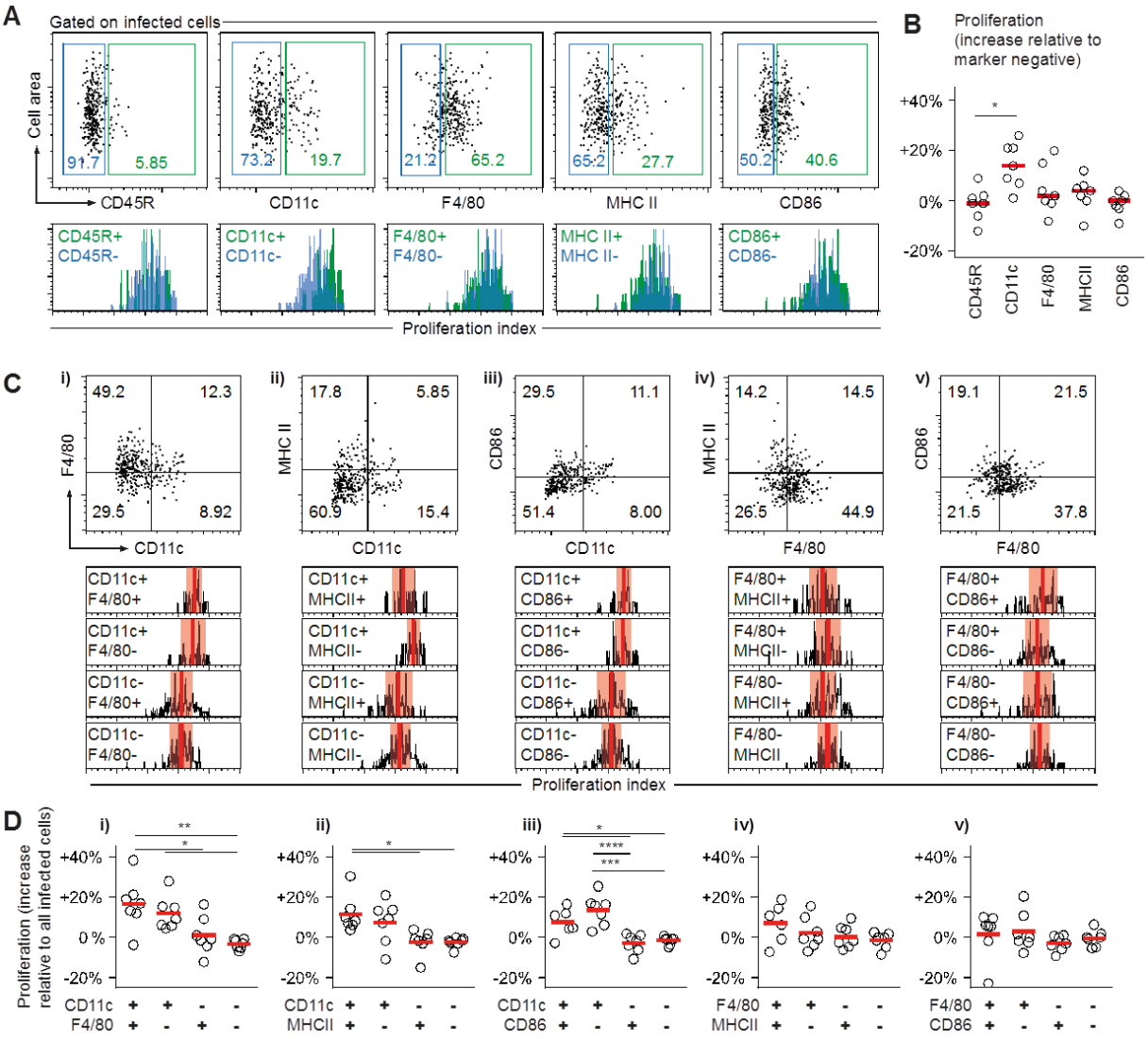

Figure 15: Multiparameter microscopy identifies CD11c⁺ cells as the main pool for high *L. major* proliferation irrespective of CD86, F4/80 and class II MHC expression. (A) (Top row) Marker positive (green gate) and marker negative (blue gate) cells were defined for each surface marker. (Bottom row) Proliferation rates of *Lm*^{SWITCH} in cell populations positive for CD45R, CD11c, F4/80, CD86 or class II MHC (green histograms) were compared with the corresponding marker-negative cell populations (blue histograms). Each plot is a representative example of 7 individual MELC experiments performed. **(B)** Quantification of 7 individual MELC experiments performed in 4 different infected mice. Each symbol represents one infection site, *p < 0.05. **(C)** (Top row) Infected cells subdivided according to CD11c versus F4/80, MHC II or CD86 expression (i, ii, iii) and F4/80 versus MHC II and CD86 (iv, v). (Bottom row) Relative proliferation rates of *Lm*^{SWITCH} in the respective subpopulations. Vertical bars denote the mean; shaded red boxes, standard deviation. **(D)** Quantification of MELC experiments according to the populations defined in (H), i though v. Each dot represents one individual MELC experiment. Relative proliferation rates were obtained by normalization of the subpopulation's proliferation indices to the

overall mean proliferation index within each sample. Horizontal bars represent the mean. ***p < 0.001; **p < 0.01; *p < 0.05.

2.2.3 Characterization of monocyte niches for high and low proliferating *L. major*

To further characterize the previously described populations of cells harboring high or low proliferating *Leishmania*, cells were analyzed again by flow cytometry using antibodies that are so far not compatible with MELC. According to the cell characterizations by Leon et al. [33] and Romano et al. [77] antibody staining against the monocyte markers CD11b, Ly6C, CCR2, as well as class II MHC was included in the analysis in order to better define the activation and maturation state of recruited monocyte-derived cells by flow cytometry. Due the limited set of fluorophores that can be used additionally to the mKikumeGR proliferation reporter, these experiments were performed with the red fluorescent *Leishmania* strain *L.m. dsRed*. When gating on $CD45^+$ cells showing high or low expression of CD11b, it became obvious that the majority of infected host cells is $CD11b^+$ (Figure 16 A). Infected $CD11b^+$ cells were further divided in the previously defined populations $CD11c^+F4/80^+$ and $CD11c^+F4/80^-$ (which have been defined as cells harboring high proliferating parasites within this study) and $CD11c^-F4/80^+$ and $CD11c^-F4/80^-$ (representing the niche for low proliferating *L. major*). These four subpopulations were further analyzed for the expression of CCR2, Ly6C and class II MHC. It was observed that Ly6C and class II MHC expression was highest in $CD11c^+F4/80^+$ populations, whereas CCR2 expression was high in both the $CD11c^+F4/80^+$ and the $CD11c^-F4/80^+$ population, but significantly lower in the $CD11c^+F4/80^-$ and $CD11c^-F4/80^-$ populations, indicating that the $CD11c^+F4/80^+$ double positive population contains the highest proportion of activated inflammatory monocytes [77].

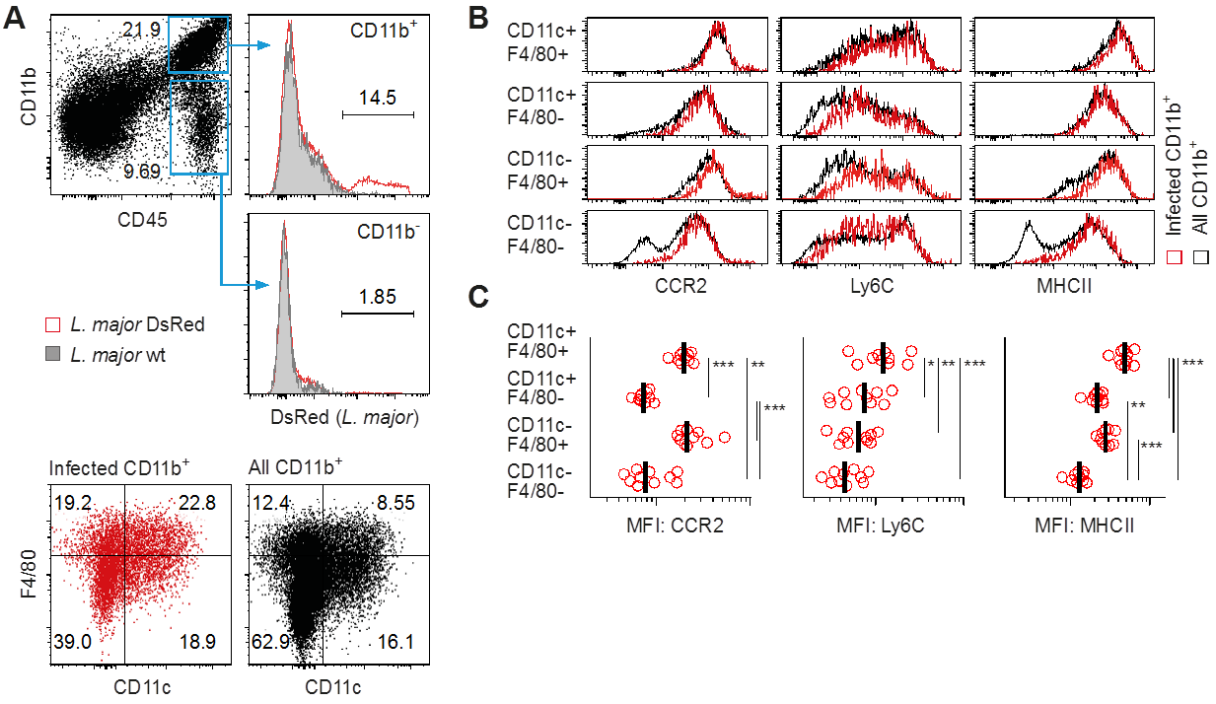

Figure 16: Characterization of cellular niches for high and low proliferating *L. major* concerning the expression of CCR2, Ly6C and class II MHC by flow cytometry. (A) C57BL/6 mice ears were infected intradermally with *L.m. dsRed*. 3 weeks post infection, ears were harvested for flow cytometry analysis. It was gated on $CD45^+$ and $CD11b^+$ (upper panel). Afterwards the four subpopulations $CD11c^+F4/80^+$, $CD11c^+F4/80^-$, $CD11c^-F4/80^+$ and $CD11c^-F4/80^-$ upon non-infected and infected cells were defined (lower panel). **(B-C)** These four subpopulations were further analyzed for the expression of CCR2, Ly6C and class II MHC. Mean fluorescence intensities are plotted. ***p < 0.001; **p < 0.01; *p < 0.05. Vertical bars denote the mean.

Since Ly6C is a very important marker for monocytes and monocyte derived cells, *L. major* proliferation related to the expression of Ly6C and CD11c was additionally analyzed by flow cytometry. To this end, the isolated cells from infected mouse ears were stained anti-CD45 to identify leukocytes, as well as CD11c and Ly6C to subdivide the infected cells into $CD11c^+Ly6C^+$, $CD11c^+Ly6C^-$, $CD11c^-Ly6C^+$, and $CD11c^-Ly6C^-$ subpopulations (Figure 17). It was observed that *L. major* proliferation was significantly higher in $CD11c^+Ly6C^+$ cells than in $CD11c^+Ly6C^-$, $CD11c^-Ly6C^-$ populations (Figure 17 B and C). Surprisingly, a high proliferation rate for *L. major* was detected in the $CD11c^-Ly6C^+$ subpopulation as well. When investigating the percentages of infected cells among the different subpopulations it became obvious that $CD11c^+Ly6C^+$ cells are strongly overrepresented among infected cells, and only a minority of infected cells was $CD11c^-Ly6C^+$ as compared to the total fraction of these cells at the site of infection (Figure 17 D). Therefore, it is comprehensive why this subpopulation was not detected in prior analysis described above (Figure 10 and Figure 15). Thus, it is conceivable that $CD11c^+Ly6C^+$ cells represent the main cellular niche for *L. major* proliferation.

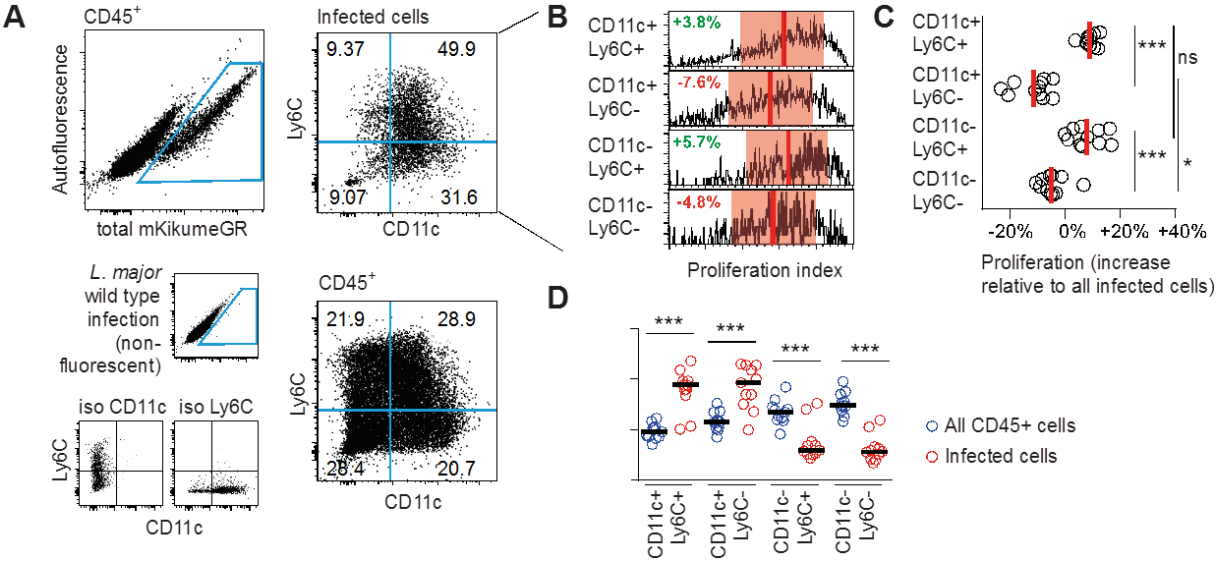

Figure 17*: L. major* proliferation in relation to the expression of Ly6C and CD11c of the host cells. **(A)** C57BL/6 mice ears were infected intradermally with *Lm*^{SWITCH}. 3 weeks post infection, parasites in the mouse ear were photoconverted and 48 h later ears were harvested for flow cytometry analysis of intracellular *L. major* proliferation (upper row). Controls infected with non-fluorescent *L. major* wt parasites were used to define the infected cells by gating on a combined mKikumeGR red and green signal (total mKikumeGR), isotype controls (iso) were used to define the gating strategy for Ly6C versus CD11c (lower row, small plots). **(B)** Relative proliferation rates of *Lm*^{SWITCH} located in the different cell compartments defined by Ly6C and CD11c staining. The shown data are each from one sample, normalized to the overall mean proliferation index within the sample. Vertical bars denote the mean and shaded red boxes the standard deviation. **(C)** Quantitative analysis of the proliferative states of *Lm*^{SWITCH} within the different cell populations. Each dot represents one mouse ear. Relative proliferation indices were obtained by normalization of the subpopulation's proliferation index to the overall mean proliferation index within each sample. Vertical bars represent the mean. **(D)** Comparison of CD11c and Ly6C expression in total and infected CD11b populations at the site of infection. Each dot represents a mouse ear. Horizontal bars represent the mean. ***p < 0.001; *p < 0.05. Data pooled from three independent experiments.

2.2.4 Newly infected host cells predominantly harbor high proliferating *L. major*

Using confocal microscopy, a slight but significantly negative correlation between *L. major* proliferation rates within individual cells and the respective cellular parasite burden was observed. This suggested that high proliferating parasites were present at lower numbers per infected cell than low proliferating parasites (Figure 18 A and B). One explanation for this could be that high proliferating *L. major* are more efficiently released from infected cells, and thus might represent the main parasite population infecting new host cells. In order to test whether newly infected cells preferentially harbor high proliferating pathogens, the arrival of newly

recruited cells was synchronized by adoptive bone marrow transfer [33,44]. For this, C57BL/6 mice (CD45.2$^+$) infected for 16 days with *Lm*^{SWITCH} were injected with 10^8 CD45.1$^+$ bone marrow cells. *Lm*^{SWITCH} infected ears were photoconverted in order to analyze pathogen proliferation five days after transfer. Thus, pathogen proliferation in infected newly recruited cells (CD45.1$^+$) could be compared to pathogen proliferation in CD45.2$^+$ cells, which are expected to be present in a steady state within the time frame observed (Figure 18 C). Of note, a shorter time frame for cell recruitment did not yield enough infected cells for proliferation analysis (Figure 19). Switched color experiments were performed to exclude an influence of the antibody staining on proliferation measurements (Figure 18 F-G). Strikingly, it was observed that pathogen proliferation in newly recruited CD45.1$^+$ cells was significantly higher than in CD45.2$^+$ cells present at the site of infection in the steady state. This suggests that high pathogen proliferation occurs in the context of the infection of new host cells (Figure 18 D-G).

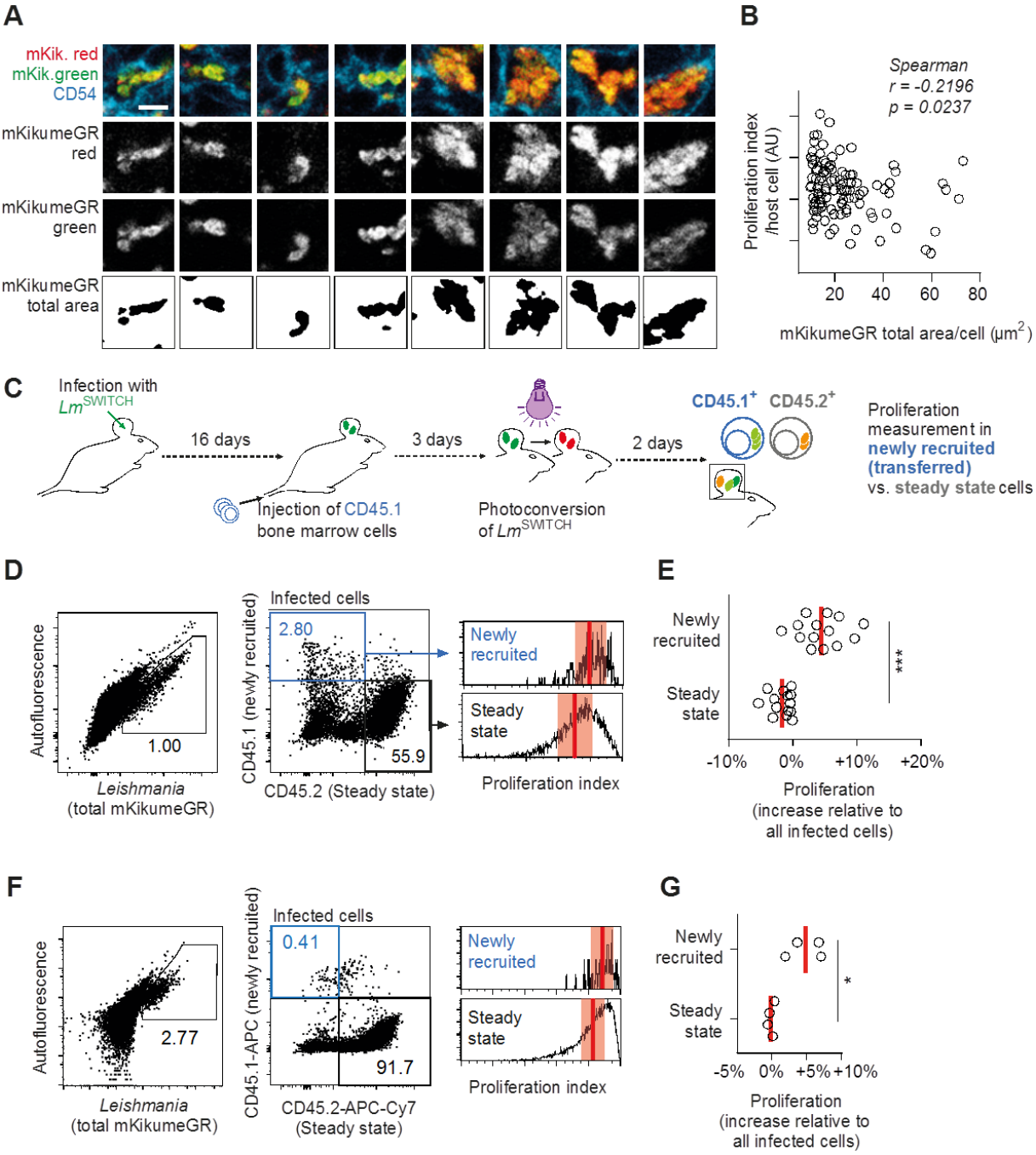

Figure 18: High *L. major* proliferation is correlated with the infection of new host cells. (A-B) *Lm*^{SWITCH} infected C57BL/6 mouse ears were photoconverted 3 weeks post infection and analyzed 48 h later by confocal immunofluorescence microscopy. Mean pathogen proliferation within individual cells was plotted against the total mKikumeGR-positive area per confocal section through the cells. Raw data reanalyzed from figure 9 A-C. Scale bar, 5 µm. **(C)** Experimental strategy to determine *L. major* proliferation in phagocytes newly recruited to the site of infection: C57BL/6 (CD45.2) mice infected with *Lm*^{SWITCH} were adoptively transferred with CD45.1 bone marrow cells 5 days prior to analysis. Photoconversion was performed 48 h prior to analysis and the relative proliferation rates of parasites in steady state (CD45.2$^+$ cells) and newly recruited (CD45.1$^+$ cells) cells were compared. **(D)** Gating strategy for detection of infected CD45.1$^+$ newly recruited and CD45.2$^+$ steady state infected cells isolated from the site of infection (left and middle panel). Proliferation rates of the infected newly recruited

and steady state population of one example site of infection are shown as histograms (right panel). Vertical bars denote the mean and shaded red boxes the standard deviation. **(E)** Quantitative analysis of *Lm*^{SWITCH} proliferation rates. Relative proliferation rates in newly recruited or steady state cells were obtained by normalization of the subpopulation's proliferation indices to the overall mean proliferation index within each sample. Each dot represents one mouse ear. Vertical bars denote the mean. ***p < 0.001. Data pooled from three independent experiments. **(F-G)** Antibody labels were switched for the anti-CD45.1 and anti-CD45.2 staining as compared to (D-E). **(F)** Gating strategy for detection of infected CD45.1$^+$ newly recruited and CD45.2$^+$ steady state infected cells isolated from the site of infection (left and middle panel). Proliferation rates of the infected newly recruited and steady state population of one example site of infection are shown as histogram (right panel). Vertical bars denote the mean and shaded red boxes the standard deviation. **(G)** Quantitative analysis of the proliferative state of *Lm*^{SWITCH} within the different cell types. Relative proliferation rates in newly recruited or steady state cells were obtained by normalization of the subpopulation's proliferation indices to the overall mean proliferation index within each sample. Each dot represents one mouse ear. Vertical bars denote the mean. *p < 0.05.

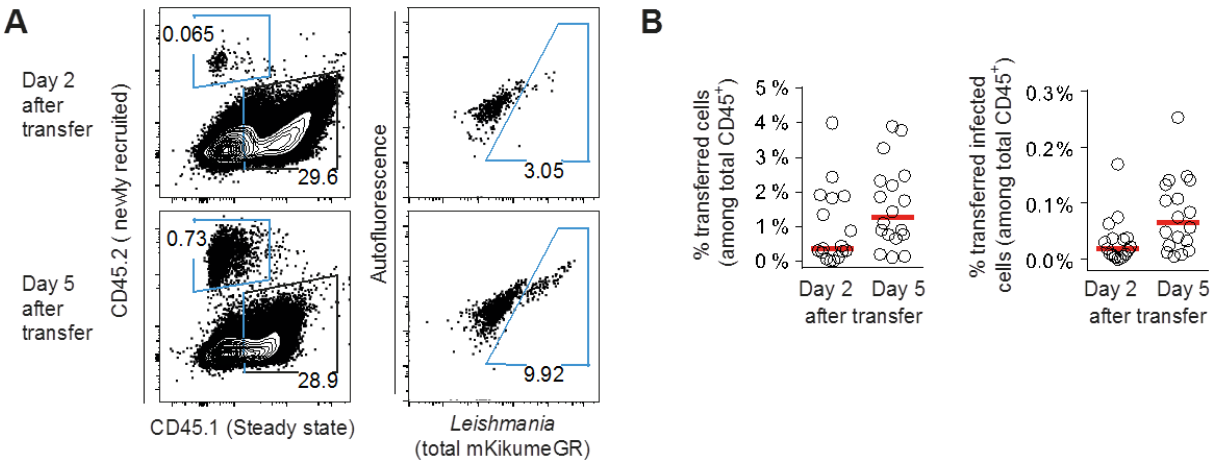

Figure 19: Comparison of infected cell numbers in newly recruited cells at day 2 and day 5 after adoptive transfer. Flow cytometry analysis of CD45.1 mice infected with *Lm*^{SWITCH}, adoptively transferred 2 or 5 days before analysis with C57BL/6 (CD45.2) bone marrow cells. **(A)** Gating strategy on CD45.2$^+$ (newly recruited) and CD45.1$^+$ (steady state) cells, infected and non-infected. **(B)** Quantification of newly recruited infected and non-infected cells at day 2 and day 5 post adoptive transfer. Each dot represents one mouse ear. Relative proliferation indices were obtained by normalization of the subpopulation's proliferation index to the overall mean proliferation index within each sample. Vertical bars represent the mean.

2.2.5 High proliferating *L. major* preferentially undergo cell-to-cell transmission

L. major has been shown to replicate once every 15 to 60 hours within host cells [72,73,108]. Thus, the high parasite proliferation observed in newly recruited host cells could be either due to the transmission of already rapidly proliferating parasites, or due to an increase of

proliferation upon infection of a new host cell. In order to determine *L. major* proliferation shortly after transmission to new host cells, *in vitro* phagocyte infections were employed. First, to visualize the spread of *L. major* to new host cells, time-lapse microscopy of infected macrophage cell cultures was performed. Strikingly, in all *de novo* infection events observed, fluorescent parasites were taken up directly from infected host cells (Figure 20 A). Specifically, in most cases, the original host cells exhibited signs of cell death (membrane blebbing) shortly before the parasites associated with them were taken up by a new phagocyte (Figure 20 B). Very often, the original host cell was eventually phagocytosed as well by the new host cell, however, transfer of the parasite preceded phagocytosis of the whole original host cell by several hours (Figure 20 C). Direct cell-to-cell transfer was also demonstrated *in vivo* via 2-photon microscopy. To this end, CD11c-YFP mice were infected with red fluorescent *L.m. dsRed*. 5 days prior to analysis, isolated bone marrow from constitutively CFP expressing mice was injected into the infected mice. Direct cell-to-cell transfer of parasites from yellow fluorescent $CD11c^+$ host cells to newly recruited CFP expressing phagocytes could be shown by intravital imaging (Figure 20 D). It was therefore concluded that the infection of new host cells mainly occurs via cell-to-cell transmission with no prolonged extracellular state of the released parasite. In order to quantitatively analyze pathogen proliferation shortly after infection of cells, the system was adapted for analyzing *de novo* infection for *in vitro* cell culture infections (see Figure 21). For this, *in vitro* differentiated $CD45.2^+$ bone marrow-derived macrophages and DC mixtures (BMMDC) were infected with serum-opsonized Lm^{SWITCH}. 24 h after infection, the parasites were photoconverted and 24 h later, $CD45.1^+$ BMMDC were added. Parasite proliferation rates were determined after 5 h of coculture by flow cytometry (Figure 21 A). Confocal microscopy of FACS-sorted newly infected $CD45.1^+$ cells revealed that the parasites were intracellular and not extracellularly adhering to the cells (Figure 21 B). Importantly, even at this very early time point after uptake into a new host cell, high proliferating parasites were significantly overrepresented in the newly infected $CD45.1^+$ phagocytes as compared to the initially infected $CD45.2^+$ cells (Figure 21 C and D, Figure 22 A-B). Control measurements, with photoconversion applied just before coculture, ensured that the recovery from photoconversion during the 5 h coculture phase was negligible (Figure 21 D, right). Furthermore, both $F4/80^+$, macrophage-like and $CD11c^+$, DC-like BM-derived cells were infected equally by high proliferating parasites, irrespective of iNOS production in the culture, probably due to the short infection times. Thus, the differences in *L. major* proliferation observed in the *in vitro* system are not attributable to the host cell type, but rather to the dissemination among phagocytes (Figure 22 C-E). In conclusion, these data suggest that high proliferating *L. major* preferentially undergo cell-to-cell transmission.

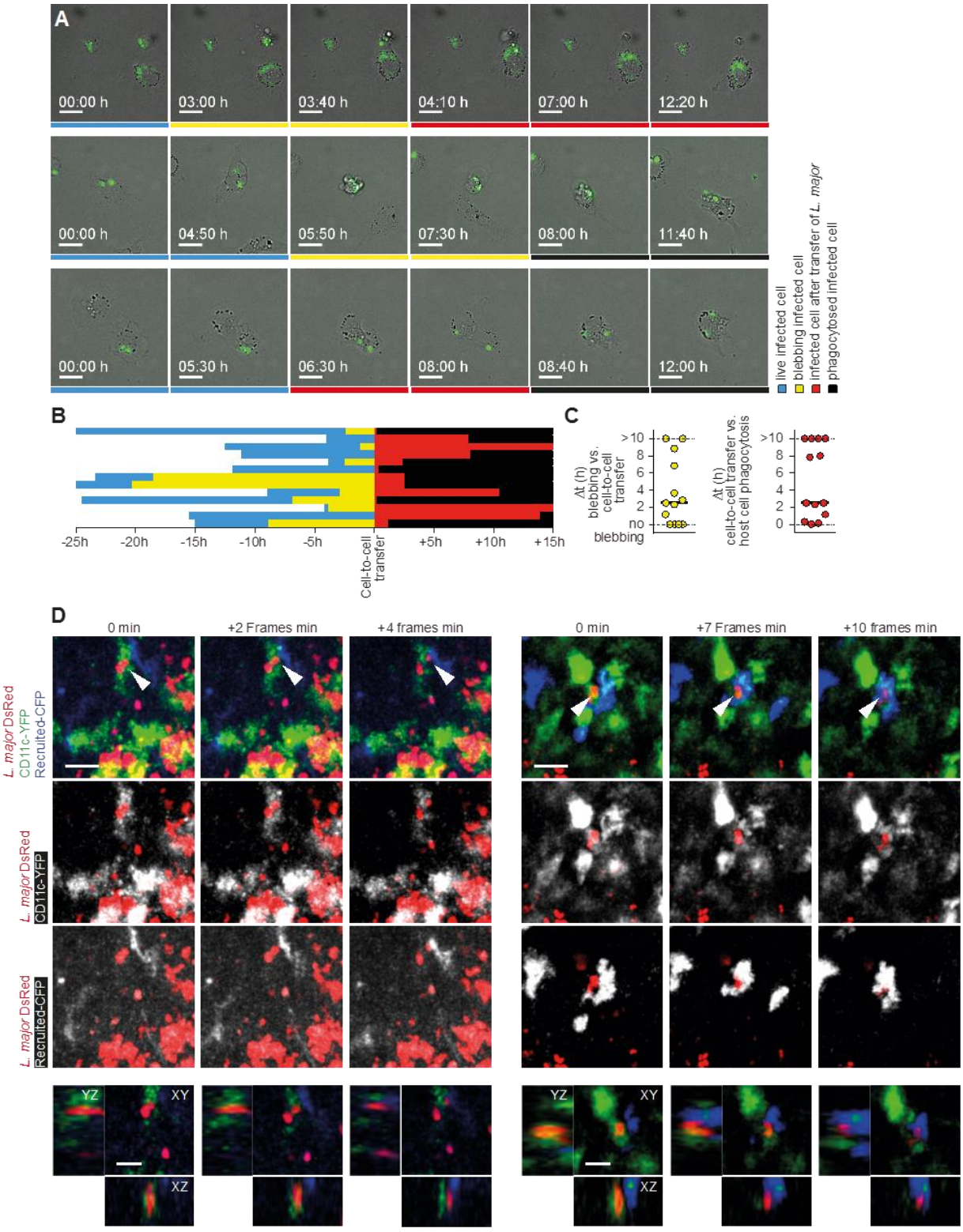

Figure 20: Cell-to-cell transfer of *L. major* among phagocytes *in vitro* and *in vivo*. Time lapse videomicroscopy of intraperitoneal macrophages infected for 24 h with fluorescently labelled *L. major*. **(A)** Three examples of cell-to-cell transfer between two phagocytes. Selected frames of the time series spaced 10 min are shown. Frames in which the originally infected cell is still alive and motile are marked blue, frames showing the original phagocyte with signs of cell death before transfer of the parasite are marked in yellow, after transfer in red. Complete phagocytosis of the original host cell is marked black.

Scale bar, 10 µm. **(B)** Analysis of the sequence of host cell death, parasite transfer and phagocytosis of the original host cell from 13 cell-to-cell transfer events analyzed, using the color code indicated in (A). **(C)** Quantification of the time between the first blebbing as a sign of cell death and cell to cell transfer (left) and the time between cell-to-cell transfer and complete phagocytosis of the original host cell. Horizontal bars denote the median. **(D)** Ears of CD11c-YFP mice were infected for 21 days with *L.m. dsRed*. 5 days prior to analysis isolated bone marrow cells from ubiquitous CFP mice were injected into the infected mice. Cell-to-cell transfer of *Leishmania* (red) from infected CD11c-YFP cells (green) to newly recruited CFP$^+$ cells (blue) was analyzed by intravital 2-photon microscopy in 3-dimensional time series.

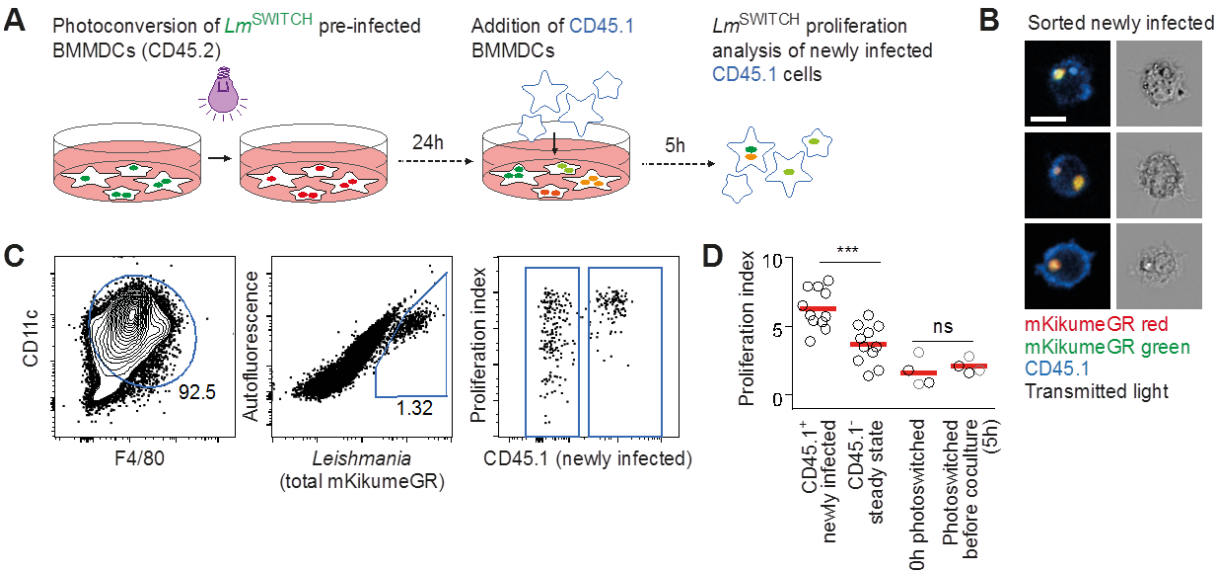

Figure 21: *De novo* infection of bone marrow macrophage and DC (BMMDC) mixtures by high-proliferating *L. major*. (A) Experimental setup for *in vitro* parasite dissemination analysis. **(B)** Confocal microscopy of sorted CD45.1$^+$ infected cells (newly infected) showing intracellular localization of fluorescent *L. major*. Images are representative of > 20 cells inspected microscopically. Scale bar, 10 µm. **(C)** Gating strategy to identify newly infected (CD45.1$^+$) and steady state (CD45.1$^-$) BMMDCs. **(D)** Quantification of proliferation rates in newly infected (CD45.1$^+$) and steady state (CD45.1$^-$) cells analyzed as shown in (A) (left), and controls photoconverted 0 h and 5 h before analysis to assess the recovery from photoconversion occurring in the 5 h of coculture (right) in newly infected (black symbols) and steady state (grey symbols) cells. Each symbol shows one individual experimental replicate. Data were pooled from three independent experiments. Horizontal bars denote the mean. ***p < 0.001; ns, not significant.

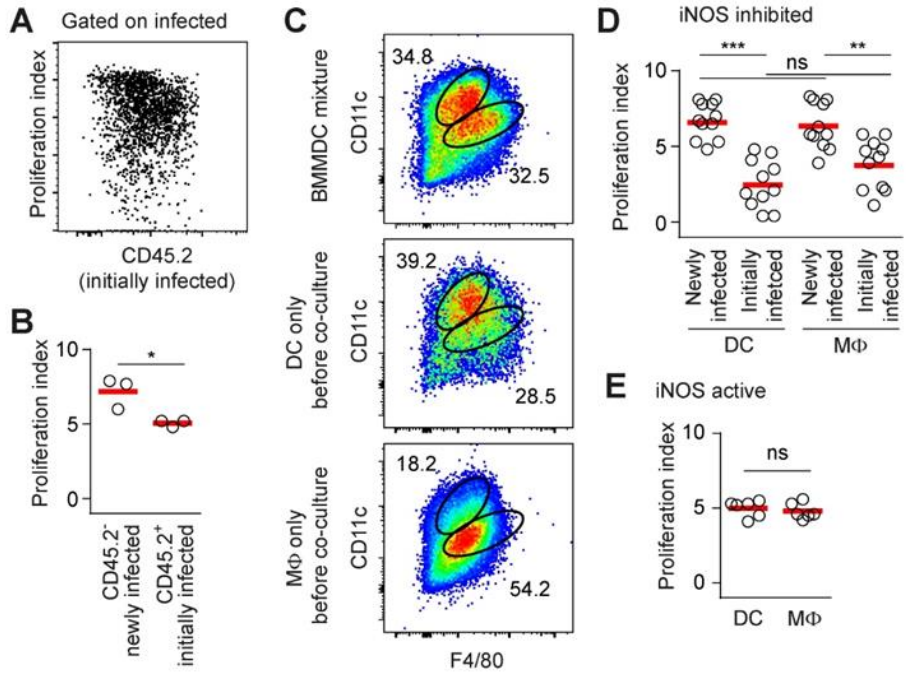

Figure 22: Color-switch control for *L. major* proliferation analysis in newly infected cells and characterization of BMMDCs *in vitro*. (A) Identification of newly infected ($CD45.2^-$) and initially infected ($CD45.2^+$) BMMDCs by flow cytometry. **(B)** Quantification of proliferation rates in newly infected and initially infected cells. *p < 0.05. **(C)** Characterization of CD11c and F4/80 expression in the total BMMDC coculture (upper panel), and DC (middle panel) and macrophage (MΦ, lower panel) single culture. **(D)** Analysis of parasite proliferation in newly infected and initially infected cells under inhibition of the nitric oxide synthase iNOS by L-NIL. **(E)** Analysis of parasite proliferation in initially infected cells without inhibition of iNOS. ***p < 0.001; **p < 0.01; *p < 0.05; ns, not significant.

2.2.6 *L. major* infects newly recruited monocytes at various differentiation stages

In order to investigate whether distinct subpopulations of newly recruited host phagocytes were preferentially infected upon arrival at the site of infection, CD11c and F4/80 expression on infected and non-infected newly recruited cells ($CD45.1^+$) and cells present at the infection site in a steady state ($CD45.2^+$) was compared (Figure 23 A-C). As expected from published work [44], the composition of the newly recruited phagocyte subsets changed substantially between day 2 and 5 after adoptive transfer. Specifically, population numbers of $CD11c^+F4/80^+$ double positive as well as $CD11c^+F4/80^-$ cells were increased significantly by day 5 as compared to day 2. Strikingly, among newly recruited cells, no differences in the composition of infected versus non-infected cells were observed (Figure 23 B). This suggests that the parasite has no preference for a specific cell type when infecting new host cells. In contrast, in the steady state cell population, more $CD11c^+F4/80^+$ double positive and less $CD11c^-F4/80^+$ single positive phagocytes were present in the infected cell population as compared to the non-infected cells

(Figure 23 C). Thus, in line with the proliferation reporter data (see Figure 10 and Figure 15), $CD11c^+F4/80^+$ phagocytes seem to represent a more suitable niche for *L. major* than $CD11c^-F4/80^+$ cells in the long-term perspective.

It has been shown that monocytes mature at the site of infection after recruitment from the bloodstream [77][33]. The late occurrence of $CD11c^+F4/80^+$ double positive cells (Figure 23 B) prompted the analysis of how long a recruited monocyte-derived cell would need to mature at the site of infection. In order to address this question, C57BL/6 mice were infected with non-fluorescent *L.m. wt* for 3 weeks and mKikumeGR-expressing bone marrow cells were adoptively transferred. 3 days after transfer, all mKikumeGR-expressing transferred cells, that had already been recruited to the ear, were marked by photoconversion. Analysis of infected tissue at 5 days after transfer would also yield non-photoconverted mKikumeGR-expressing cells, which consequently must have been recruited between day 3 and 5 (Figure 23 D and E). Therefore, it was possible to compare the surface marker expression of cells present at the site of infection for longer (photoconverted), or shorter (not photoconverted) than two days. Control experiments showed that cell metabolism-related recovery from photoconversion in leukocytes is slow enough to use mKikumeGR to mark cells over several days (Figure 23 E, lower panel). Importantly, it could be observed that the large majority of cells expressing CD11c and F4/80 were photoconverted, thus had been present in the lesion at least for 2 days. As conclusion, these cells had matured at the site of infection from cells recruited between day 1 and 3 after transfer (Figure 23 E and F). Taken together, these data underline that newly recruited monocyte-derived cells are infected by *L. major* irrespective of their differentiation state.

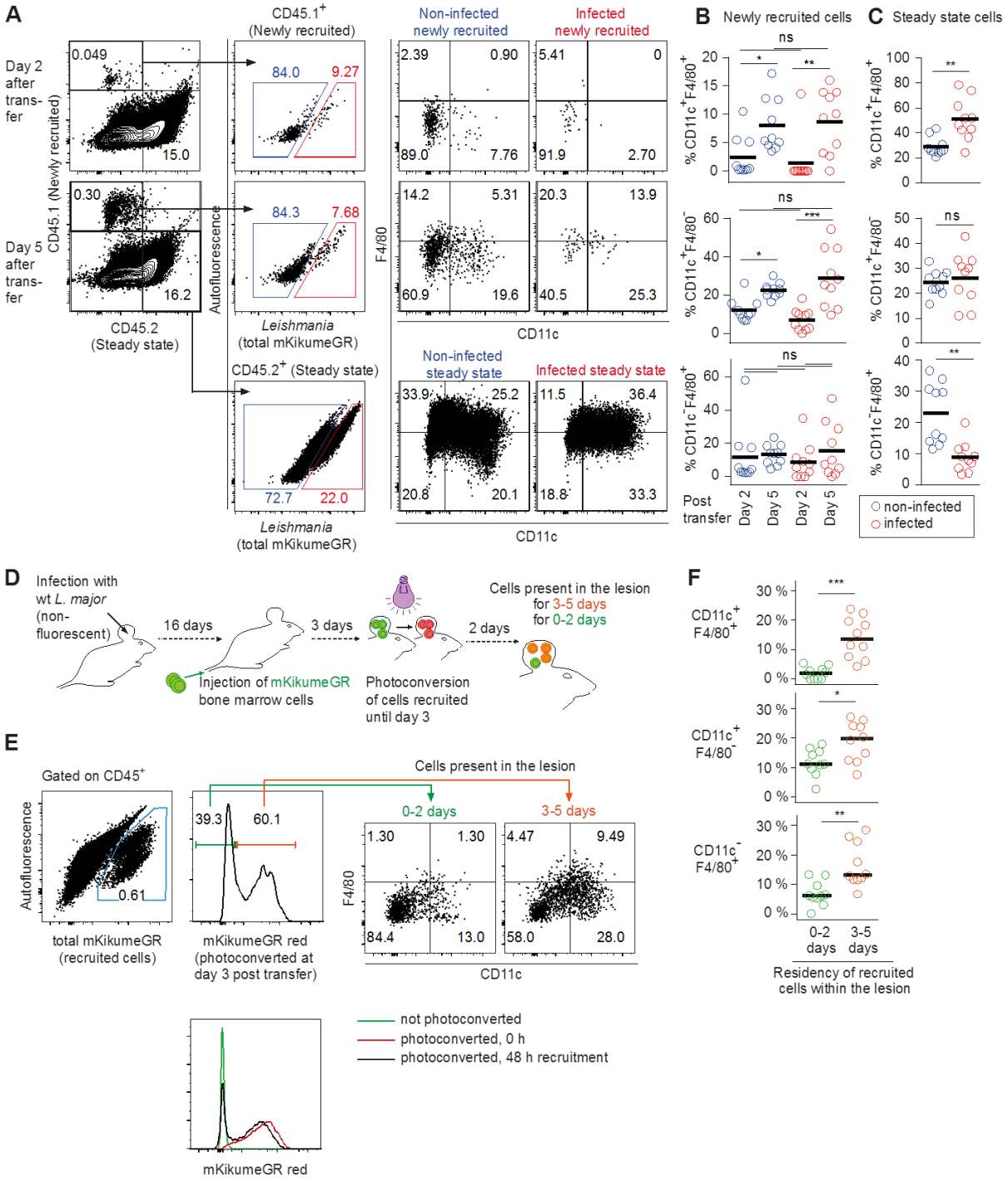

Figure 23: *L. major* infects newly recruited monocyte-derived cells independently of their differentiation stage. (A) Flow cytometry analysis of C57BL/6 (CD45.2) mice infected with *Lm*^{SWITCH}, adoptively transferred 2 or 5 days before analysis with CD45.1 bone marrow cells. Gating strategy on CD45.1$^+$ (newly recruited) and CD45.2$^+$ (steady state) infected and non-infected cells. **(B)** Quantification of infected (red) and non-infected (blue) CD11c$^+$ F4/80$^+$ double positive (upper panel) and CD11c$^+$ F4/80$^-$ single positive (lower panel) among newly recruited cells at day 2 and day 5 post adoptive transfer. **(C)** Analysis as in (B) for steady state cells. Data in A-C are reanalyzed from figure 19. **(D)** Experimental strategy to identify newly recruited cells present for 0-2 versus 3-5 days post adoptive transfer. Mice infected with non-fluorescent *L. major* wt received mKikumeGR-expressing bone marrow

cells 5 days prior to analysis. Photoconversion at 3 days post transfer identifies cells recruited to the site of infection until day 3 in mKikumeGR red fluorescence, while cells recruited after photoconversion (0-2 days prior to analysis) exhibit green mKikumeGR fluorescence. **(E)** After gating on $CD45^+$ cells, all adoptively transferred cells are identified by total mKikumeGR fluorescence. Transferred cells which were at the infection site for 0-2 days (showing no red fluorescence) can be clearly distinguished from cells that were recruited to the site of infection 3-5 days before analysis (and thus photoconverted, showing a high red fluorescence). The two populations were analyzed for CD11c and F4/80 expression. (Lower panel) Control samples were photoconverted 0 h prior to analysis or not photoconverted at all and fluorescence was compared with cells being photoconverted for 48 h. **(F)** Quantitative analysis of $CD11c^+F4/80^+$ double positive (upper panel) and $CD11c^+F4/80^-$ single positive (lower panel) present at the site of infection for 0-2 days (green) and 3-5 days (red), respectively. Each dot represents one mouse ear. Horizontal bars denote the mean. *$p < 0.05$; **$p < 0.01$; ***$p < 0.001$; ns, not significant.

2.3 Perspectives for future analysis

2.3.1 iNOS, but not NADPH oxidase, impacts on *L. major* proliferation cell-intrinsically

To examine possible mechanisms behind the observation of different pathogen proliferation rates within distinct cell types, cell-intrinsic effects of iNOS and NADPH oxidase were examined. So far, it had been shown that iNOS can work cell-extrinsically via the diffusion of nitric oxide across cell membranes [44] (see chapter 1.2.4). Since the results described above indicate that a cellular niche-specific mode of action within different cell types might contribute to the control of pathogen proliferation, a potential cell-intrinsic role was to be considered. A second important mechanism that might control *Leishmania* infection in macrophages cell-intrinsically is the production of ROS by NADPH oxidase [45] (see chapter 1.2.4). In order to test these possibilities, mixed bone marrow chimera of 50% C57BL/6 wt cells (expressing the surface marker CD45.1) and 50% iNOS knock out cells ($iNOS^{-/-}$), or 50% NADPH oxidase k.o. cells, respectively ($NADPH^{-/-}$) (expressing the surface marker CD45.2), were injected into irradiated CD45.1 mice. Such reconstituted mice were infected with Lm^{SWITCH} and proliferation rates of parasites were evaluated in k.o. compared to wt cells. Infected mouse ears were analyzed by flow cytometry (Figure 24). To this end, wt and k.o. cells were identified by antibody staining for CD45 and CD45.1. As a control, mixed bone marrow chimera of CD45.1 and CD45.2 wt cells were generated and assessed the same way. When investigating overall *Leishmania* proliferation, proliferation rates in $iNOS^{-/-}$ cells were increased in comparison to *Leishmania* proliferation in wt cells (Figure 24), suggesting that a cell-intrinsic control mechanism of iNOS is operative in addition to the described cell-extrinsic mode of action [44]. In contrast, when analyzing parasite proliferation of Lm^{SWITCH} in $NADPH^{-/-}$ versus wt cells, no significant differences were observable in *Leishmania* proliferation between parasite containing wt and $NADPH^{-/-}$ cells.

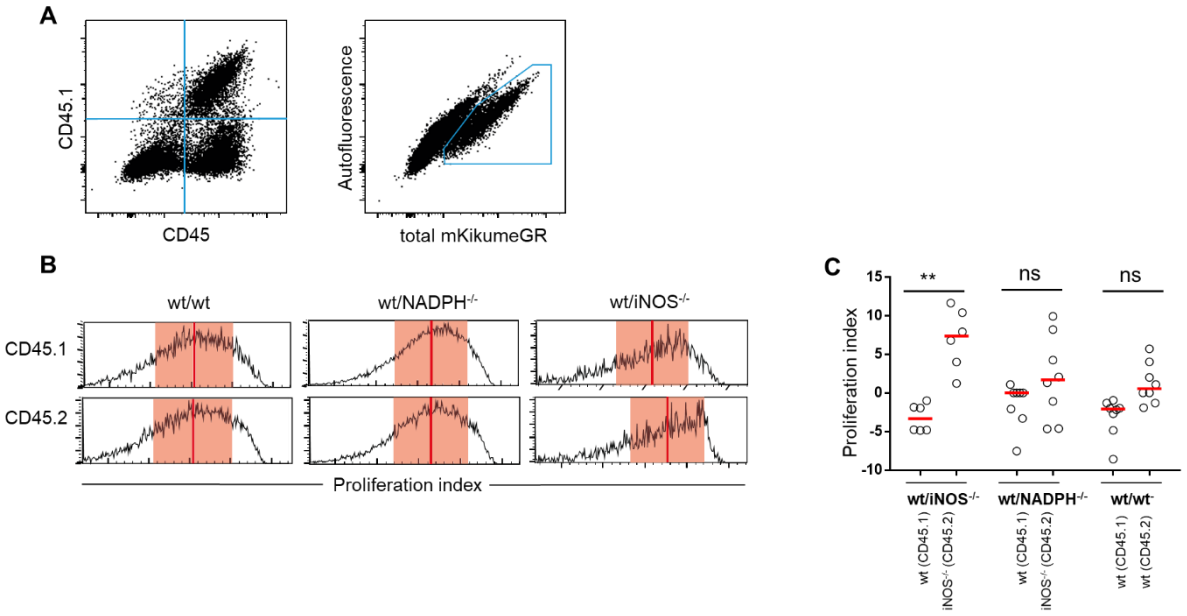

Figure 24: iNOS seems to control *L. major* proliferation cell-intrinsically. (A) Mixed bone marrow chimera of 50% C57BL/6 wt cells (expressing the surface marker CD45.1) and 50% iNOS k.o. cells (iNOS$^{-/-}$) or 50% NADPH oxidase k.o. cells (NADPH$^{-/-}$) (expressing the surface marker CD45.2) were injected into irradiated CD45.1 mice and analyzed by flow cytometry. As a control, mixed bone marrow chimera of CD45.1 and CD45.2 wt cells were generated. *Lm*^{SWITCH}-infected cells were analyzed for *L. major* proliferation. **(B)** Examples for relative proliferation rates of *Lm*^{SWITCH} located in wt and k.o. cells defined by CD45.1 and CD45.2 staining. Left panels show the control with CD45.1 and CD45.2 wt cells. Vertical bars denote the mean and shaded red boxes the standard deviation. **(C)** Quantitative analysis of the proliferative states of *Lm*^{SWITCH} within the different cell populations. Each dot represents one mouse ear. Relative proliferation indices were obtained by normalization of the subpopulation's proliferation index to the overall mean proliferation index within each sample. Horizontal bars represent the mean. **p < 0.01; ns, not significant.

2.3.2 Impact of *L. major* proliferation on interactions between APCs and T helper cells

Initiation of an effective T cell response plays an important role for the efficient control of *Leishmania* infection [3] (see chapter 1.2.4). Interactions between infected antigen presenting cells with CD4$^+$ T helper 1 cells induce the release of IFNγ by T cells and therefore lead to the activation of iNOS. Consequently, this process leads to the production of nitric oxide within the host cells, which is essential to cure *L. major* infection. Since a heterogenic distribution of APC-T cell interactions within the *Leishmania* infection has already been demonstrated [63] (see chapter 1.2.4), this raised the question if there is a correlation between the T cell behavior and pathogen proliferation. Thus, a system to study the influence of the proliferative state of parasites on APC-T cell interactions in the ongoing infection was set up.

Generation of an ovalbumin expressing Lm^{SWITCH} *strain to provide a system to investigate antigen-specific APC-T cell interactions*

To examine antigen-specific interactions between infected host cells and CD4$^+$ T cells, the well-established ovalbumin system was used [122]. Therefore, a new *Leishmania* strain was constructed expressing ovalbumin (OVA) on its surface. To obtain this, the *Leishmania* hydrophilic acylated surface protein B (HASPB) export sequence was fused to the OVA sequence to generate an HASPB fusion protein. It has been shown that the expression of this fusion protein by *Leishmania* leads to OVA expression on the parasitic plasma membrane [123], and is subsequently presented on the surface of infected antigen presenting cells via class II MHC molecules. Therefore, a new *Lm*^{SWITCH} strain, expressing additionally an HASPB-OVA fusion protein, was generated. In brief, an OVA-HASPB encoding DNA sequence was cloned into a pLEXSY_hyg2 vector (Jena Bioscience) wherein the hygromycin resistance cassette was exchanged with a neomycin resistance cassette. This enabled stable insertion of the OVA-HASPB sequence into the *Lm*^{SWITCH} genome via homologous recombination into rDNA loci. Transfection was done by electroporation. The selection of successfully transfected *Leishmania* was performed via the neomycin and hygromycin resistance cassettes. The successful generation of a photoconvertible *Leishmania* strain that expresses additionally the OVA protein on a HASPB sequence, hereafter termed *Lm*$^{SWITCH\_OVA}$, was proved on the basis of fluorescence and protein production (Figure 25). Photoconversion in the newly generated *Lm*$^{SWITCH\_OVA}$ *Leishmania* strain (Figure 25 A, right) was as efficient as in the original strain (Figure 25 A, left) (Figure 25 B). The effective expression of the OVA protein could be demonstrated by western blot analysis (Figure 25 C).

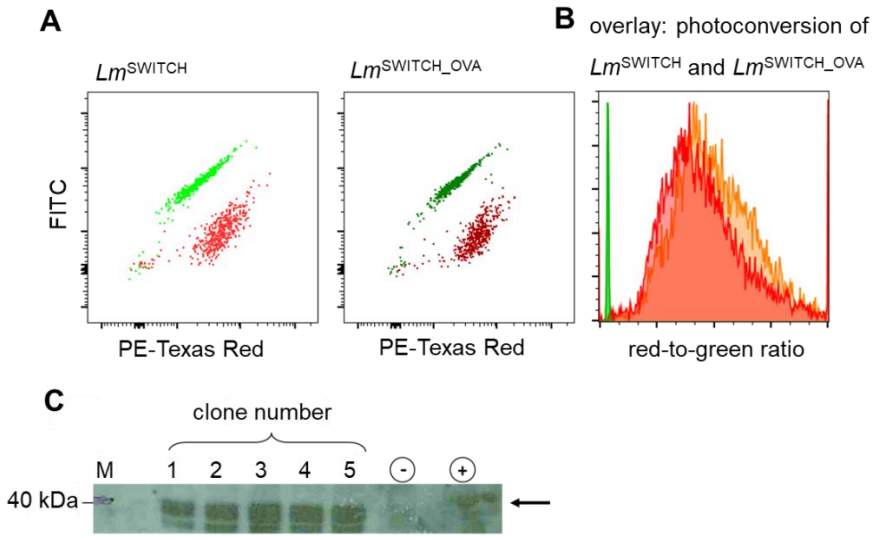

Figure 25: Successful generation of an OVA-expressing *Lm*^{SWITCH} proliferation reporter strain. A HASPB-OVA sequence was stably transfected into *Lm*^{SWITCH}. **(A)** To verify photoconvertibility of the newly generated *L. major* strain, *Lm*^{SWITCH} (left) and *Lm*$^{SWITCH\_OVA}$ (right) cultures were photoconverted

by a 2x2 diode array for 1 min. Efficiency of photoconversion was subsequently analyzed via flow cytometry by comparing non-photoconverted (green population) with photoconverted (red population) *Leishmania* cultures. **(B)** Overlay and comparison of red-to-green ratios before and after photoconversion of Lm^{SWITCH_OVA} and Lm^{SWITCH} (light green population: non-photoconverted Lm^{SWITCH}, red population: photoconverted Lm^{SWITCH}, dark green population: non-photoconverted Lm^{SWITCH_OVA}, orange population: Lm^{SWITCH_OVA}). **(C)** Verification of OVA expression by Lm^{SWITCH_OVA} by western blot analysis. Expected protein size: 43 kDa.

Measurement of parasite proliferation in Lm^{SWITCH_OVA} *infected APCs interacting with CD4⁺ T cells via intravital 2-photon microscopy*

To measure *Leishmania* proliferation in antigen presenting cells interacting with $CD4^+$ T cells, B6 albino wt mice were infected in a pilot experiment in the ear dermis with the newly generated Lm^{SWITCH_OVA} strain. 2 days prior to analysis, Magnetic Activated Cell Sorting (MACS)-isolated OT-II $CD4^+$ T cells, that had been *in vitro* differentiated into Th1 cells, were labelled with the far-red dye SNARF and injected intravenously into the infected mice. Therefore, APC-T cell interactions could be investigated via intravital 2-photon microscopy (Figure 26). 3-dimensional time series were recorded to analyze stable interactions (Figure 26 A). Contacts of more than 30 min between OT-II $CD4^+$ T cells (shown in purple) and high or low proliferating *Leishmania* (shown in green and red) were defined as stable interactions. The arrested T cells participating in these interactions were identified via a self-developed heat-map generator that presents long T cell dwell time as hotspots (Figure 26 B) (see appendix supplementary macro 3 for details). Subsequently, the proliferation index of *Leishmania* overlapping with these resting T cells was calculated via the Imaris software. Proliferation indices of *Leishmania* that are in contact with OT-II $CD4^+$ T cells were normalized to the average proliferation index of all imaged parasites at the site of infection (Figure 26 C). One important result concerning the *in vivo* analysis is the fact that stable interactions were observed, indicating the successful presentation of OVA at the surface of infected APCs. In this pilot experiments, the red-to-green ratio of parasites that are in contact with arrested T cells did not show a different proliferation index than the average population of all parasites in the imaged area, indicating there might be no strong preference of T cells to interact with APCs containing high proliferating *Leishmania*. As control, a scrambled control with arbitrary photoconversion right before proliferation measurement was analyzed. For this purpose, Lm^{SWITCH_OVA} in the ear were photoconverted at random by using a grid as explained and demonstrated in chapter 2.2.1 (Figure 11 and Figure 26 D). Because of a naturally high signal-to-noise ratio within this experimental set-up, further experiments will have to be done to confirm the results of this pilot study. Nevertheless, the data suggest that the system for analyzing stable T cell-APC interactions in the context of *L. major* proliferation is working as intended.

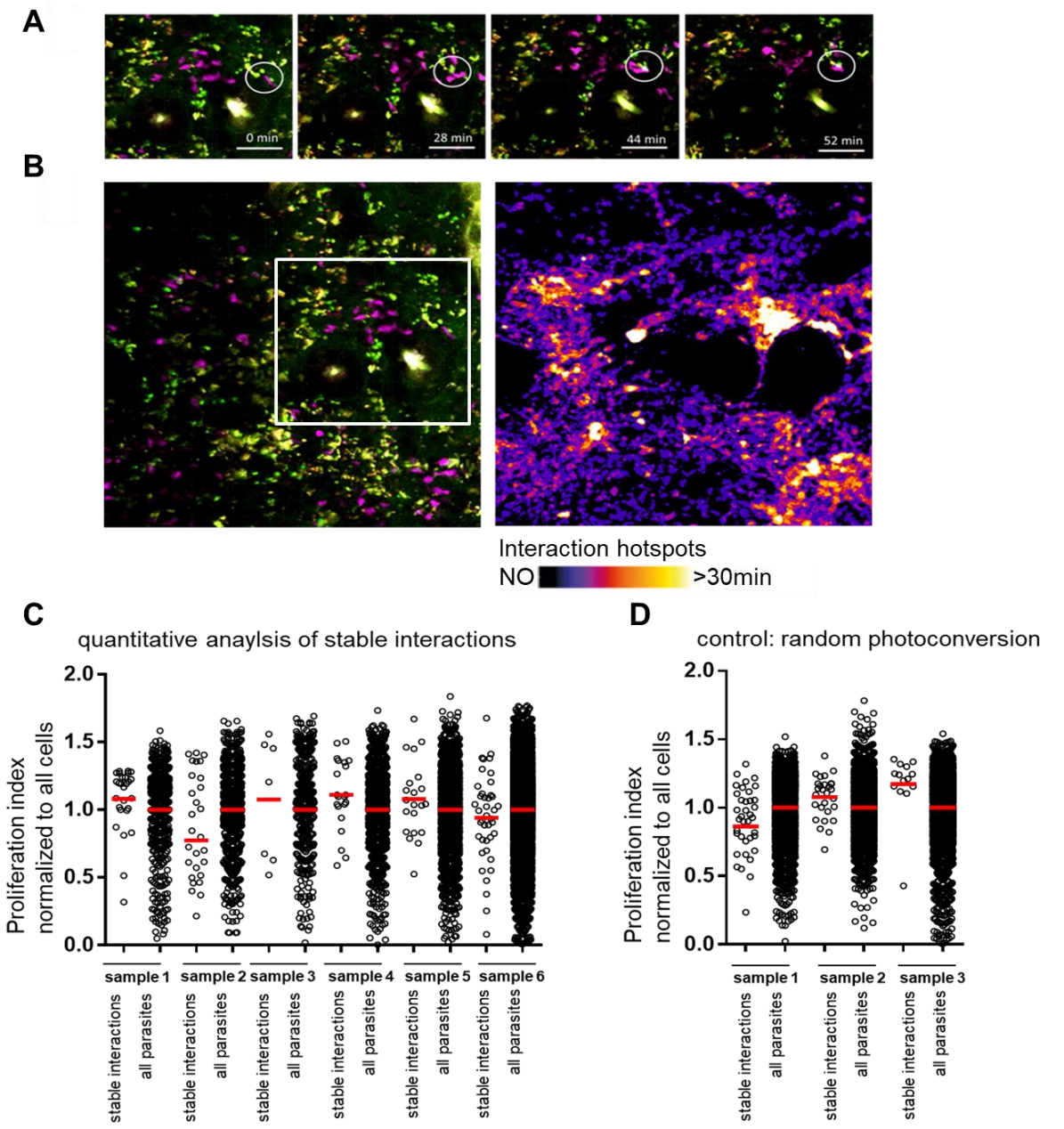

Figure 26: Measurement of parasite proliferation in *Lm*$^{SWITCH\_OVA}$ infected APCs interacting with CD4$^+$ Th1 cells via intravital 2-photon microscopy. *Lm*$^{SWITCH\_OVA}$ infected B6 albino wt mouse ears were photoconverted 8 days post infection and OT-II CD4$^+$ T cells that had been *in vitro* differentiated into Th1 cells, were labelled with the far-red dye SNARF and injected intravenously into the infected mice. T cell interactions related to *L. major* proliferation were analyzed 48 h later via intravital 2-photon microscopy. **(A)** Stable interactions between OVA specific injected OT II cells and *Leishmania* were analyzed by 3-dimensional time series. Contacts of more than 30 min were defined as stable interactions. **(B)** Resting T cells were identified via a self-developed heat-map generator that presents long T cell dwell time as hotspots. White box in the left panel marks the region that is shown magnified in (A). **(C)** Proliferation indices of *Leishmania* that are in contact with OT-II CD4$^+$ T cells were normalized to the average proliferation indices of all imaged parasites at the site of infection. Each dot represents a single parasite. **(D)** As a control *Lm*$^{SWITCH\_OVA}$ in the ear were randomly photoconverted straight before

analysis and proliferation indices of *Leishmania*, that show contacts with SNARF labelled T cells, were normalized to the average proliferation indices of all imaged parasites at the site of infection. Each dot represents a single parasite.

3 Discussion

To understand the interaction between the immune system and a pathogen, it is indispensable to extract data on the proliferation states of infectious microorganisms, and to define the niches in which differentially proliferating pathogen populations are located. For bacteria, e.g. *M. tuberculosis*, non-replicating forms have been defined despite the high proliferating states at the infection site. In those infections, antibiotic treatment often leads to a biphasic "hockey-stick" like killing curve, since a non-replicating subpopulation shows antibiotic resistance. These populations have been defined as "phenotypically tolerant", since they were shown to retain the possibility to entry cycles of replication again and therefore cause disease [124,125]. The mechanisms behind this are not completely understood and are believed to be the result of a complex of different molecular mechanisms that have been proposed so far to be involved in the formation of persistent populations [126,125]. However, it is indispensable to further investigate these mechanisms in order to dissect the development of antibiotic resistance and thereby to understand how to effectively treat a pathogen.

3.1 Characterization of the mKikumeGR reporter system

Measuring proliferation of pathogens *in vivo* is still a big challenge in biomedical research. There are different methods that have been established to investigate this difficult but important task of the influence of pathogen proliferation within the infection.

One possibility is the incorporation of BrdU (5-Bromo-2′-deoxyuridine) into the mitochondrial DNA and the nucleus of a pathogen, which has been used for determining *L. major* proliferation [72]. Parasite replication is therefore indicated upon the increase in *Leishmania* positive for BrdU. By using this application, subpopulations of high and low proliferating parasites among the persistent populations were identified. Nevertheless, this system is limited by the fact that samples need to be chemically fixed for monitoring BrdU incorporation. The rather harsh fixation conditions required, restrict this method in that a concomitant analysis of the cellular niche of the pathogens is difficult. In particular, it is incompatible with most antibody staining procedures.

Another approach to measure the physiological state and proliferation of *Leishmania* was developed by Kloehn et al. [108] using heavy water labelling. Thereby infected mice are treated with $^{2}H_2O$ for a defined period of time and the turnover rate of proteins and DNA from parasites is calculated from the amount of deuterium within the parasites. However, analysis of parasite replication on a cellular level is hard to implement by this approach, making it incompatible with intravital or multiparameter host cell analysis, which is indispensable for investigating a link between the impact of *L. major* proliferation and host cell tropism.

An alternative method to measure protein turnover is the application of so called fluorescent timer proteins [127,128]. Thereby, the fluorescence color of proteins is dependent on the protein age and changes by time. A problem of using fluorescent timers is e.g. that the kinetics of maturation are highly dependent on the oxygenation of the tissue. Further limitations are the time the proteins need to mature that might not be well-adapted to the observed proliferation rate of the pathogen, as well as photoinstability [128]. Another problem might be the exact definition of a starting point for the measurement of protein turnover, which therefore constitutes a problem to accurately compare different experimental conditions in parallel.

Photoconvertible proteins can overcome many of these problems. By the use of this approach, the starting point in the change of the fluorescence color can be tightly controlled by the activation of a light pulse anytime during an infection. Several photoconvertible proteins have been described [129] [130,116,131]. Since the heterologous expression of multimeric forms of proteins, e.g. in bacteria, often turns out to be difficult, one obstacle for the efficient use of photoconvertible proteins for analysis is that the protein should be present in its monomeric form. This is challenging since most fluorescent proteins exist naturally as tetramers or dimers [129]. mKikumeGR is a photoconvertible protein that could be stably synthesized in its monomeric form [116]. Furthermore, it was shown to be successfully expressed in *L. major*, while expression of new protein is coupled to cell division [73]. Thus, mKikumeGR exhibits perfect conditions to act as an indicator for microbial proliferation. Specifically, the green fluorescence of mKikumeGR can be converted irreversibly into red after illumination with violet light. Production of non-photoconverted green fluorescent protein upon cell division leads to a dilution of the red fluorescence and therefore to recovery from photoconversion. Additionally, it was proven that parasite proliferation via the mKikumeGR reporter can be investigated directly *in vivo* by intravital 2-photon microscopy [73].

One aim of this thesis was to further characterize the mKikumeGR reporter to enable the analysis of *Leishmania* proliferation via various applications and methods like flow cytometry and histological analysis e.g. Multi-Epitope Ligand Cartography. To this end, the photoconversion approach was extended first to large areas, such as the whole infected ear skin. So far, photoconversion had only been performed by epifluorescence illumination during intravital microscopy, or by confocal laser scanning [73,116,132]. In the presented thesis, a diode array was established to photoconvert *Lm*^{SWITCH} in the ear tissue as well as *in vitro*. The efficient photoconversion of *Lm*^{SWITCH} as well as the successful recovery from photoconversion via the diode array was proven (see chapter 2.1.1). Thus, the application spectrum of *Lm*^{SWITCH} as well as the area that can be photoconverted is substantially enhanced by the use of a diode array. Hence, more flexibility in the usage of the mKikumeGR reporter for the analysis of *L. major* proliferation was obtained. Furthermore, preservation of fluorescence after chemical

fixation of photoconverted ear samples could be demonstrated, verifying the stability of the mKikumeGR protein within fixation protocols for example for confocal microscopy analysis or Multi-Epitope Ligand Cartography. Since the mKikumeGR reporter is compatible with immunofluorescence, conditions to efficiently analyze *Lm*^{SWITCH} infected mouse ears by flow cytometry were also defined successfully within this thesis (see chapter 2.1.4). In conclusion, mKikumeGR was demonstrated to be a highly reliable reporter protein to measure *Leishmania* proliferation *in vivo* and *in vitro* e.g. via intravital microscopy, MELC and flow cytometry.

3.2 Defining the niche of high and low proliferating *L. major*

In line with previous BrdU-based proliferation measurements [72], it was shown that *L. major* parasites grow at a broad spectrum of different proliferation rates in an established infection. While the harsh fixation conditions in bioorthogonal labelling experiments preclude a concomitant analysis of the cellular niche of the pathogens, it could be shown, using the photoconversion-based biosensor, that individual host cells contain parasites with a proliferation rate which is similar among all *L. major* within the same cell (Figure 9). Thus, it can be concluded that *L. major* proliferation rate is linked to the cellular niche in which the parasite resides. Within in the established infection, this niche is constituted mainly of macrophage- and DC like monocyte-derived phagocytes, which have been shown to mature at the site of infection [104,33]. Whether one of these cell types would be particularly permissive for higher pathogen proliferation had been unclear. By using cell type-specific gene ablation, it was shown recently that Interleukin-10 receptor signaling in DCs, respectively $CD11c^+$ cells, is involved in regulating *L. major* burden at the site of infection, since the parasite burden in the infected ear was reduced significantly upon knock out of the IL-10 receptor on $CD11c^+$ cells [133]. IL-10 plays an important role during immune regulation and is thus crucial for persistence in the host organism [68,66,67]. In contrast, it was proven that infection was cleared completely in IL-10 knock out mice in the skin and the draining lymph nodes, leading to sterile immunity. However, the impact on pathogen proliferation on a cellular level had remained uncharacterized. Using flow cytometry, $CD11c^+$ cells were defined in the presented thesis as the major niche for *L. major* proliferation (Figure 10). These results were confirmed by transient depletion of $CD11c^+$ cells in *L. major* infected mice which subsequently show a significantly lower overall pathogen burden compared to *L. major* infected control mice (Figure 12). Thus, these data suggest that a major niche for parasite proliferation is lost upon depletion of $CD11c^+$ cells. The cell populations containing high or low proliferating parasites were further investigated by a multiparameter analysis approach that suggests that $CD11c^+$ phagocytes which are recruited to the site of infection represent a niche of increased *L. major* proliferation, irrespective of their expression level of F4/80, class II MHC and CD86, with class II MHC and CD86 serving as markers for defining the activation state of the different subpopulations. However, when investigating pathogen proliferation in cells which were CD11c negative but positive for F4/80, CD86 or class II MHC, respectively, no differences were observed between the several subpopulations regarding the proliferation state of the parasites. Hence, $F4/80^+$ but $CD11c^-$ cells, irrespective of their activation state, do not provide a reservoir for high *Leishmania* proliferation (Figure 15). These data fit with the publication of Girard-Madoux et al. which showed that upon on the knock down of the important immune regulator IL-10 in $CD11c^+$ DCs, the pathogen burden in the whole infection is decreased. This already indicated that

Leishmania proliferation in $CD11c^+$ cells might play an important role regarding the total *Leishmania* proliferation in the overall infection. By investigating *Leishmania* proliferation in relation to the surface markers CD11c combined with the important monocyte marker Ly6C it was observed that *L. major* proliferation is high in $CD11c^+Ly6C^+$ double positive cells. Interestingly, the $CD11c^-Ly6C^+$ subpopulation was found to also harbor high proliferating parasites. By investigating the percentage of infected cells within this subpopulation, it became however clear that this subpopulation represents only a very small part of the infected cells in the entire infection, thus explaining why it was not identifiable in analysis performed with CD11c and F4/80. Instead, these cells might be recently recruited immature monocytes, in which it would be expectable to mainly detect parasites that have recently undergone cell-to-cell transfer and therefore are rapidly proliferating (see below). Overall, these results confirm the majority of $CD11c^+$ monocyte-derived cells as main niche for *L. major* proliferation.

In-depth characterization of *L. major* infected cells via flow cytometry combining the surface markers CD11c, F4/80, Ly6C, class II MHC, CCR2 and CD11b showed that Ly6C and class II MHC expression is highest in $CD11c^+F4/80^+$ cells compared to $CD11c^+F4/80^-$ or CD11c negative populations. CCR2 expression was high in $CD11c^+F4/80^+$ and $CD11c^-F4/80^+$ but significantly lower in $CD11c^+F4/80^-$ and $CD11c^-F4/80^-$ populations (Figure 16). Monocytes infiltrating *Leishmania* infections were characterized in referred publications as $CD11b^+Ly6C^+CCR2^+$class II $MHC^-CD11c^-F4/80^-$ [92,77,33] which than mature and become activated upon arrival at the infection site. The results obtained within this study indicate that the main population of parasite containing cells within the skin after 3 weeks of infection are monocyte-derived. Furthermore, mainly according to the data from Leon et al. and Romano et al. $CD11c^+$ $F4/80^+$ cells which are additionally $CD11b^+$, $CCR2^{high}$ and class II MHC^{high} seem to be matured and highly activated monocytes. Moreover, the observed intermediate to high expression level of Ly6C for this subpopulation seems to fit to the mentioned publications. $CD11c^+F4/80^-$ cells also express Ly6C but not significantly more than $CD11c^+F4/80^+$ which is not in complete agreement with the findings of Leon et al. 2007. Those slight differences in the characterized cell types at the infection site might be due to the fact that there are differences in the experimental settings between the current study and the studies of Leon et al. and Romano et al. The studies for example differ in the amount of *L. major* that were injected into the skin. Additionally, Leon et al. and Romano et al. worked with footpad infections whereas, within this study, the ear dermis was infected. Furthermore, Romano et al. characterized monocytes during primary and secondary *L. major* infection and defined different roles for monocytes in these different settings. Nevertheless, they did not describe monocyte characterization after 3 weeks of primary infection as it was performed in the presented study. Indeed, the 3 weeks time point might represent an intermediate state between early primary infection and secondary infection, investigated by Romano et al., referred to as concomitant

immunity. Along this line, while $CD11c^+$ monocyte-derived cells seem to constitute a niche for high pathogen proliferation, there might be other functions of these cells at the infection site which promote immunity to reinfection: Collins et al. have shown recently that the CCR2-dependent sustained accumulation of $CD11c^+$class II MHC^+ antigen presenting cells to the site of herpes simplex virus infection is responsible for efficiently promoting local T-cell mediated immunity [134]. Thus, it might be possible that these cells, in *L. major* infection, have an ambivalent role in harboring high proliferating pathogens and promoting effector T cell responses.

Moreover, based on the surface marker expression of infected cells discussed above, it can be assumed that the major cell type, containing high proliferating parasites, might be monocyte-derived DCs, irrespective of their activation state. These data are in line with previous findings defining monocyte derived dermal DCs as the most important DC type in the ongoing *L. major* infection [6,98,98,77,104]. Strikingly, De Trez et al. defined inflammatory DCs in the lymph node, positive for CD11b, CD11c, F4/80, Ly6C and class II MHC, as major iNOS producing cell types that show the same phenotype as TNF/iNOS producing DCs, so called TipDCs [104]. The seemingly paradox situation in which exactly the cell type, in which pathogen proliferation is highest, might also be a main producer of iNOS underlines the question to what extent cell-intrinsic control mechanisms control *Leishmania* during infection. Previous work had shown that several layers of cell-extrinsic *L. major* containment are in place. First, a gradient of IFNγ mediates induction of iNOS, the main cellular defense mechanism against the parasite, also in cells that are not directly engaged by effector T cells [65]. Second, diffusible nitric oxide produced by iNOS seems to provide another layer of cooperative control of the pathogen on the tissue level [44]. In contrast to these findings, the data ascertained within the current study show proliferation rates linked with a specific cell type suggesting that additional cell-intrinsic control mechanisms against *L. major* proliferation exist.

To further analyze the potential cell-intrinsic control mechanisms of *L. major* proliferation, a cell-intrinsic effect of iNOS beyond its cell-extrinsic function was considered. When comparing *Leishmania* proliferation within all infected wt cells with *Leishmania* proliferation in $iNOS^{-/-}$ cells at the same infection site, preliminary data show that the *L. major* proliferation rate within the wt situation was significantly reduced compared to cells which are not able to produce iNOS (Figure 24). Since wt and $iNOS^{-/-}$ cells were located at the same infection site this indicates a possible cell-intrinsic control mechanism of iNOS.

An additional reason for cell type specific proliferation rates might be the differential production of ROS within different cell types. ROS is generated through the induction of the NADPH oxidase machinery at the phagosomal membrane in macrophages [45,89] (see chapter 1.2.4). Nitric oxide, together with reactive oxygen, can form highly toxic peroxynitrite, which has a

diffusion range of less than 5 µm from its site of production [135,136]. Thus, while nitric oxide seems to diffuse to neighboring cells, peroxynitrite formation at sites of high NADPH oxidase activity might represent a cell-intrinsic component of *L. major* containment. Another possible explanation for distinct proliferation rates within different cells might be the capacity of the parasites to counteract cellular defense mechanisms by deactivating NADPH oxidase assembly, by producing detoxifying enzymes or interfering with host phagocyte signaling pathways linked to antimicrobial activity, which might not be equally efficient in all cell types [137,15]. Therefore, *Leishmania* proliferation within infected wt cells was compared with *Leishmania* proliferation in $NADPH^{-/-}$ cells at the same site of infection. However, no significant differences were seen concerning parasite proliferation between wt and $NADPH^{-/-}$ cells. Nevertheless, since these are preliminary data a cell-intrinsic/specific effect of NADPH oxidase cannot be completely excluded and will be an interesting subject to follow up further. Furthermore, parasite proliferation within the different $CD11c^{+}$ and $CD11c^{-}$ subpopulations in $iNOS^{-/-}$ respectively $NADPH^{-/-}$ cells should be studied since effects within these subpopulations might not be observed by analyzing the total amount of infected cells at once.

Finally, while a tissue-wide mode of *L. major* control could be mainly shown for $CD4^{+}$ T cell-dependent effector functions, $CD8^{+}$ cytotoxic T cells and NK cells might mediate target cell-intrinsic containment mechanisms [138,59,46]. IFNγ production by $CD8^{+}$ T cells or NK cells, which is dependent on IL-12 signaling via Tyk2 in these cell types [138], plays an additional important role in the further induction of an efficient Th1 response. Alternatively cytotoxicity can also be activated within these cell types leading to the release of granulysin, perforin and granzymes into an infected cell [59]. Therefore, influence of NK cells and $CD8^{+}$ T cells on intracellular pathogen proliferation within the different cell types should be investigated in the future.

3.3 Exit strategies of *L. major*

Strategies of intracellularly proliferating pathogens to exit infected cells in order to be transmitted into a new cellular niche are critical for survival of pathogens especially in long-lasting infections [31]. This process has profound implications for the cell tropism of the pathogens, as well as immune activation, and has been extensively characterized for example for *Plasmodium*. The life cycle of these parasites, which are transmitted by mosquitos into the mammalian host, consists of four stages. Via lysis of the parasitophorus vacuolar membrane so called merozoites are released from hepatocytes into the bloodstream [139] where they are taken up by red blood cells. Therein they proliferate in a lytic cycle. By destabilization of the cytoskeleton of the red blood cells, *Plasmodium* parasites can escape from their host cells [140]. In a next step, gametocytes are taken up by a mosquito and are released in its midgut for fertilization [141]. In the fourth stage sporozoites are released from the oocyst and are ready to migrate into the salivary glands of the mosquito [31]. Another example for well-defined exit strategies is the bacterium *Salmonella*, which can induce apoptosis in infected macrophages. Nevertheless, in systemic infections necrosis and pyroptosis represent the main mechanisms of *Salmonella* exit from host cells [142]. Thereby, caspase-1 activation, as well as releasing inflammatory cytokines, leads to phagolysosome exocytosis [143].

In contrast to these pathogens, the mechanism of egress of *L. major* from infected host cells and infection of new host cells has not been extensively studied so far and has been completely unknown in the established infection. *In vitro* evidence from *L. amazonensis* suggests direct cell-to-cell transfer via LAMP1-rich extrusions [32]. Furthermore, intravital 2-photon microscopy of very early events after infection had shown that *L. major* is taken up by neutrophils immediately after inoculation of the skin, and is then phagocytosed by both macrophage and DC-like phagocytes, a process that might involve the apoptosis of the neutrophils [76,144]. While in the established infection later on, macrophages and DCs represent the main infected cell type, nothing is known about how *L. major* disseminates to new host cells during this phase of the disease [104,33]. In the presented thesis, synchronization of the arrival of newly recruited phagocytes revealed that high proliferating parasites are more efficiently transmitted to newly recruited host cells (Figure 18). It is conceivable that eventually, a subpopulation of newly infected cells is able to dampen pathogen proliferation, resulting in the observed overall distribution of high proliferating parasites in $CD11c^+$ and low proliferating parasites in $CD11c^-$ negative host cells. *In vitro* data suggest that the high pathogen proliferation detected in newly recruited cells is due to the successful transmission of *L. major* which were already exhibiting a higher proliferation rate, and not due to an increase in proliferation upon infection of a new host cell (Figure 21). This conclusion is based on the fact that during *in vitro* analysis newly infected cells are analyzed

5 h after they were added to the cell culture, which is a timespan that is too short for efficient *L. major* proliferation (Figure 21). It can therefore be proposed that the $CD11c^+$ monocyte-derived phagocytes not only represent a cellular niche of high *L. major* proliferation, but also represent the main source of parasites disseminating to new cells. In contrast, it is likely that CD11c-negative phagocytes, e.g. monocyte-derived macrophages or neutrophils, although infected as efficiently as the $CD11c^+$ cells, might represent a dead end in the cycle of parasite release, reinfection and intracellular replication. Also, a possible extracellular proliferation before entering new host cells can be excluded by the presented data, as direct cell-to-cell transmission from resident host cells to newly added cells could be observed by time-lapse microscopy *in vitro*. Furthermore, direct cell-to-cell transfer of *Leishmania* from $CD11c^+$ cells to cells newly recruited to the infection site could be demonstrated within this study *in vivo* via intravital 2-photon microscopy (Figure 20).

3.4 Differentiation of cells recruited to the infection site

It has been described that monocytes infiltrating the site of infection may be found in a variety of maturation states [33,77]. Strikingly, it was observed within this project that $CD11c^+$ monocytes harbor high proliferating *Leishmania* irrespective of the different expression of activation markers like CD86, class II MHC, and F4/80. When investigating the development of monocytes newly arrived at the infection site to more mature forms, it was observed that the number of differentiated cells is significantly increased between day 2 and day 5 after recruitment. This indicates that mainly immature monocytes are recruited to the infection site which than mature to $CD11c^+F4/80^+$, $CD11c^+F4/80^-$ and $CD11c^-F4/80^+$ cells. This was proven by the use of mKikumeGR expressing cells, which were injected into *L.m. wt* infected C57BL/6 mice. By using these cells, the time of residency for cells which infiltrated the infection site can be determined (Figure 23). Thus, it could be concluded that the majority of recruited monocytes mature at the site of the established *L. major* infection. Interestingly, it was proven that *L. major* uptake can dampen the maturation of infected host cells [77], thus, photoconvertible approaches for comparing the time of residency at the site of infection with maturation could constitute an important tool to characterize the impact of *L. major* infection on monocyte differentiation at the site of infection.

Comparison of infected and total cell populations was performed to determine if newly recruited phagocytes are infected by *L. major* dependent on their differentiation state. Strikingly, newly arriving cells turned out to be infected rather randomly and equally distributed irrespective of the cell type (Figure 23), whereas in non-transferred and thus previously present cells of the host, $CD11c^+F4/80^+$ as well as $CD11c^+Ly6C^+$ cells turned out to be the most frequently infected cell type (compared to the infection of $CD11c^+F4/80^-$, $CD11c^-F4/80^+$, or $CD11c^+Ly6C^-$ cells). Therefore, these data confirm that when infecting new host cells *Leishmania* do not differentiate which cell type they infect but later on during the steady state $CD11c^+$ cells constitute the most convenient niche for *L. major*.

Taken together, while monocyte-derived DCs have been mainly studied in the context of inducing adaptive immune responses against *L. major* [33,36,98], these findings now elucidate a role for monocyte-derived $CD11c^+$ cells as a reservoir for rapidly proliferating parasites that disseminate at the site of infection.

3.5 Impact of *L. major* proliferation on interactions between APCs and T helper cells

L. major infection represents an efficient and well-established system to study Th1 or Th2 T cell responses, respectively. The Th2 response is studied in susceptible BALB/c mice whereas a protective Th1 response is induced in C57BL/6 mice [3]. By analyzing interactions between APCs infected with *L. major* and Th1 cells via intravital 2-photon microscopy in the skin, Filipe-Santos et al. could show that T cells exhibiting stable, long-lasting interactions with APCs are not distributed equally at the site of infection, but instead form so-called antigen-recognition clusters [63]. Thus, there are some infected APCs that do not form stable interactions with $CD4^+$ helper T cells within the ongoing *L. major* infection. Müller et al. have shown that differential class II MHC expression is an unlikely explanation for such heterogenic behaviors [65]. To better understand T cell immunity upon infections with intracellular parasites the influence of *L. major* proliferation on the heterogenic distribution of T helper cell contacts should be investigated within this study.

For the analysis of interactions between Th1 cells and antigen presenting cells harboring *Leishmania* of different proliferative states, the chicken ovalbumin (OVA)- OT-II system was employed, since OVA is one of the best characterized model antigens, and OVA specific TCR transgenic OT-II mice are available [122]. These transgenic TCRs recognize specifically the OVA presented on the class II MHC complexes on APCs. Successful expression of ovalbumin at the plasma membrane of *Leishmania* and subsequent presentation of the peptide via the class II MHC molecules of the infected antigen presenting cell has been established [123]. Prickett et al. demonstrated that the location of ovalbumin expression plays an important role for the induction of an efficient T cell response. Thus, a new *L. major* strain was generated expressing the mKikumeGR proliferation reporter and additionally the full-length ovalbumin at the plasma membrane. Efficient photoconversion in the new Lm^{SWITCH_OVA} strain was verified to be as effective as in Lm^{SWITCH}. Furthermore, efficient recruitment of OVA specific OT-II T cells to the site of infection as well as stable interactions were demonstrated, indicating the successful presentation of processed ovalbumin by class II MHC molecules of antigen presenting cells (Figure 26). Thus, a system to reliably analyze interactions between APCs, containing *L. major* of different proliferation states, with specific Th1 $CD4^+$ cells in the living host organism via 2-photon microscopy could be established within this thesis. Since, the full-length ovalbumin is expressed by Lm^{SWITCH_OVA} this system represents also a very elegant tool to study class I MHC-mediated APC interactions with $CD8^+$ T cells in further studies.

When investigating stable interactions related to the proliferation state of the parasites, there was no obvious tendency observable in that T cells would interact preferentially with green,

high proliferating, parasites (i.e. APCs containing high proliferating parasites) (Figure 26). This implication can be made by normalizing the proliferation index of interacting parasites to the average proliferation index of all imaged parasites at the site of infection. As a control to exclude artefacts due to spectral overlap between the labelled T cells with mKikumeGR fluorescence, a scrambled photoconversion was performed right before the analysis and controls were analyzed the same way as the specimen. Nevertheless, the results obtained so far can only give a hint towards the behavior of Th1 $CD4^+$ cells in the ongoing *L. major* infection in terms of parasite proliferation, since the data are not significant and totally conclusive, yet. One reason for this might be the high signal-to-noise ratio within these experiments. This is caused for example by the fact that antigen presenting cells which are harboring *Leishmania* are not visible by fluorescence microscopy and thus all *Leishmania* overlapping with resting T cells must first be assumed to be interacting APCs. Therefore, it is possible that *Leishmania* which are considered to be interacting are located in a different host cell than the neighboring parasites and thus might reside in an APC that does not interact with a T cell. This scenario is not detectable within the established system. Nevertheless, since the system is very well controlled by constant application of the scrambled control with arbitrary photoconversion, it represents a promising method to investigate the correlation of *L. major* proliferation and Th1 $CD4^+$ cell interaction *in vivo*. Thus, it would be highly promising to optimize the analysis of T cell-APC contacts by enhanced resolution, or improved image analysis approaches, and to clarify the question of the impact of pathogen proliferation on these interactions, since there might be several important implications for proliferation specific APC – T cell interactions. For example, it is known that innate immune cells are often able to differ between dead and alive pathogens, via the recognition of viability, so called vita-PAMPs [112] [114] (see chapter 1.3.2). Thus, although no dramatic differences in the activation markers tested on cells infected with high versus low proliferating *L. major* were detected, it might be possible that APCs harboring high proliferating *Leishmania* might interact differently with T cells compared to APCs containing low proliferating parasites. For the detection of vita-PAMPs, the innate adaptor molecules MyD88 and TRIF often play an essential role [112] [114]. Therefore, to further investigate the role of MyD88 and TRIF within the context of *Leishmania* proliferation, APC - Th1 $CD4^+$ cell interactions in Lm^{SWITCH_OVA} infected wt mice should be compared with APC - Th1 $CD4^+$ cell interactions in Lm^{SWITCH_OVA} infected $MyD88^{-/-}$ respectively $TRIF^{-/-}$ mice by intravital imaging analysis. Furthermore, if T cells preferentially interact with APCs containing high proliferating parasites, this would suggest that the niche of high proliferating *L. major* also represents the main population of antigen presenting cells. One explanation might be that high pathogen proliferation could therefore trigger an increase of the antigen dose. Deeper analyses of this hypothesis can be done by performing intravital microscopy with Lm^{SWITCH_OVA} infected CD11c reporter mice and investigating CD4 interactions with $CD11c^+$ cells related to the

proliferation state of the parasites. By the use of antibodies specific for *Leishmania* peptide presented on class II MHC, an increase of presented antigens on interacting- compared to non-interacting APCs could be investigated [19].

In summary, the work of the current thesis provides for the first time a quantification of *L. major* proliferation rates with respect to different host cell types, and to different phases in the cell-to-cell transfer cycle, in an unperturbed infection setting. This is of great interest for the understanding of how the residency within a specific cellular niche enables *Leishmania* parasite to efficiently multiply and persist at the site of infection.

4 Materials and Methods

4.1 Methods

Ethics Statement

All animal experiments were approved by the Ethics Committee of the Office for Veterinary Affairs of the State of Saxony-Anhalt, Germany, under the permit license numbers 42502-2-1253 Uni MD, and 42502-2-1314 Uni MD.

4.1.1 Mouse and parasite strains and infections

Parasites and mouse infections

L. major LRC-L137 V121 wt, mKikumeGR expressing *Lm*^{SWITCH} or dsRed expressing *L.m. dsRed* parasites, were previously described [73,145,146,104]. *L. major* that are co-expressing mKikumeGR and ovalbumin (*Lm*$^{SWITCH\_OVA}$) were generated within the current study (see chapter 2.3.2). Parasites were grown in M119 medium complemented with 10% heat-inactivated fetal calf serum, 0.1 mM adenine, 1 mg/ml biotin, 5 mg/ml hemin, and 2 mg/ml biopterin for maximally 6 passages.

Wt C57BL/6J, CD45.1 (B6.SJL-*Ptprc*^{a}*Pepc*^{b}/BoyJ), mKikumeGR expressing (Tg(CAG-KikGR)33Hadj/J), CFP expressing (B6.129(ICR)-Tg(CAG-ECFP)CK6Nagy/J), and CD11c-GFP-DTR (B6.FVB-1700016L21Rik$^{Tg(Itgax-DTR/EGFP)57Lan}$/J) mice were purchased from Jackson Laboratories (Bar Harbor, MA), B6N-Tyrc BrdCrCrl (B6 albino wt) mice, were obtained from Charles River (Sulzfeld, Germany). Mice expressing the transgenic OTII T cell receptor (B6-Tg(TcraTcrb)425Cbn) (available at Jackson Laboratories (Bar Harbor, MA)) were generated originally by Barnden et al. [122] and CD11c-YFP mice (C57BL/6 CD11c$^{tm(EYFP\ Venus)_RUNY}$) were generated by Lindquist et al. [147]. All mice were bred under specific pathogen-free conditions at Otto-von-Guericke-University, Magdeburg. For the infection of mice, stationary phase parasites were centrifuged (3500 g, 5 min, RT) and resuspended in PBS. $2x10^6$ parasites were subsequently injected in 10 µl PBS into the ear dermis. Analysis was performed 3 weeks post infection. For intravital 2-photon microscopy analysis of APC-T cell interactions (see chapter 2.3.2) B6 albino wt mice were infected with $2x10^5$ parasites/mouse ear and analysis was performed 9 days post infection.

4.1.2 Microscopy

Intravital Imaging

Mice were anaesthetized by intraperitoneal injection of ketamine (100 mg/kg body weight) and xylazine (10 mg/kg body weight) and prepared for intravital microscopy. To this end, mice were

positioned on a metal plate heated to 37°C and one infected mouse ear was fixed. A parafilm-framed coverslip was fastened onto the mouse ear and covered with water. 2-photon microscopy imaging was performed with a W Plan-Apochromat 20x/1,0 DIC VIS-IR objective on a LSM 700 confocal laser scanning microscope and a Mai Tai DeepSee laser tuned at 920 nm. The emitted signal from the *Lm*^{SWITCH} parasites was split with 625 nm long pass, 495 nm long pass, and 555 nm long pass dichroic mirrors and filtered with 470/20, 525/50 and 600/40 nm filters before collection with nondescanned detectors. SNARF signal of injected T cells was detected with 625 nm long pass dichroic mirror and 640-710 filter. Fluorescence signals of *L.m. dsRed*, YFP and CFP expressing cells were excited with the laser tuned at 880 nm. Signals were split with 520 nm long pass, 490 nm long pass, and 555 nm long pass dichroic mirrors and filtered with 509/22, SP485 and 560-625 nm filters. Typically, imaging volumes of 0.8 */ mm^3 for automated analysis were obtained by collecting 4 µm spaced z stacks using the ZEN acquisition software.

Multi-Epitope Ligand Cartography (MELC)

Ears of mice were harvested and incubated for 2 h at 4°C in 4% paraformaldehyde in PBS before incubation in 20% sucrose in PBS at 4°C overnight. Samples were frozen in Tissue-Tek® O.C.T.™ Compound by liquid nitrogen and stored at -80°C. 10 µm cryosections were transferred on a 0.1% Poly-L-Lysin in H_2O coated Superfrost slides and air-dried. MELC was performed using a MM3.2 Toponome Imaging Cycler (MelTec, Magdeburg) at the Institute of Molecular and Clinical Immunology of the Otto-von-Guericke-University, Magdeburg [120]. In brief, directly labelled antibodies (see chapter 4.2.5) were incubated consecutively and image stacks of the fluorescence signal were acquired by a DMI6000B microscope equipped with a 40x/NA1.25 lens and a KX4 CCD camera resulting in 3D images of 2048 × 2048 × 16 or 8 voxels (voxel size 225 × 225 × 500 or 1000 nm^3). The fluorescence signals were then removed by bleaching of the directly coupled fluorophores. Using the corresponding phase contrast images acquired with every staining cycle, the fluorescence images were automatically aligned voxel-wise with accuracy of 1/10 pixel in XY direction and ½ pixel in Z direction. Illumination faults of the fluorescence images were eliminated using flat-field correction before the resolution of the wide field fluorescent image stacks were improved by applying a deconvolution/deblurring algorithm (XCOSM software package), an interface to Computational Optical Sectioning Microscopy algorithms for removing out-of-focus light in 3D image volumes (Washington University St. Louis, MO).

Confocal microscopy

Ears were harvested and incubated for 2 h at 4°C in 4% paraformaldehyde in PBS before incubation in 20% sucrose in PBS at 4°C overnight. Samples were frozen in Tissue-Tek® O.C.T.™ Compound in liquid nitrogen and stored at -80°C. 10 µm cryosections were prepared, transferred onto Poly-L-Lysin (0.1% in H_2O for coating) coated Superfrost slides and air-dried. Samples were blocked with Fc-block using anti-CD16/32 antibody (1:25) for 30 min and stained with the primary antibody Armenian hamster anti-CD54 (1:100 in PBS) for 30 min at RT. Samples were washed afterwards 3 times with PBS before the secondary antibody DyLight649-conjugated goat anti-Armenian hamster IgG (1:100 in PBS) was added for 1 h at RT in the dark. Analysis was performed by confocal laser scanning microscopy. 488 nm excitation and 491-526 nm emission were used for non-photoconverted mKikumeGR, 561 nm excitation and 571-620 nm emission for photoconverted mKikumeGR, and 633 nm excitation and 640-720 nm for detection of the CD54 staining. Image analysis was done with the Fiji software (NIH, https://imagej.nih.gov/ij/).

4.1.3 Data analysis

MELC image segmentation and analysis

Deconvolved and aligned image stacks (Z vs. XY ratio of 2.5 or 5) of CD11b, CD45 and CD54 stainings were used separately as membrane input, the corresponding propidium iodide staining served as seed input for the Real-time Accurate Cell-shape Extractor (RACE) program developed by Stegmaier et al. [121] with ITK RACE acceleration, SSH Fusion Heuristic and the following settings: Max Threads: 16, Min Closing Radius: 1, Max Closing Radius: 4, Min Seed Area: 1, Min 3D Cell Volume: 3000, and Binary Threshold: 0.00080. Max 2D Segment Areas, Max 3D Cell Volumes, H-Maxima Levels and Slice-by-Slice Watershed Levels were varied according to table 3 in order to identify a maximal number of infected cells and found to be optimal at Max 2D Segment Area: 3000, Max 3D Cell Volume: 10000, H-Maxima Level: 0.5, and Slice-by-Slice Watershed Level: 3.

From the resulting image stacks of gray level-coded 2D objects, regions of interest (ROIs) were generated in three planes spaced 3 micron apart around the Z centre of the stacks using the Fiji software (NIH, https://imagej.nih.gov/ij/). CD11b-seeded stacks were processed first, subsequently, the ROIs were supplemented with RACE data from the CD45-seeded stacks, and finally from the CD54-seeded stacks. The cellular ROIs were used for mKikumeGR fluorescence measurement. 2 pixel (0.4 micron) rim masks generated from the ROIs were used for surface marker measurements. The mean fluorescence of the cellular and rim ROIs were extracted (see appendix supplementary macro 1) for each cell and fluorescence channel.

In order to normalize image-to-image differences in background and overall staining intensity, the individual ROI fluorescence values were normalized

$$100 + \left(100 * \frac{Fluo_{\,ROI} - Fluo_{\,20th\ Percentile,\ all\ ROIs\ in\ image}}{Fluo_{\,80th\ Percentile,\ all\ ROIs\ in\ image}}\right)_{rounded\ to\ the\ nearest\ integer}$$

with the factor and constant 100 introduced in order to obtain positive integers as fluorescence values. The resulting data tables were converted into .fcs files using the DiscIT software [118] and analyzed using the FlowJo software.

For defining fluorescence thresholds for gating within FlowJo, 30 marker-positive and 30 marker-negative cells were selected from images of three different sites of infection and a high-specificity cutoff was defined (i.e. no marker-negative cells in the positive gate).

RACE parameters were optimized in order to detect the largest number of cells and highest percentage of infected cells (Table 3). To this end deconvolved 400 x 400 x 8 micron stacks were segmented with the RACE settings indicated. Three infection sites from different mice (Site1-Site3) and two Z planes per site (ZPl1-ZPl2) were converted into flow cytometry datasets and analyzed as described. The number of total and infected cells detected at each site/plane is indicated in the upper part of the table, the rank within one plane and site is shown in the lower part. The optimized condition is boxed.

Table 3: Optimization of RACE conditions for single cell detection.

Absolute values

Max 2D Segment Area	Max. 3D Cell Volume	H-Maxima Level	Slice-by-Slice Watershed level	Total cells detected						Infected cells detected					
				Site1 ZPl1	Site1 ZPl2	Site2 ZPl1	Site2 ZPl2	Site3 ZPl1	Site3 ZPl2	Site1 ZPl1	Site1 ZPl2	Site2 ZPl1	Site2 ZPl2	Site3 ZPl1	Site3 ZPl2
2000	8000	0.25	1	1389	1123	1559	1421	1460	1647	252	214	299	255	259	303
2000	8000	0.5	3	1595	1162	1642	1481	1524	1740	271	221	308	256	290	333
2000	8000	1	5	1138	777	1390	1130	1105	1460	241	127	248	239	186	257
3000	10000	0.25	1	1505	1165	1634	1804	1491	1716	267	220	325	304	281	326
3000	10000	0.5	3	1573	1190	1636	1500	1566	1760	280	224	318	271	300	331
3000	10000	1	5	1140	798	1468	1168	1148	1546	240	133	271	242	193	277
4000	12000	0.25	1	1529	1172	1653	1459	1519	1760	280	219	325	258	288	336
4000	12000	0.5	3	1549	1189	1711	1531	1541	1783	277	219	329	257	300	335
4000	12000	1	5	1170	802	1417	1180	1155	1506	250	131	258	247	191	267

Ranked values

Max 2D Segment Area	Max. 3D Cell Volume	H-Maxima Level	Slice-by-Slice Watershed level	Total cells detected						Infected cells detected					
				Site1 ZPl1	Site1 ZPl2	Site2 ZPl1	Site2 ZPl2	Site3 ZPl1	Site3 ZPl2	Site1 ZPl1	Site1 ZPl2	Site2 ZPl1	Site2 ZPl2	Site3 ZPl1	Site3 ZPl2
2000	8000	0.25	1	6	6	6	6	6	6	6	6	6	6	6	6
2000	8000	0.5	3	1	5	3	4	3	4	4	2	5	5	3	3
2000	8000	1	5	9	9	9	9	9	9	8	9	9	9	9	9
3000	10000	0.25	1	5	4	5	1	5	5	5	3	2	1	5	5
3000	10000	0.5	3	2	1	4	3	1	2	1	1	4	2	1	4
3000	10000	1	5	8	8	7	8	8	7	9	7	7	8	7	7
4000	12000	0.25	1	4	3	2	5	4	2	1	4	2	3	4	1
4000	12000	0.5	3	3	2	1	2	2	1	3	4	1	4	1	2
4000	12000	1	5	7	7	8	7	7	8	7	8	8	7	8	8

Condition rank: best 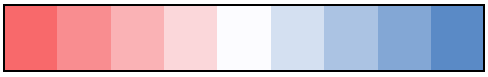 worst

Proliferation analysis

The relative proliferation index of *L. major* within the different cell populations for both flow cytometry and MELC was defined as

$$1 - \frac{\left(\frac{mKikume\ Red}{mKikumeGreen}\right)_{cell}}{\left(\frac{mKikumeRed}{mKikumeGreen}\right)_{mean\ (all\ infected\ cells)}}$$

and represented as percent deviation from the total infected cell population within one sample or imaged infection site. For visualizing qualitative comparisons within the same sample using the FlowJo software, values were plotted as

$$C - \frac{100 * \left(\frac{mKikume\ Red}{mKikumeGreen}\right)_{cell}}{\left(\frac{mKikumeRed}{mKikumeGreen}\right)_{mean\ (all\ infected\ cells)}}$$

with chosen C between 100 and 250 and kept constant within the same sample for which the comparison was made, and the factor 100 introduced in order to analyze integer fluorescence values in FlowJo.

For *in vitro* determination and inter-experiment standardization of proliferation indices, a non-photoconverted (green control) and fully photoconverted (0 h recovery from photoconversion, red control) sample were measured with each experiment, and for each infected cell, the proliferation index was defined as

$$10 - \frac{100 * \left(\frac{mKikume\ Red}{mKikumeGreen}\right)_{cell} - 100 * \left(\frac{mKikume\ Red}{mKikumeGreen}\right)_{mean\ (all\ infected\ cells,\ \ green\ control)}}{100 * \left(\frac{mKikume\ Red}{mKikumeGreen}\right)_{mean\ (all\ infected\ cells,\ \ red\ control)} - 100 * \left(\frac{mKikume\ Red}{mKikumeGreen}\right)_{mean\ (all\ infected\ cells,\ \ green\ control)}}$$

with the factor 100 introduced in order to analyze integer fluorescence values in FlowJo, and the constant 10 in order to obtain positive values.

Analysis of T cell-APC interactions via 2-photon microscopy

Imaging data from intravital APC-T cell interactions (see Chapter 2.3.2) were analyzed via Imaris and Fiji software. Resting T cells were defined by running a heatmap generating macro script which was self-designed within Fiji (see appendix supplementary macro 3). Afterwards, the grey values of combined red and green fluorescence signals (see Intravital Imaging) of *Leishmania* overlapping with these of resting T cells and of non-overlapping *Leishmania* were extracted via the Imaris software. Subsequently, proliferation indices of *Leishmania* that are in contact with T cells were calculated and normalized to the average proliferation index of all imaged parasites at the site of infection.

Statistical Analysis

Spearman correlations and all comparisons between groups were calculated using the Prism 7 software. Statistical analysis of multiple cell populations was performed with one-way analysis of variance (ANOVA) with a Tukey post-test for multiple cross-comparisons, or a Bonferroni post-test for comparison with a control condition, respectively. To analyze the impact of two different independent variables related to a continual dependent variable, two-way ANOVA tests were performed, followed by a Bonferroni test. Comparisons with only two experimental conditions were performed using a Mann Whitney test. P values under 0.05 were regarded as significant and marked with an asterisk. P values lower than 0.01 or 0.001 were hence allocated two or three asterisks, respectively.

4.1.4 Immunological Methods

Photoconversion

Lm^{SWITCH} parasites in the mouse ear were photoconverted with violet light at 405 nm wavelength with an assembly of 2x2 LED diodes (half-viewing angle: 15°; Radiant Power:

10 mW) spaced 5 mm apart. For this, the ears of anaesthetized mice were fixed and illuminated from each side for 1 minute in a distance of 1.3 cm. The photoconverted parasites were analyzed after 48 h by flow cytometry, multi-epitope ligand cartography, confocal microscopy or intravital microscopy. For *in vitro* analysis of *de novo* infection, parasites were photoconverted in 24-well plates via illumination with 405 nm wavelength with an assembly of 3x3 diodes for 1 minute and analyzed after 24 h via flow cytometry.

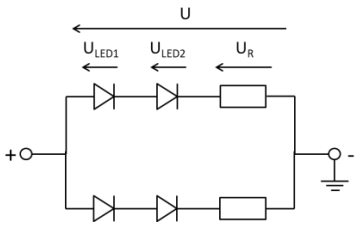

Figure 27: Diode array for photoconversion of *L.m.*^{SWITCH}. LED specifications: Wavelength; 405 nm; Half-viewing angle: 15°; Radiant Power: 10 mW; Forward current: 30 mA; Forward Voltage: 3.8 V.

Flow cytometry

Ears of mice were separated in two sheets (ventral and dorsal) using forceps and enzymatically digested in RPMI 1640 medium containing 1 mg/ml collagenase and 50 ng/ml DNase for 60 min at 600 rpm and 37°C and passed through a 70 µm cell strainer. Cells were centrifuged at 4°C with 300 g for 10 min. Afterwards, cells were washed with PBS and FACS buffer before surface staining of cells was done by using surface marker specific antibodies (see chapter 4.2.5). Samples were blocked with Fc-block using anti-CD16/32 antibody (1:25 in FACS buffer) for 15 min on ice before the antibody staining. Antibodies were applied with a final concentration of 1:200. *Lm*^{SWITCH} infections were analyzed with a FACS ARIA III flow cytometer/sorter using lasers at 405 nm, 488 nm, 561 nm, and 633 nm. Mice infected with *L.m. dsRed* were analyzed using a FACS Fortessa flow cytometer using lasers at 405 nm, 488 nm, and 633 nm. Photoconverted or non-photoconverted mKikumeGR fluorescence was read out at 561 nm excitation and 610/20 nm emission, or 488 nm excitation and 530/30 nm emission, respectively. An autofluorescence signal was recorded at 488 excitation and 695/40 nm emission. Data were analyzed by using the FlowJo X software.

Bone marrow isolation and cell transfer

Bone marrow cells were isolated from tibia and femur of mice and passed through a 70 µm cell strainer. After centrifugation at 4°C with 300 g for 10 min 8-10 x 10^7 cells were resuspended in 300 µl PBS and intravenously injected into the recipient mice 2 or 5 days before the analysis.

Cell culture infections

Isolated bone marrow cells (see Bone marrow isolation and cell transfer) from either C57BL/6 or CD45.1 wt mice were filtered through a 70 µm cell strainer in PBS before they were differentiated *in vitro* into macrophages and DCs. For differentiation of macrophages, cells were centrifuged at RT with 300 g for 5 min and plated in RPMI 1640 supplemented with 10% FCS and 20% 3T3 cell culture supernatant and incubated at 37°C and 5% CO_2. Three days later, the medium was exchanged for fresh medium and after another four days of incubation macrophages were harvested by taking the medium and incubating the cell culture plate afterwards with for 15 min at 37°C with trypsin. Harvested macrophages were used for infection experiments. DCs were differentiated by culturing isolated bone marrow cells in BM-DC medium (1x NEAA, 5% FCS, 2 mM L-Glutamin, 50 µM β-Mercaptoethanol, 50 µg/ml Gentamycin, 100 U/ml IL-4, 255 U/ml GM-CSF) at 37°C and 5 % CO_2 for three days. Afterwards, the medium was exchanged for fresh medium and after another four days of incubation DCs were harvested by collecting the medium and incubating the cell culture plate afterwards for 15 min at 37°C with trypsin. DCs were then used for infection experiments.

For infection, differentiated macrophages and DCs from C57BL/6 mice (CD45.2) were pooled in a ratio of 1:1 and *Lm*^{SWITCH} stationary phase promastigotes (opsonized with 5% mouse immune serum for 30 min at 26°C) were added with a MOI of 5. 24 h later, parasites were photoconverted (see Photoconversion). Cells were induced with IFNγ (0.01 ng/µl) and LPS (1 µg/ml) and optionally, the nitric oxide synthase iNOS was inhibited by addition of 0.023 µg/µl N6-(1-iminoethyl)-L-lysine hydrochloride (L-NIL). After another 24 h, a 1:1 mixture of CD45.1 macrophages and DCs was added to the cell culture. After 5 h of coculture at 37°C and 5 %, cells were analyzed by flow cytometry. For isolation of peritoneal macrophages mice were sacrificed and subsequently 5 ml of cold PBS were injected intraperitoneally. The cell suspension was aspirated and cells were seeded in RPMI 1640 supplemented with 10% heat-inactivated fetal bovine serum for infection and live cell imaging. Time-lapse microscopy of cell culture infections was performed with the use of a DMI6000B inverted microscope or a CellR imaging workstation using an upright microscope stage (BX61) equipped with a 20x dry objectives. Images were automatically acquired every 10 minutes and movies were processed with the Fiji software (NIH, https://imagej.nih.gov/ij/).

Limiting dilutions

Limiting dilutions were performed to analyze parasite burden in the infected ear tissue. To do so, 10% of cell suspension that was obtained from squeezing the enzymatically digested ears of *L. major* infected mice through a 70 µM cell strainer (see Flow cytometry) were centrifuged (3500 g, 5 min, RT) and resuspended in complete M199 medium. Afterwards parasites were

diluted 16 times in 1:2 steps and cultured in 100 µl complete M199 medium in parafilm-sealed 96-well plates. This dilution was performed in quadruplicates for every sample. Plates were incubated for 2 weeks before parasite growth within the single wells was read out via transmitted light microscopy.

Construction of bone marrow chimera

Recipient mice were anesthetized and irradiated with 13 Gy. Bone marrow cells were isolated from tibia and femur of two different donor mice and a 1:1 mixture of 2-3 x 10^7 bone marrow cells from both donor mice were injected intravenously into recipient mice. After 8 weeks mice were infected with *L. major*.

Depletion of CD11c cells in mice

To enable depletion of $CD11c^+$ cells in CD11c-GFP-DTR mice infected with *L.m. dsRed,* 100 ng/25 g mouse weight of diphtheria toxin was injected intraperitoneally 48 h prior to analysis. Depletion efficiency was validated by flow cytometry analysis of GFP and CD11c surface staining of cells isolated from the site of infection.

$CD4^+$ T cell isolation and Th1 differentiation

Inguinal, axial, cervical lymph nodes and the spleen were harvested from OT-II mice. $CD4^+$ T cells were isolated via the CD4 T cell negative isolation Kit. Subsequently cells were seeded in 24 well plates (2 million/well) with RPMI+10%FCS+1% P/S+10 µg/ml anti IL4 + 10 ng/ml IL12 and incubated at 37°C and 5% CO_2 for 72 h. Plates were coated in advance over night at 4°C with 3 µg/ml anti CD3 und 5µg/ml anti CD28 in 1xPBS. After 72 h cells were diluted 1:1 in warm cell culture medium, split into two wells and incubated for additional 24 h at 37°C and 5% CO_2.

T cell labelling

Differentiated T cells were centrifuged (10 min, 300 g, 4°C), washed with PBS and resuspended in PBS (10 million/ml). SNARF diluted in DMSO was added in a final concentration of 1:4000 and incubated for 10 min at 37°C. The labelling reaction was stopped by addition of 10% FCS. Afterwards the samples were centrifuged again and washed with 10% FCS in PBS. Subsequently cells were washed again with PBS and resuspended in an appropriate amount of PBS for intravenous injection into infected mice.

4.1.5 Molecular biology Techniques

Construction of new L. major strains (Transfection of L. major)

Genes of interest were incorporated into the *Leishmania* DNA via homologous recombination. Therefore, specific genes were cloned into the pLEXSY hyg2 vector, 30-40 µg DNA were then linearized by enzymatic digestion with SwaI (NEB). Molecules were separated and purified via agarose gel electrophoresis and *L. major* were subsequently electroporated with the purified DNA. For this, *Leishmania* culture was centrifuged and afterwards washed and resuspended in cytomix buffer before 5 µg of the purified DNA were added to the parasites and cells were electroporated two times with a break of 10 sec with a capacity of 25 µF and a voltage of 1500 V. Electroporated parasites were cultured as described above for 24 h and subsequently each time 10 µl were plated in 12 well plates filled up with 2 ml complete M199 medium, additionally appropriate antibiotics were added. *Leishmania* cultures were sealed air-tight and incubated for 2 weeks at 26°C before they were screened by transmitted light microscopy for efficient plasmid incorporation. From wells in which parasite growth could be observed, limiting dilutions (see Limiting dilutions) were performed to obtain single clones. Afterwards 40.000.000 *L. major*/ml were stored in 90% FCS and 10% glycerol at -180°C in liquid nitrogen.

Enzymatic digestion of nucleotide sequences

Specific digestion of DNA was implemented by the use of appropriate restriction enzymes from NEB. Reaction conditions were thereby chosen according to information of the manufacturer.

In this study, the HASPB-OVA sequence as well as a neomycin resistance cassette Neo^R were inserted into the pLEXSY-Hyg2 (from Jena Biosciences) vector. To this end, the PCR amplified Neo^R gene (see Polymerase Chain Reaction (PCR)) from an pEYFP-N1 vector (Clontech) (see Vectors and constructs) was first ligated into pS001-pLEXSY_blemKikume (contructed in the laboratory of Andreas Müller from the plasmid pLEXSY_I-blecherry3 and the insert mKikumeGR, which was originally amplified from the pEX-KikumeGR plasmid). Therefore, PCR product and pS001-pLEXSY_blemKikume were digested with BamHI and SpeI. In parallel HASPB-OVA sequence, *de novo* synthesized according to Prickett et al., from Eurofins Genomics, was cloned into pLEXSY-Hyg2 via the restriction sites BGlII and NotI leading to the pS002- pLEXSY_hyg2_HASPb_OVA plasmid. Subsequently, the generated plasmids were enzymatically digested with SpeI and NotI to ligate the Neo^R gene into the pS002-pLEXSY_hyg2_HASPb_OVA. Therefore, the pLEXSY_NEO_HASPb_OVA vector was generated.

Enzymatically digested vectors were dephosphorylated after enzymatic digestion by addition of 1 µl antarctic phosphatase (NEB) to the batch. Samples were incubated for 10 min at 37°C

and the phosphatase was inactivated afterwards for 5 min at 75°C. For efficient transfection of *Lm*^{SWITCH} pLEXSY_NEO_HASPb_OVA was digested with SwaI (see Construction of new *L.* major strains (Transfection of *L. major)*). Afterwards samples were analyzed via agarose gel electrophoresis (see Agarose gel electrophoresis).

Polymerase Chain Reaction (PCR)

PCR was used to amplify a neomycin resistance cassette from pEYFP-N1 vector (Clontech) with appropriate restriction sites for cloning into a pLEXSY_hyg2 vector (from Jena Bioscience). An additional sequence was integrated into the sequence of the forward primer to amplify a Neo^{R} gene as used by Jena Bioscience in the pLEXSY system. Template DNA (pEYFP-N1 vector) (100 ng/µl) was mixed with Coral Load Buffer (1x), Q-Solution (1x), dNTPs (10 mM), forward and reverse primers (10 mM) and Taq-polymerase (Qiagen). DNA samples were incubated in a gradient cycler. 34 cycling steps were performed with 94°C denaturing temperature for 30 sec, 58°C annealing temperature for 30 sec and 72°C extending temperature for 1 min. PCR products were controlled via agarose gel electrophoresis (see Agarose gel electrophoresis).

Ligation

The HASPB-OVA sequence with appropriate restriction sites (see Enzymatic digestion of nucleotide sequences) was ligated into a pLEXSY_hyg2 vector, therefore pS002-pLEXSY_hyg2_HASPb_OVA was generated. Additionally, amplified Neo^{R} gene was ligated into the enzymatically digested pS001-pLEXSY_blemKikume vector (see Vectors and constructs). Afterwards the neomycin resistance cassette was enzymatically digested and Neo^{R} gene was ligated into the pS002- pLEXSY_hyg2_HASPb_OVA vector to generate pLEXSY_NEO_HASPb_OVA, whereby the hygromycin resistance cassette (hyg2) was exchanged by the neomycin resistance. A insert/vector molecule ratio of 5/1 was used and mixed with T4 ligation buffer (1x) and T4 ligase (NEB). Samples were incubated for 3 h at RT or at 16°C over night, before *E. coli* was transformed with the generated constructs (see Transformation of *E. coli*).

Transformation of E. coli

Transformation of *E. coli* was done with NEB 5-alpha competent *E. coli* cells. For transformation of chemically competent *E. coli* cells, 200 µl of cells were mixed with 1-5 µl of 1 pg-100 ng of the appropriate DNA and incubated on ice for 30 min. Following the heat-shock at exactly 42°C for 30 sec and cooling on ice for 1-2 min. 500 µl SOC-medium was added to

the cells and incubated for 1 h at 220 rpm and 37°C. Subsequently bacteria were plated on LB agar and incubated over night at 37°C on appropriate antibiotics.

Mini- and Maxi-DNA preparation from E. coli

Mini-DNA preparation was done by using the Plasmid Mini Prep-Kits according to manufacturer´s conditions. For Maxi-DNA preparation the NucleoBond® PC 500 EF Kit was used according to manufacturer´s instructions.

Agarose gel electrophoresis

For DNA analysis samples were mixed with 5 x DNA loading dye. DNA fragments were subsequently loaded on a cured 1% agarose gel which was produced in heated TAP buffer and dosed with 1 µg/ml ethidium bromide. Agarose gel was placed in a BIO-RAD Mini DNA system which was filled with TAP buffer at 100 V. DNA fragments were visualized by UV light with the gel documentation station. Quick-Load® 2-Log DNA Ladder (0,1 – 10,0 kb) (NEB) was used to analyze the size of the DNA fragments.

DNA extraction from agarose gels

DNA extraction from agarose gels was done by using the Nucleo Spin® Extract II Kit according to manufacturer's conditions.

DNA concentration

To determine DNA concentration, DNA was dissolved in ddH_2O and concentration was measured via NanoDrop 2000 spectrophotometer.

4.1.6 Biochemical Methods

Sodium dodecyl sulfate polyacrylamide gel electrophoresis (SDS PAGE)

Protein expression was analyzed via discontinuous procedure published by Laemmli [148]. Separating gels (2.25 ml 4x separating buffer, 4.5 ml acrylamid/bisacrylamid (37.5%), 60 µl APS, 10 µl TEMED, 2.25 ml ddH_2O) had an amount of 15% acrylamide. These were overlayed by a stacking gel of 4% acrylamide (1.05 ml 4x stacking buffer, 0.65 ml acrylamid/bisacrylamid (37.5%), 30 µl APS, 10 µl TEMED, 2.57 ml ddH_2O). *Leishmania* were centrifuged (3500 g, 5 min, RT) before they were resuspended in lysis buffer, incubated for 30 min on ice and centrifuged for 10 min at 15.000 g. Supernatant was taken and mixed with 5x SDS-loading buffer before samples were incubated for 10 min at 100°C. After applying the samples onto the gel, the electrophoretic separation in a Mini-PROTEAN II unit with 100 V (stacking gel) and

130 V (separating gel) was ensued. As marker the PageRuler Plus Prestained Protein Ladder was used. Afterwards gels were used for western blot analysis (see Western Blot).

Western Blot

After electrophoretic separation, proteins were immobilized via a semi-dry western blotting device on nitrocellulose membranes (Hybond-C Extra). Transfer was implemented using a Mini-PROTEAN II unit according to manufacturer's information. The device was run with 140 mA for 1 h. When the transfer was completed, nitrocellulose membrane was blocked slowly shaking for 30 min in 3% BSA in PBS. Afterwards membranes were washed 3 x in PBS with 0,05% Tween (PBS-T). This was followed by adding the primary antibody, polyclonal anti-OVA antibody, 1:4000 in TBS-T for 1 h at RT shaking slowly, before membranes were washed again 3 x with PBS-T under fast shaking conditions. Secondary antibody, peroxidase conjugated affinity pure goat anti-rabbit IgG, was added then 1:10.000 in PBS-T, slowly shaking for 1 h at RT. Membranes were washed 3 x in PBS-T subsequently. The membranes were then developed by incubating with Thermo Scientific Western Blotting Substrate according to manufacturer´s instructions. Signals from peroxidase were detected by the use of hyperfilms and the developing machine Cawomat 2000IR.

4.2 Materials

4.2.1 Used nucleotide sequences (primers and vectors)

Primers

Name	Nucleotide sequence
Neo_pEYFP_fw	GCTTACGGATCCAATATGGGATCGGCCATTGAACAAGATGGATTGCACG
Neo_pEYFP_rev	GCTAACACTAGTTCAGAAGAACTCGTCAAGAAGGC

Vectors and constructs

Name	Source
pEX-K4-HASPbOVA	Eurofins Genomics
pS001-pLEXSY_blemKikume	generated in the laboratory of Andreas Müller (Magdeburg) out of pLEXSY_I-blecherry3 (Jena Bioscience) and the insert mKikumeGR, which was originally amplified from the pEX-KikumeGR plasmid
pLEXSY-Hyg2	Jena Bioscience
pLEXSY_I-blecherry3	Jena Bioscience
pS002-pLEXSY_hyg2_HASPb_OVA	generated by Sandrina Heyde (see Ligation and Enzymatic digestion of nucleotide sequences)
pEYFP-N1	Clontech
pLEXSY_NEO_HASPb_OVA	generated by Sandrina Heyde (see Ligation and Enzymatic digestion of nucleotide sequences)

4.2.2 Buffers

Cytomix

KCl	120 mM
$CaCl_2$	0.15 mM
HEPES (pH 7.5)	25 mM
EDTA	2 mM
$MgCl_2$	5 mM
K_2HPO_4	10 mM

Fill up with ddH_2O.

pH 7.6

Lysis buffer

NaCl	0.5 M
$MgCl_2$	0.1 M
Tris (pH 7.4)	0.5 M
EDTA	50 mM
protease inhibitor cocktail tablet (Roche)	0.5/ml

Fill up with ddH_2O.

PBS

NaCl	140 mM
KCl	2.7 mM
Na_2HPO_4	8 mM
KH_2PO_4	1.8 mM

pH 7,4

Fill up with ddH_2O.

FACS/MACS

FCS	0.5% (w/v)
EDTA	2.5 mM

Fill up with PBS.

4 x Stacking buffer

Tris	30.2 g
SDS	2 g
ddH_2O	500 ml

pH 6.8

Separating buffer

Tris	90.75 g
SDS	2 g
ddH_2O	500 ml

pH 8.8

5x SDS-loading buffer

glycerol	50% (w/v),
Tris	100 mM
SDS	5% (w/v)
bromophenol blue	1% (w/v)
β-mercaptoethanol	10% (v/v)

Fill up with ddH_2O.

Running Buffer (10x)

Glycine	288 g
Tris	60 g
SDS	20 g

Fill up with ddH_2O to 2 l.

Transfer Buffer (1x)

Glycine	32.5 g
Tris	5 g
Methanol	400 ml

Fill up with ddH_2O to 2 l.

TBS-T

NaN_3	0.02%
Tween	0.05%
BSA	0.5%
Tris/HCl (pH 7.5)	50 mM
NaCl	150 mM

Fill up with ddH_2O.

TAP Buffer

Tris	242 g
37 % acidic acid	57.1 ml
EDTA	37.3 g

Fill up with ddH_2O to 100 ml.

4.2.3 Kits

Kit	Supplier
$CD4^+$ T cell isolation kit, mouse	Miltenyi Biotec
Nucleo Spin® Extract II	MACHEREY-NAGEL
Peroxidase detection Kit	Thermo Fisher Scientific
Plasmid Mini Prep-Kit	Qiagen
NucleoBond® PC 500 EF Kit	MACHEREY-NAGEL

4.2.4 Software

Software	Source/Supplier
deconvolution/deblurring algorithm	XCOSM software package
DiscIT	Reference [118]
Fiji software	NIH, http://rsb.info.nih.gov/ij/
FlowJo X software	FlowJo, LLC
Imaris	Bitplane
Prism 7 software	GraphPad Inc. Software
RACE tool	Reference [121]
ZEN acquisition software	Zeiss

4.2.5 Antibodies

Antibody specifity	Clone/ Clonality	Supplier	Dilution from commercial stock	Label
CCR2	SA203G11	Biolegend	1:200	FITC
CD3	145	Biolegend	3 µg/ml	non-labelled
CD11b	M1/70	eBioscience	1:80	Alexa 488
CD11b	M1/70	Biolegend	1:200	APC
CD11b	M1/70	Biolegend	1:200	APC-Cy7
CD11c	N418	eBioscience	1:40	Alexa 488
CD11c	N418	Biolegend	1:80	Alexa 488
CD11c	N418	Biolegend	1:200	APC
CD11c	N418	Biolegend	1:200	APC Fire
CD11c	N418	Biolegend	1:200	PeCy7
CD16/32	93	Biolegend	1:25	non-labelled
CD28	2C1137.51	Biolegend	5 µg/ml	non-labelled
CD45	30-F11	Biolegend	1:200	PerCP Cy5.5
CD45	30-F11	BD Bioscience	1:240	FITC
CD45.1	A20	Biolegend	1:200	APC
CD45.1	A20	Biolegend	1:200	APC-Cy7
CD45.1	A20	Biolegend	1:200	BV510
CD45.1	A20	Biolegend	1:200	PerCP Cy5.5
CD45.2	104	Biolegend	1:200	APC

Antibody specifity	Clone/ Clonality	Supplier	Dilution from commercial stock	Label
CD45.2	104	Biolegend	1:200	APC-Cy7
CD45.2	104	Biolegend	1:200	BV510
CD45R	RA3-6B3	BD Bioscience	1:240	Alexa 488
CD54 (armenian hamster)	3E2	BD Biosciences	1:100	non-labelled
CD86	GL-1	Biolegend	1:80	Alexa 488
class II MHC	M5/114.15.2	Biolegend	1:200	BV510
class II MHC	2G9	BD Bioscience	1:500	FITC
F4/80	BM8	Biolegend	1:200	BV421
F4/80	BM8	eBioscience	1:240	Alexa 488
Ly6C	HK 1.4	Biolegend	1:200	PeCy7
goat anti-Armenian hamster IgG (H+L)	polyclonal	Jackson ImmunoResearch	1:200	DyLight649
ICAM-1	YN1/1.7.4	Biolegend	1:120	Alexa 488
IL-4 (LEAF purified)	11B11	Biolegend	10 µg/ml	non-labelled
ovalbumin	polyclonal	Abcam	1:4000	non-labelled
peroxidase conjugated affini pure goat anti-rabbit IgG	polyclonal	Jackson Immuno Research	1:10000	peroxidase conjugated
propidium iodide		Sigma	1:5000	non-labelled

4.2.6 Biochemical and chemical reagents

Reagents	Source/Supplier
2-Propanol	Carl Roth
3T3 supernatant	obtained from 3T3 fibroblast cell line provided by *Helmholtz Zentrum für Infektionsforschung*, Braunschweig
Acetic acid (96% v/v)	Carl Roth
Acrylamide/BIS 37.5%/1%	Carl Roth
Adenine	Sigma
Ampicillin	Carl Roth
Ammoniumpersulfat (APS)	Carl Roth
Chloramphenicol	Carl Roth
BD FACS Flow™ Sheath Fluid	BD Bioscience
BD FACS™ Clean Solution	BD Bioscience
BD FACS™ Rinse Solution	BD Bioscience
BD Perm/Wash	BD Bioscience
Biopterin	Sigma
Biotin	Sigma
BM-DC medium (1x NEAA)	Gibco
β-Mercaptoethanol	Gibco
Bovine Serum Albumin (BSA) fraction V PAA	NEB
Bromophenol Blue	Carl Roth
Calciumchloride ($CaCl_2$)	Carl Roth
Collagenase	Sigma

Reagents	Source/Supplier
Coral Load Buffer	Qiagen
Deoxyribonucleoside triphosphate (dNTP) Set	Thermo Fisher Scientific
Dimethyl sulfoxide (DMSO)	Carl Roth
Diphtheria toxin	Sigma
DNA loading dye	Fermentas
DNase	Sigma-Aldrich
Ethanol (99% v/v)	Carl Roth
Ethidium bromide	Carl Roth
Ethylenediaminetetraacetic acid (EDTA)	Carl Roth
Fetal Calf Serum (FCS)	Pan Biothech GmbH
Gentamycin	Gibco
Glycerol	Carl Roth
GM-CSF	obtained from supernatant produced by cell lines, produced in the lab of Thomas Blankenstein, MDC, Berlin
Hemin	Sigma
IL-12 (p70), recombinant mouse	BioLegend
IL-4	obtained from supernatant produced by cell lines, produced in the lab of Thomas Blankenstein, MDC, Berlin
IFNγ	R&D Systems
Ketamine	Medistar
L-Glutamin	Gibco
LB Agar	Carl Roth
LB Medium	Carl Roth

Reagents	Source/Supplier
L-Glutamin	Gibco
LPS (1µg/ml, E. coli O26:B6)	Sigma-Aldrich
M119 medium	Biochrom
Mouse Immune Serum	recovered from *L. major* infected mice
NEAA	Gibco
N6-(1-iminoethyl)-L-lysine hydrochloride (L-NIL)	Sigma-Aldrich
PageRuler Plus Prestained Protein Ladder	Thermo Fisher Scientific
Paraformaldehyde (PFA)	Carl Roth
PBS Dulbecco (phosphate-buffered saline, without (w/o) Ca2+, Mg2+)	Biochrom AG
Penicillin/Streptomycin (10000U/10000µg/ml)	Biochrom AG Carl Roth
Poly-L-Lysin	Sigma-Aldrich
Q-Solution	Qiagen
Quick-Load® 2-Log DNA Ladder (0,1 – 10,0 kb)	NEB
1 Carboxylic Acid, Acetate, Succinimidyl Ester (SNARF)	Invitrogen
RPMI 1640 medium	Merck
Sea Kem Le Agarose	BMA
Serva 4-(2-hydroxyethyl)-1-piperazineethanesulfonic acid (HEPES)	Carl Roth
SOC-medium	NEB
Sodium azide (NaN3)	Carl Roth
Sodium chloride (NaCl)	Carl Roth
Sodium dodecyl sulfate (SDS)	Carl Roth

Reagents	Source/Supplier
Sucrose	Carl Roth
T4 ligation buffer	NEB
Tertamethylethylenediamine (TEMED)	Carl Roth
Tissue-Tek® O.C.T.™ Compound	Sakura
Tris (hydroxymethyl)-aminomethan (Tris)	Carl Roth
Triton X-100	Sigma-Aldrich
Trypane Blue Solution (0.4%)	Sigma-Aldrich
Trypsine/EDTA	Merck Millipore
Tween 20	Carl Roth
Xylazine (Rompun 2%)	Bayer

4.2.7 Technical equipment

Equipment	Supplier
2-Photon LSM 700 confocal laser scanning microscope	Zeiss
Cawomat 2000IR	CAWO
CellR imaging workstation	Olympus
Centrifuges	Hereaus
Confocal microscope TCS SP8 Confocal	Leica
DMI6000B microscope equipped with a 40x/NA1.25 lens and a KX4 CCD camera	Leica, Apogee Instruments
Electrophoresis system Mini-PROTEAN® 3 Cell	BIO-RAD
Electrophoresis Mini DNA system	BIO-RAD
FACS Fortessa	BD Biosciences

Equipment	Supplier
Gel documentation station (camera: E.A.S.Y. B-455-F)	Herolab
Gradient Cycler	BIO-RAD
Hyperfilms	Amersham
Incubator Hera Therm	Thermo Fisher Scientific
Incubator Hera Cell 150, CO_2 Incubator	Thermo Fisher Scientific
LED diodes	Strato
Mai Tai DeepSee laser	Spectra-Physics
Milli-Q® Integral Water Purification System	Merck Millipore
NanoDrop 2000 spectrophotometer	Thermo Fisher Scientific
Nitrocellulose membranes, Hybond-C Extra	Amersham
Semi-dry western blotting device	PEQLAB
Sorter FACS ARIA III	BD Biosciences
Superfrost slides	Thermo Scientific
Time-lapse microscopy DMI6000B inverted microscope	Leica Microsystems
MM3.2 Toponome Imaging Cycler	MelTec, Magdeburg
Upright microscope stage (BX61)	Olympus
W Plan-Apochromat 20x/1,0 DIC VIS-IR objective	Zeiss

5 References

1. Murphy KP, Travers P, Walport M, Janeway C, Seidler L et al. (2009) Janeway Immunologie. Heidelberg: Spektrum Akademischer Verlag. 1093 p.
2. Kaye P, Scott P (2011) Leishmaniasis. Complexity at the host-pathogen interface. Nature reviews. Microbiology 9 (8): 604–615.
3. Frederick P. Heinzel, Michaeld. Sadick, Bettie J. Holaday, Robert L. Coffmanj and Richard M. Locksley (1989) Reciprocal Expression of Interferon y OR Interleukin 4 during the Resolution or Progression of Murine Leishmaniasis. Evidence for Expansion ofDistinct Helper T Cell Subsets. Journal of Experimental Medicine (169): 59–72.
4. Sacks D, Noben-Trauth N (2002) The immunology of susceptibility and resistance to Leishmania major in mice. Nature reviews. Immunology 2 (11): 845–858.
5. Rogers KA, DeKrey GK, Mbow ML, Gillespie RD, Brodskyn CI et al. (2002) Type 1 and type 2 responses to Leishmania major. FEMS microbiology letters 209 (1): 1–7.
6. Scott P, Novais FO (2016) Cutaneous leishmaniasis. Immune responses in protection and pathogenesis. Nature reviews. Immunology 16 (9): 581–592.
7. Stamm LM, Räisänen-Sokolowski A, Okano M, Russell ME, David JR et al. (1998) Mice with STAT6-targeted gene disruption develop a Th1 response and control cutaneous leishmaniasis. The Journal of Immunology 161 (11): 6180–6188.
8. Moura TR de, Novais FO, Oliveira F, Clarêncio J, Noronha A et al. (2005) Toward a novel experimental model of infection to study American cutaneous leishmaniasis caused by Leishmania braziliensis. Infection and immunity 73 (9): 5827–5834.
9. Qi H, Popov V, Soong L (2001) Leishmania amazonensis-Dendritic Cell Interactions In Vitro and the Priming of Parasite-Specific CD4+ T Cells In Vivo. Journal of immunology (Baltimore, Md. : 1950) 167 (8): 4534–4542.
10. Ji J, Sun J, Qi H, Soong L (2002) Analysis of T helper cell responses during infection with Leishmania amazonensis. The American journal of tropical medicine and hygiene 66 (4): 338–345.
11. Dostálová A, Volf P (2012) Leishmania development in sand flies. Parasite-vector interactions overview. Parasites & vectors 5: 276.
12. Giraud E, Lěstinová T, Derrick T, Martin O, Dillon RJ et al. (2018) Leishmania proteophosphoglycans regurgitated from infected sand flies accelerate dermal wound repair and exacerbate leishmaniasis via insulin-like growth factor 1-dependent signalling. PLoS pathogens 14 (1): e1006794.
13. Rogers M, Kropf P, Choi B-S, Dillon R, Podinovskaia M et al. (2009) Proteophosophoglycans regurgitated by Leishmania-infected sand flies target the L-

arginine metabolism of host macrophages to promote parasite survival. PLoS pathogens 5 (8): e1000555.

14. McConville MJ, Naderer T (2011) Metabolic pathways required for the intracellular survival of Leishmania. Annual review of microbiology 65: 543–561.
15. van Assche T, Deschacht M, da Luz RAI, Maes L, Cos P (2011) Leishmania-macrophage interactions: insights into the redox biology. Free radical biology & medicine 51 (2): 337–351.
16. Belkaid Y, Mendez S, Lira R, Kadambi N, Milon G et al. (2000) A natural model of Leishmania major infection reveals a prolonged "silent" phase of parasite amplification in the skin before the onset of lesion formation and immunity. Journal of immunology (Baltimore, Md. : 1950) 165 (2): 969–977.
17. Liu D, Uzonna JE (2012) The early interaction of Leishmania with macrophages and dendritic cells and its influence on the host immune response. Frontiers in cellular and infection microbiology 2: 83.
18. Forestier C-L, Gao Q, Boons G-J (2014) Leishmania lipophosphoglycan: how to establish structure-activity relationships for this highly complex and multifunctional glycoconjugate. Frontiers in cellular and infection microbiology 4: 193.
19. Muraille E, Gounon P, Cazareth J, Hoebeke J, Lippuner C et al. (2010) Direct visualization of peptide/MHC complexes at the surface and in the intracellular compartments of cells infected in vivo by Leishmania major. PLoS pathogens 6 (10): e1001154.
20. Segawa H, Soares RP, Kawakita M, Beverley SM, Turco SJ (2005) Reconstitution of GDP-mannose transport activity with purified Leishmania LPG2 protein in liposomes. The Journal of biological chemistry 280 (3): 2028–2035.
21. McConville MJ, Mullin KA, Ilgoutz SC, Teasdale RD (2002) Secretory Pathway of Trypanosomatid Parasites. Microbiology and Molecular Biology Reviews 66 (1): 122–154.
22. McCall L-I, Matlashewski G (2010) Localization and induction of the A2 virulence factor in Leishmania. Evidence that A2 is a stress response protein. Molecular microbiology 77 (2): 518–530.
23. Contreras I, Gómez MA, Nguyen O, Shio MT, McMaster RW et al. (2010) Leishmania-induced inactivation of the macrophage transcription factor AP-1 is mediated by the parasite metalloprotease GP63. PLoS pathogens 6 (10): e1001148.
24. Cameron P, McGachy A, Anderson M, Paul A, Coombs GH et al. (2004) Inhibition of Lipopolysaccharide-Induced Macrophage IL-12 Production by Leishmania mexicana Amastigotes. The Role of Cysteine Peptidases and the NF-κB Signaling Pathway. Journal of immunology (Baltimore, Md. : 1950) 173 (5): 3297–3304.

25. Rub A, Dey R, Jadhav M, Kamat R, Chakkaramakkil S et al. (2009) Cholesterol depletion associated with Leishmania major infection alters macrophage CD40 signalosome composition and effector function. Nature immunology 10 (3): 273–280.
26. Guimarães-Costa AB, Nascimento MTC, Froment GS, Soares RPP, Morgado FN et al. (2009) Leishmania amazonensis promastigotes induce and are killed by neutrophil extracellular traps. Proceedings of the National Academy of Sciences of the United States of America 106 (16): 6748–6753.
27. Rochael NC, Guimarães-Costa AB, Nascimento MTC, DeSouza-Vieira TS, Oliveira MP et al. (2015) Classical ROS-dependent and early/rapid ROS-independent release of Neutrophil Extracellular Traps triggered by Leishmania parasites. Scientific reports 5: 18302.
28. Novais FO, Santiago RC, Báfica A, Khouri R, Afonso L et al. (2009) Neutrophils and macrophages cooperate in host resistance against Leishmania braziliensis infection. Journal of immunology (Baltimore, Md. : 1950) 183 (12): 8088–8098.
29. van Zandbergen G, Klinger M, Mueller A, Dannenberg S, Gebert A et al. (2004) Cutting Edge. Neutrophil Granulocyte Serves as a Vector for Leishmania Entry into Macrophages. The Journal of Immunology 173 (11): 6521–6525.
30. Hurrell BP, Schuster S, Grün E, Coutaz M, Williams RA et al. (2015) Rapid Sequestration of Leishmania mexicana by Neutrophils Contributes to the Development of Chronic Lesion. PLoS pathogens 11 (5): e1004929.
31. Friedrich N, Hagedorn M, Soldati-Favre D, Soldati T (2012) Prison break. Pathogens' strategies to egress from host cells. Microbiology and molecular biology reviews : MMBR 76 (4): 707–720.
32. Real F, Florentino PTV, Reis LC, Ramos-Sanchez EM, Veras PST et al. (2014) Cell-to-cell transfer of Leishmania amazonensis amastigotes is mediated by immunomodulatory LAMP-rich parasitophorous extrusions. Cellular microbiology 16 (10): 1549–1564.
33. León B, López-Bravo M, Ardavín C (2007) Monocyte-derived dendritic cells formed at the infection site control the induction of protective T helper 1 responses against Leishmania. Immunity 26 (4): 519–531.
34. Lopes MF, Costa-da-Silva AC, DosReis GA (2014) Innate immunity to Leishmania infection. Within phagocytes. Mediators of inflammation 2014: 754965.
35. Stebut E von, Metz M, Milon G, Knop J, Maurer M (2003) Early macrophage influx to sites of cutaneous granuloma formation is dependent on MIP-1alpha /beta released from neutrophils recruited by mast cell-derived TNFalpha. Blood 101 (1): 210–215.
36. Kautz-Neu K, Schwonberg K, Fischer MR, Schermann AI, Stebut E von (2012) Dendritic cells in Leishmania major infections. Mechanisms of parasite uptake, cell activation and

evidence for physiological relevance. Medical microbiology and immunology 201 (4): 581–592.

37. Maurer M, Lopez Kostka S, Siebenhaar F, Moelle K, Metz M et al. (2006) Skin mast cells control T cell-dependent host defense in Leishmania major infections. FASEB journal : official publication of the Federation of American Societies for Experimental Biology 20 (14): 2460–2467.
38. Wershil BK, Theodos CM, Galli SJ, Titus RG (1994) Mast cells augment lesion size and persistence during experimental Leishmania major infection in the mouse. Journal of immunology (Baltimore, Md. : 1950) 152 (9): 4563–4571.
39. Bidri M, Vouldoukis I, Mossalayi MD, Debré P, Guillosson JJ et al. (1997) Evidence for direct interaction between mast cells and Leishmania parasites. Parasite immunology 19 (10): 475–483.
40. Mekori YA, Metcalfe DD (1999) Mast cell-T cell interactions. The Journal of allergy and clinical immunology 104 (3 Pt 1): 517–523.
41. Heinzel FP, Schoenhaut DS, Rerko RM, Rosser LE, Gately MK (1993) Recombinant interleukin 12 cures mice infected with Leishmania major. The Journal of experimental medicine 177 (5): 1505–1509.
42. Sypek JP, Chung CL, Mayor SE, Subramanyam JM, Goldman SJ et al. (1993) Resolution of cutaneous leishmaniasis. Interleukin 12 initiates a protective T helper type 1 immune response. The Journal of experimental medicine 177 (6): 1797–1802.
43. Fromm PD, Kling JC, Remke A, Bogdan C, Körner H (2015) Fatal Leishmaniasis in the Absence of TNF Despite a Strong Th1 Response. Frontiers in microbiology 6: 1520.
44. Olekhnovitch R, Ryffel B, Müller AJ, Bousso P (2014) Collective nitric oxide production provides tissue-wide immunity during Leishmania infection. The Journal of clinical investigation 124 (4): 1711–1722.
45. Blos M, Schleicher U, Soares Rocha FJ, Meissner U, Röllinghoff M et al. (2003) Organ-specific and stage-dependent control of Leishmania major infection by inducible nitric oxide synthase and phagocyte NADPH oxidase. European journal of immunology 33 (5): 1224–1234.
46. Diefenbach A, Schindler H, Röllinghoff M, Yokoyama WM, Bogdan C (1999) Requirement for type 2 NO synthase for IL-12 signaling in innate immunity. Science (New York, N.Y.) 284 (5416): 951–955.
47. Schleicher U, Liese J, Knippertz I, Kurzmann C, Hesse A et al. (2007) NK cell activation in visceral leishmaniasis requires TLR9, myeloid DCs, and IL-12, but is independent of plasmacytoid DCs. The Journal of experimental medicine 204 (4): 893–906.
48. Chatelain R, Varkila K, Coffman RL (1992) IL-4 induces a Th2 response in Leishmania major-infected mice. The Journal of Immunology 148 (4): 1182–1187.

49. Kane MM, Mosser DM (2001) The role of IL-10 in promoting disease progression in leishmaniasis. The Journal of Immunology 166 (2): 1141–1147.
50. Launois P, Maillard I, Pingel S, Swihart KG, Xénarios I et al. (1997) IL-4 Rapidly Produced by Vβ4 Vα8 CD4+ T Cells Instructs Th2 Development and Susceptibility to Leishmania major in BALB/c Mice. Immunity 6 (5): 541–549.
51. Julia V, Rassoulzadegan M, Glaichenhaus N (1996) Resistance to Leishmania major induced by tolerance to a single antigen. Science (New York, N.Y.) 274 (5286): 421–423.
52. Stetson DB, Mohrs M, Mallet-Designe V, Teyton L, Locksley RM (2002) Rapid expansion and IL-4 expression by Leishmania-specific naive helper T cells in vivo. Immunity 17 (2): 191–200.
53. Scott P, Eaton A, Gause WC, Di Zhou X, Hondowicz B (1996) Early IL-4 production does not predict susceptibility to Leishmania major. Experimental parasitology 84 (2): 178–187.
54. Launois P, Pingel S, Himmelrich H, Locksley R, Louis J (2007) Different epitopes of the LACK protein are recognized by V beta 4 V alpha 8 CD4+ T cells in H-2b and H-2d mice susceptible to Leishmania major. Microbes and infection 9 (11): 1260–1266.
55. Himmelrich H, Parra-Lopez C, Tacchini-Cottier F, Louis JA, Launois P (1998) The IL-4 rapidly produced in BALB/c mice after infection with Leishmania major down-regulates IL-12 receptor beta 2-chain expression on CD4+ T cells resulting in a state of unresponsiveness to IL-12. The Journal of Immunology 161 (11): 6156–6163.
56. Carrera L, Gazzinelli RT, Badolato R, Hieny S, Muller W et al. (1996) Leishmania promastigotes selectively inhibit interleukin 12 induction in bone marrow-derived macrophages from susceptible and resistant mice. The Journal of experimental medicine 183 (2): 515–526.
57. Roberts M, Mock BA, Blackwell JM (1993) Mapping of genes controlling Leishmania major infection in CXS recombinant inbred mice. European journal of immunogenetics : official journal of the British Society for Histocompatibility and Immunogenetics 20 (5): 349–362.
58. Shankar AH, Titus RG (1995) T cell and non-T cell compartments can independently determine resistance to Leishmania major. The Journal of experimental medicine 181 (3): 845–855.
59. Dotiwala F, Mulik S, Polidoro RB, Ansara JA, Burleigh BA et al. (2016) Killer lymphocytes use granulysin, perforin and granzymes to kill intracellular parasites. Nature medicine 22 (2): 210–216.
60. Novais FO, Carvalho LP, Graff JW, Beiting DP, Ruthel G et al. (2013) Cytotoxic T cells mediate pathology and metastasis in cutaneous leishmaniasis. PLoS pathogens 9 (7): e1003504.

61. Belkaid Y, Stebut E von, Mendez S, Lira R, Caler E et al. (2002) CD8+ T cells are required for primary immunity in C57BL/6 mice following low-dose, intradermal challenge with Leishmania major. Journal of immunology (Baltimore, Md. : 1950) 168 (8): 3992–4000.
62. Bousso P, Moreau HD (2012) Functional immunoimaging: the revolution continues. Nature reviews. Immunology 12 (12): 858–864.
63. Filipe-Santos O, Pescher P, Breart B, Lippuner C, Aebischer T et al. (2009) A dynamic map of antigen recognition by CD4 T cells at the site of Leishmania major infection. Cell host & microbe 6 (1): 23–33.
64. Honda T, Egen JG, Lämmermann T, Kastenmüller W, Torabi-Parizi P et al. (2014) Tuning of antigen sensitivity by T cell receptor-dependent negative feedback controls T cell effector function in inflamed tissues. Immunity 40 (2): 235–247.
65. Müller AJ, Filipe-Santos O, Eberl G, Aebischer T, Späth GF et al. (2012) CD4+ T cells rely on a cytokine gradient to control intracellular pathogens beyond sites of antigen presentation. Immunity 37 (1): 147–157.
66. Belkaid Y, Hoffmann KF, Mendez S, Kamhawi S, Udey MC et al. (2001) The role of interleukin (IL)-10 in the persistence of Leishmania major in the skin after healing and the therapeutic potential of anti-IL-10 receptor antibody for sterile cure. The Journal of experimental medicine 194 (10): 1497–1506.
67. Belkaid Y, Piccirillo CA, Mendez S, Shevach EM, Sacks DL (2002) CD4+CD25+ regulatory T cells control Leishmania major persistence and immunity. Nature 420 (6915): 502–507.
68. Aebischer T, Moody SF, Handman E (1993) Persistence of virulent Leishmania major in murine cutaneous leishmaniasis. A possible hazard for the host. Infection and immunity 61 (1): 220–226.
69. Anderson CF, Oukka M, Kuchroo VJ, Sacks D (2007) CD4(+)CD25(-)Foxp3(-) Th1 cells are the source of IL-10-mediated immune suppression in chronic cutaneous leishmaniasis. The Journal of experimental medicine 204 (2): 285–297.
70. Peters NC, Pagán AJ, Lawyer PG, Hand TW, Henrique Roma E et al. (2014) Chronic parasitic infection maintains high frequencies of short-lived Ly6C+CD4+ effector T cells that are required for protection against re-infection. PLoS pathogens 10 (12): e1004538.
71. Glennie ND, Volk SW, Scott P (2017) Skin-resident CD4+ T cells protect against Leishmania major by recruiting and activating inflammatory monocytes. PLoS pathogens 13 (4): e1006349.
72. Mandell MA, Beverley SM (2017) Continual renewal and replication of persistent Leishmania major parasites in concomitantly immune hosts. Proceedings of the National Academy of Sciences of the United States of America 114 (5): E801-E810.

73. Müller AJ, Aeschlimann S, Olekhnovitch R, Dacher M, Späth GF et al. (2013) Photoconvertible pathogen labeling reveals nitric oxide control of Leishmania major infection in vivo via dampening of parasite metabolism. Cell host & microbe 14 (4): 460–467.
74. Bogdan C, Donhauser N, Döring R, Röllinghoff M, Diefenbach A et al. (2000) Fibroblasts as host cells in latent leishmaniosis. The Journal of experimental medicine 191 (12): 2121–2130.
75. Belachew EB (2018) Immune Response and Evasion Mechanisms of Plasmodium falciparum Parasites. Journal of immunology research 2018: 6529681.
76. Peters NC, Egen JG, Secundino N, Debrabant A, Kimblin N et al. (2008) In vivo imaging reveals an essential role for neutrophils in leishmaniasis transmitted by sand flies. Science (New York, N.Y.) 321 (5891): 970–974.
77. Romano A, Carneiro MBH, Doria NA, Roma EH, Ribeiro-Gomes FL et al. (2017) Divergent roles for Ly6C+CCR2+CX3CR1+ inflammatory monocytes during primary or secondary infection of the skin with the intra-phagosomal pathogen Leishmania major. PLoS pathogens 13 (6): e1006479.
78. Hurrell BP, Beaumann M, Heyde S, Regli IB, Müller AJ et al. (2017) Frontline Science. Leishmania mexicana amastigotes can replicate within neutrophils. Journal of leukocyte biology 102 (5): 1187–1198.
79. Arcanjo AF, LaRocque-de-Freitas IF, Rocha JDB, Zamith D, Costa-da-Silva AC et al. (2015) The PGE2/IL-10 Axis Determines Susceptibility of B-1 Cell-Derived Phagocytes (B-1CDP) to Leishmania major Infection. PloS one 10 (5): e0124888.
80. Gonzaga WFKM, Xavier V, Vivanco BC, Lopes JD, Xander P (2015) B-1 cells contribute to susceptibility in experimental infection with Leishmania (Leishmania) chagasi. Parasitology 142 (12): 1506–1515.
81. Scott P, Natovitz P, Sher A (1986) B lymphocytes are required for the generation of T cells that mediate healing of cutaneous leishmaniasis. The Journal of Immunology 137 (3): 1017–1021.
82. Woelbing F, Kostka SL, Moelle K, Belkaid Y, Sunderkoetter C et al. (2006) Uptake of Leishmania major by dendritic cells is mediated by Fcgamma receptors and facilitates acquisition of protective immunity. The Journal of experimental medicine 203 (1): 177–188.
83. Esterre P, Dedet JP, Guerret S, Chevallier M, Frenay C et al. (1991) Matrix remodelling and fibroblast phenotype in early lesions of human cutaneous leishmaniasis. Pathology, research and practice 187 (8): 924–930.
84. Corte-Real S, Santos CB, Meirelles MN (1995) Differential expression of the plasma membrane Mg2+ ATPase and Ca2+ ATPase activity during adhesion and interiorization

of Leishmania amazonensis in fibroblasts in vitro. Journal of submicroscopic cytology and pathology 27 (3): 359–366.

85. Dedet JP, Ryter A, Vogt E, Hosli P, da Silva LP (1983) Uptake and killing of Leishmania mexicana amazonensis amastigotes by human skin fibroblasts. Annals of tropical medicine and parasitology 77 (1): 35–44.
86. Da Silva RP, Hall BF, Joiner KA, Sacks DL (1989) CR1, the C3b receptor, mediates binding of infective Leishmania major metacyclic promastigotes to human macrophages. The Journal of Immunology 143 (2): 617–622.
87. Miles SA, Conrad SM, Alves RG, Jeronimo SMB, Mosser DM (2005) A role for IgG immune complexes during infection with the intracellular pathogen Leishmania. The Journal of experimental medicine 201 (5): 747–754.
88. Muleme HM, Reguera RM, Berard A, Azinwi R, Jia P et al. (2009) Infection with arginase-deficient Leishmania major reveals a parasite number-dependent and cytokine-independent regulation of host cellular arginase activity and disease pathogenesis. Journal of immunology (Baltimore, Md. : 1950) 183 (12): 8068–8076.
89. Scorza BM, Carvalho EM, Wilson ME (2017) Cutaneous Manifestations of Human and Murine Leishmaniasis. International journal of molecular sciences 18 (6).
90. Ammon C, Meyer SP, Schwarzfischer L, Krause SW, Andreesen R et al. (2000) Comparative analysis of integrin expression on monocyte-derived macrophages and monocyte-derived dendritic cells. Immunology 100 (3): 364–369.
91. Ng LG, Hsu A, Mandell MA, Roediger B, Hoeller C et al. (2008) Migratory dermal dendritic cells act as rapid sensors of protozoan parasites. PLoS pathogens 4 (11): e1000222.
92. Goncalves R, Zhang X, Cohen H, Debrabant A, Mosser DM (2011) Platelet activation attracts a subpopulation of effector monocytes to sites of Leishmania major infection. The Journal of experimental medicine 208 (6): 1253–1265.
93. Bursch LS, Wang L, Igyarto B, Kissenpfennig A, Malissen B et al. (2007) Identification of a novel population of Langerin+ dendritic cells. The Journal of experimental medicine 204 (13): 3147–3156.
94. Brewig N, Kissenpfennig A, Malissen B, Veit A, Bickert T et al. (2009) Priming of CD8+ and CD4+ T cells in experimental leishmaniasis is initiated by different dendritic cell subtypes. Journal of immunology (Baltimore, Md. : 1950) 182 (2): 774–783.
95. López-Bravo M, Ardavín C (2008) In vivo induction of immune responses to pathogens by conventional dendritic cells. Immunity 29 (3): 343–351.
96. Soong L (2008) Modulation of dendritic cell function by Leishmania parasites. Journal of immunology (Baltimore, Md. : 1950) 180 (7): 4355–4360.

97. Misslitz AC, Bonhagen K, Harbecke D, Lippuner C, Kamradt T et al. (2004) Two waves of antigen-containing dendritic cells in vivo in experimental Leishmania major infection. European journal of immunology 34 (3): 715–725.
98. Iborra S, Martínez-López M, Cueto FJ, Conde-Garrosa R, Del Fresno C et al. (2016) Leishmania Uses Mincle to Target an Inhibitory ITAM Signaling Pathway in Dendritic Cells that Dampens Adaptive Immunity to Infection. Immunity 45 (4): 788–801.
99. Ravindran R, Rusch L, Itano A, Jenkins MK, McSorley SJ (2007) CCR6-dependent recruitment of blood phagocytes is necessary for rapid CD4 T cell responses to local bacterial infection. Proceedings of the National Academy of Sciences of the United States of America 104 (29): 12075–12080.
100. Swiecki M, Colonna M (2015) The multifaceted biology of plasmacytoid dendritic cells. Nature reviews. Immunology 15 (8): 471–485.
101. Parlato S, Chiacchio T, Salerno D, Petrone L, Castiello L et al. (2018) Impaired IFN-α-mediated signal in dendritic cells differentiates active from latent tuberculosis. PloS one 13 (1): e0189477.
102. Chistiakov DA, Orekhov AN, Sobenin IA, Bobryshev YV (2014) Plasmacytoid dendritic cells. Development, functions, and role in atherosclerotic inflammation. Frontiers in physiology 5: 279.
103. McKenna K, Beignon A-S, Bhardwaj N (2005) Plasmacytoid dendritic cells. Linking innate and adaptive immunity. Journal of virology 79 (1): 17–27.
104. Trez C de, Magez S, Akira S, Ryffel B, Carlier Y et al. (2009) iNOS-producing inflammatory dendritic cells constitute the major infected cell type during the chronic Leishmania major infection phase of C57BL/6 resistant mice. PLoS pathogens 5 (6): e1000494.
105. Lewis K (2007) Persister cells, dormancy and infectious disease. Nature reviews. Microbiology 5 (1): 48–56.
106. Helaine S, Cheverton AM, Watson KG, Faure LM, Matthews SA et al. (2014) Internalization of Salmonella by macrophages induces formation of nonreplicating persisters. Science (New York, N.Y.) 343 (6167): 204–208.
107. Tuchscherr L, Medina E, Hussain M, Völker W, Heitmann V et al. (2011) Staphylococcus aureus phenotype switching. An effective bacterial strategy to escape host immune response and establish a chronic infection. EMBO molecular medicine 3 (3): 129–141.
108. Kloehn J, Saunders EC, O'Callaghan S, Dagley MJ, McConville MJ (2015) Characterization of metabolically quiescent Leishmania parasites in murine lesions using heavy water labeling. PLoS pathogens 11 (2): e1004683.
109. Cheers C, Zhan Y (1996) How do macrophages distinguish the living from the dead. Trends in microbiology 4 (11): 453–455.

110. Detmer A, Glenting J (2006) Live bacterial vaccines--a review and identification of potential hazards. Microbial cell factories 5: 23.
111. Brockstedt DG, Bahjat KS, Giedlin MA, Liu W, Leong M et al. (2005) Killed but metabolically active microbes. A new vaccine paradigm for eliciting effector T-cell responses and protective immunity. Nature medicine 11 (8): 853–860.
112. Barbet G, Sander LE, Geswell M, Leonardi I, Cerutti A et al. (2018) Sensing Microbial Viability through Bacterial RNA Augments T Follicular Helper Cell and Antibody Responses. Immunity 48 (3): 584-598.e5.
113. Sander LE, Davis MJ, Boekschoten MV, Amsen D, Dascher CC et al. (2011) Detection of prokaryotic mRNA signifies microbial viability and promotes immunity. Nature 474 (7351): 385–389.
114. Rigby RE, Webb LM, Mackenzie KJ, Li Y, Leitch A et al. (2014) RNA:DNA hybrids are a novel molecular pattern sensed by TLR9. The EMBO journal 33 (6): 542–558.
115. Aguilera A, García-Muse T (2012) R loops: from transcription byproducts to threats to genome stability. Molecular cell 46 (2): 115–124.
116. Habuchi S, Tsutsui H, Kochaniak AB, Miyawaki A, van Oijen AM (2008) mKikGR, a monomeric photoswitchable fluorescent protein. PloS one 3 (12): e3944.
117. Tsutsui H, Karasawa S, Shimizu H, Nukina N, Miyawaki A (2005) Semi-rational engineering of a coral fluorescent protein into an efficient highlighter. EMBO reports 6 (3): 233–238.
118. Moreau HD, Lemaître F, Terriac E, Azar G, Piel M et al. (2012) Dynamic in situ cytometry uncovers T cell receptor signaling during immunological synapses and kinapses in vivo. Immunity 37 (2): 351–363.
119. Jung S, Unutmaz D, Wong P, Sano G-I, los Santos K de et al. (2002) In vivo depletion of CD11c+ dendritic cells abrogates priming of CD8+ T cells by exogenous cell-associated antigens. Immunity 17 (2): 211–220.
120. Philipsen L, Engels T, Schilling K, Gurbiel S, Fischer K-D et al. (2013) Multimolecular analysis of stable immunological synapses reveals sustained recruitment and sequential assembly of signaling clusters. Molecular & cellular proteomics : MCP 12 (9): 2551–2567.
121. Stegmaier J, Amat F, Lemon WC, McDole K, Wan Y et al. (2016) Real-Time Three-Dimensional Cell Segmentation in Large-Scale Microscopy Data of Developing Embryos. Developmental cell 36 (2): 225–240.
122. Barnden MJ, Allison J, Heath WR, Carbone FR (1998) Defective TCR expression in transgenic mice constructed using cDNA-based alpha- and beta-chain genes under the control of heterologous regulatory elements. Immunology and cell biology 76 (1): 34–40.

123. Prickett S, Gray PM, Colpitts SL, Scott P, Kaye PM et al. (2006) In vivo recognition of ovalbumin expressed by transgenic Leishmania is determined by its subcellular localization. The Journal of Immunology 176 (8): 4826–4833.
124. Nathan C (2012) Fresh Approaches to Anti-Infective Therapies. Nature medicine 4 (140): 140sr2-140sr2.
125. Saito K, Warrier T, Somersan-Karakaya S, Kaminski L, Mi J et al. (2017) Rifamycin action on RNA polymerase in antibiotic-tolerant Mycobacterium tuberculosis results in differentially detectable populations. Proceedings of the National Academy of Sciences of the United States of America 114 (24): E4832-E4840.
126. Harms A, Maisonneuve E, Gerdes K (2016) Mechanisms of bacterial persistence during stress and antibiotic exposure. Science (New York, N.Y.) 354 (6318).
127. Subach FV, Subach OM, Gundorov IS, Morozova KS, Piatkevich KD et al. (2009) Monomeric fluorescent timers that change color from blue to red report on cellular trafficking. Nature chemical biology 5 (2): 118–126.
128. Knop M, Edgar BA (2014) Tracking protein turnover and degradation by microscopy: photo-switchable versus time-encoded fluorescent proteins. Open biology 4: 140002.
129. Hoi H, Shaner NC, Davidson MW, Cairo CW, Wang J et al. (2010) A monomeric photoconvertible fluorescent protein for imaging of dynamic protein localization. Journal of molecular biology 401 (5): 776–791.
130. Subach OM, Patterson GH, Ting L-M, Wang Y, Condeelis JS et al. (2011) A photoswitchable orange-to-far-red fluorescent protein, PSmOrange. Nature methods 8 (9): 771–777.
131. Ando R, Hama H, Yamamoto-Hino M, Mizuno H, Miyawaki A (2002) An optical marker based on the UV-induced green-to-red photoconversion of a fluorescent protein. Proceedings of the National Academy of Sciences of the United States of America 99 (20): 12651–12656.
132. Hatta K, Tsujii H, Omura T (2006) Cell tracking using a photoconvertible fluorescent protein. Nature protocols 1 (2): 960–967.
133. Girard-Madoux MJH, Kautz-Neu K, Lorenz B, Ober-Blöbaum JL, Stebut E von et al. (2015) IL-10 signaling in dendritic cells attenuates anti-Leishmania major immunity without affecting protective memory responses. The Journal of investigative dermatology 135 (11): 2890–2894.
134. Collins N, Hochheiser K, Carbone FR, Gebhardt T (2017) Sustained accumulation of antigen-presenting cells after infection promotes local T-cell immunity. Immunology and cell biology 95 (10): 878–883.

135. Alvarez MN, Piacenza L, Irigoín F, Peluffo G, Radi R (2004) Macrophage-derived peroxynitrite diffusion and toxicity to Trypanosoma cruzi. Archives of biochemistry and biophysics 432 (2): 222–232.
136. Radi R (2004) Nitric oxide, oxidants, and protein tyrosine nitration. Proceedings of the National Academy of Sciences of the United States of America 101 (12): 4003–4008.
137. Nandan D, Reiner NE (2005) Leishmania donovani engages in regulatory interference by targeting macrophage protein tyrosine phosphatase SHP-1. Clinical immunology (Orlando, Fla.) 114 (3): 266–277.
138. Schleicher U, Mattner J, Blos M, Schindler H, Röllinghoff M et al. (2004) Control of Leishmania major in the absence of Tyk2 kinase. European journal of immunology 34 (2): 519–529.
139. Sturm A, Amino R, van de Sand C, Regen T, Retzlaff S et al. (2006) Manipulation of host hepatocytes by the malaria parasite for delivery into liver sinusoids. Science (New York, N.Y.) 313 (5791): 1287–1290.
140. Glushakova S, Yin D, Li T, Zimmerberg J (2005) Membrane transformation during malaria parasite release from human red blood cells. Current biology : CB 15 (18): 1645–1650.
141. Sologub L, Kuehn A, Kern S, Przyborski J, Schillig R et al. (2011) Malaria proteases mediate inside-out egress of gametocytes from red blood cells following parasite transmission to the mosquito. Cellular microbiology 13 (6): 897–912.
142. Watson KG, Holden DW (2010) Dynamics of growth and dissemination of Salmonella in vivo. Cellular microbiology 12 (10): 1389–1397.
143. Bergsbaken T, Fink SL, den Hartigh AB, Loomis WP, Cookson BT (2011) Coordinated host responses during pyroptosis: caspase-1-dependent lysosome exocytosis and inflammatory cytokine maturation. Journal of immunology (Baltimore, Md. : 1950) 187 (5): 2748–2754.
144. Ribeiro-Gomes FL, Peters NC, Debrabant A, Sacks DL (2012) Efficient capture of infected neutrophils by dendritic cells in the skin inhibits the early anti-leishmania response. PLoS pathogens 8 (2): e1002536.
145. Misslitz A, Mottram JC, Overath P, Aebischer T (2000) Targeted integration into a rRNA locus results in uniform and high level expression of transgenes in Leishmania amastigotes. Molecular and biochemical parasitology 107 (2): 251–261.
146. Sörensen M, Lippuner C, Kaiser T, Misslitz A, Aebischer T et al. (2003) Rapidly maturing red fluorescent protein variants with strongly enhanced brightness in bacteria. FEBS letters 552 (2-3): 110–114.
147. Lindquist RL, Shakhar G, Dudziak D, Wardemann H, Eisenreich T et al. (2004) Visualizing dendritic cell networks in vivo. Nature immunology 5 (12): 1243–1250.

148. Laemmli UK (1970) Cleavage of structural proteins during the assembly of the head of bacteriophage T4. Nature 227 (5259): 680–685.

6 Appendix

6.1 Supplementary macro 1: ROI Generator for MELC image segmentation and analysis

From the image stacks resulting of grey level-coded 2D objects, regions of interest (ROIs) were generated in three planes spaced 3 micron apart around the Z centre of the stacks using the Fiji software (NIH, https://imagej.nih.gov/ij/).

```
roiManager("reset");
run("Clear Results");
zplane=getString("enter Z plane to be analysed", "default")
folder=getString("enter image folder plane to be analysed")
imagesizeX=getString("enter X dimension", "default")
imagesizeY=getString("enter Y dimension", " default ")
open("File path and name");
run("Duplicate...", "duplicate range="+zplane+"-"+zplane+"");
run("Set Measurements...", "mean centroid redirect=None decimal=3");
run("Properties...", "channels=1 slices=1 frames=1 unit=inch pixel_width=1 pixel_height=1
voxel_depth=1.0000000");
selectWindow("File name");
close();
selectWindow("File name");
setForegroundColor(0, 0, 0);
for (i=0; i<imagesizeX; i=i+15) {
        for (j=0; j<imagesizeY; j=j+15) {
        makeRectangle(i, j, 1, 1);
        run("Measure");
        floodFill(i, j);
        }
}
selectWindow("File name");
close();
open("File path and name");
```

```
run("Duplicate...", "duplicate range="+zplane+"-"+zplane+"");

run("Set Measurements...", "mean centroid redirect=None decimal=3");

run("Properties...", "channels=1 slices=1 frames=1 unit=inch pixel_width=1 pixel_height=1
voxel_depth=1.0000000");

selectWindow("File name");

close();

selectWindow("File name");

RegionCount=nResults();

Mean=newArray(RegionCount);

RoiX=newArray(RegionCount);

RoiY=newArray(RegionCount);

for (i=0; i<RegionCount; i++) {

        Mean[i]=getResult("Mean", i);

        RoiX[i]=getResult("X", i);

        RoiY[i]=getResult("Y", i);

        if (Mean[i]>0) {

   doWand(RoiX[i], RoiY[i]);

        roiManager("add");

  }

}

open("File path and name");

run("Duplicate...", "duplicate range="+zplane+"-"+zplane+"");

run("Set Measurements...", "mean centroid redirect=None decimal=3");

run("Properties...", "channels=1 slices=1 frames=1 unit=inch pixel_width=1 pixel_height=1
voxel_depth=1.0000000");

selectWindow("File name");

close();

selectWindow("File name");

RegionCount=nResults();

Mean=newArray(RegionCount);

RoiX=newArray(RegionCount);

RoiY=newArray(RegionCount);

for (i=0; i<RegionCount; i++) {
```

```
        Mean[i]=getResult("Mean", i);
        RoiX[i]=getResult("X", i);
        RoiY[i]=getResult("Y", i);
        if (Mean[i]>0) {
   floodFill(RoiX[i], RoiY[i]);
  }
}
open("File path and name");
run("Duplicate...", "duplicate range="+zplane+"-"+zplane+"");
run("Set Measurements...", "mean centroid redirect=None decimal=3");
run("Properties...", "channels=1 slices=1 frames=1 unit=inch pixel_width=1 pixel_height=1
voxel_depth=1.0000000");
selectWindow("File name");
close();
selectWindow("File name");
RegionCount=nResults();
Mean=newArray(RegionCount);
RoiX=newArray(RegionCount);
RoiY=newArray(RegionCount);
for (i=0; i<RegionCount; i++) {
        Mean[i]=getResult("Mean", i);
        RoiX[i]=getResult("X", i);
        RoiY[i]=getResult("Y", i);
        if (Mean[i]>0) {
   floodFill(RoiX[i], RoiY[i]);
  }
}
//Measures CD45
run("Clear Results");
selectWindow("File name");
run("Duplicate...", " ");
selectWindow("File name");
setForegroundColor(0, 0, 0);
```

```
for (i=0; i<imagesizeX; i=i+15) {
        for (j=0; j<imagesizeY; j=j+15) {
        makeRectangle(i, j, 1, 1);
        run("Measure");
        floodFill(i, j);
        }
}
selectWindow("File name");
RegionCount=nResults();
Mean=newArray(RegionCount);
RoiX=newArray(RegionCount);
RoiY=newArray(RegionCount);
for (i=0; i<RegionCount; i++) {
        Mean[i]=getResult("Mean", i);
        RoiX[i]=getResult("X", i);
        RoiY[i]=getResult("Y", i);
        if (Mean[i]>0) {
   doWand(RoiX[i], RoiY[i]);
        roiManager("add");
  }
}
selectWindow("File name");
RegionCount=nResults();
Mean=newArray(RegionCount);
RoiX=newArray(RegionCount);
RoiY=newArray(RegionCount);
for (i=0; i<RegionCount; i++) {
        Mean[i]=getResult("Mean", i);
        RoiX[i]=getResult("X", i);
        RoiY[i]=getResult("Y", i);
        if (Mean[i]>0) {
   floodFill(RoiX[i], RoiY[i]);
  }
```

```
}
//Measures CD54
run("Clear Results");
selectWindow("File name");
run("Duplicate...", " ");
selectWindow("File name ");
setForegroundColor(0, 0, 0);
for (i=0; i<imagesizeX; i=i+15) {
        for (j=0; j<imagesizeY; j=j+15) {
        makeRectangle(i, j, 1, 1);
        run("Measure");
        floodFill(i, j);
        }
}
selectWindow("File name");
RegionCount=nResults();
Mean=newArray(RegionCount);
RoiX=newArray(RegionCount);
RoiY=newArray(RegionCount);
for (i=0; i<RegionCount; i++) {
        Mean[i]=getResult("Mean", i);
        RoiX[i]=getResult("X", i);
        RoiY[i]=getResult("Y", i);
        if (Mean[i]>0) {
   doWand(RoiX[i], RoiY[i]);
        roiManager("add");
  }
}
roiManager("Save", " File path and name ");
count=roiManager("count");
for (i=0; i<count; i++) {
        roiManager("Select", i);
        run("Area to Line");
```

```
        run("Line to Area");
        run("Enlarge...", "enlarge=1");
        roiManager("Update");
}
roiManager("Save", " File path and name ");
run("Clear Results");
selectWindow("File name ");
close();
selectWindow("File name ");
close();
selectWindow("File name ");
close();
selectWindow("File name ");
close();
selectWindow("File name ");
close();
```

6.2 Supplementary macro 2: Data extraction for MELC image analysis

The mean fluorescence of the cellular and rim ROIs were extracted for each cell and fluorescence channel using the Fiji software.

```
roiManager("reset");
run("Clear Results");


zplane=getString("Enter Z plane number")
folder=getString("Enter folder")
chnumberRed=getString("Enter Red channel number")
//extractCD80=getString("Extract CD80?", "yes=1")


//loads Band Masks
roiManager("Open", " File path and name");
//loads and measures CD3
open("File path and name");
count=roiManager("count");
for (i=0; i<count; i++) {
        roiManager("select", i);
        run("Measure");
}
selectWindow("File name "+zplane+".png");
close();
//loads and measures CD8
open("File path and name"+zplane+".png");
run("Set Measurements...", "area mean median redirect=None decimal=3");
count=roiManager("count");
for (i=0; i<count; i++) {
        roiManager("select", i);
        run("Measure");
}
selectWindow("File name"+zplane+".png");
```

```
close();
for (m=count; m<nResults; m++) {
	newparameter=getResult("Mean", m);
	setResult("MeanCD8", m-count, newparameter);
	newparameter=getResult("Median", m);
	setResult("MedianCD8", m-count, newparameter);
}
IJ.deleteRows(count, nResults-1);
//loads and measures NK1.1
open("File path and name"+zplane+".png");
run("Set Measurements...", "area mean median redirect=None decimal=3");
count=roiManager("count");
for (i=0; i<count; i++) {
	roiManager("select", i);
	run("Measure");
}
selectWindow("File name"+zplane+".png");
close();
for (m=count; m<nResults; m++) {
	newparameter=getResult("Mean", m);
	setResult("MeanNK11", m-count, newparameter);
	newparameter=getResult("Median", m);
	setResult("MedianNK11", m-count, newparameter);
}
IJ.deleteRows(count, nResults-1);
//loads and measures CD45R
open("File path and name"+zplane+".png");
run("Set Measurements...", "area mean median redirect=None decimal=3");
count=roiManager("count");
for (i=0; i<count; i++) {
	roiManager("select", i);
	run("Measure");
}
```

```
selectWindow("File name "+zplane+".png");
close();
for (m=count; m<nResults; m++) {
        newparameter=getResult("Mean", m);
        setResult("MeanCD45R", m-count, newparameter);
        newparameter=getResult("Median", m);
        setResult("MedianCD45R", m-count, newparameter);
}
IJ.deleteRows(count, nResults-1);
//loads and measures CD11b
open("File path and name "+zplane+".png");
run("Set Measurements...", "area mean median redirect=None decimal=3");
count=roiManager("count");
for (i=0; i<count; i++) {
        roiManager("select", i);
        run("Measure");
}
selectWindow("File name"+zplane+".png");
close();
for (m=count; m<nResults; m++) {
        newparameter=getResult("Mean", m);
        setResult("CD11b", m-count, newparameter);
}
IJ.deleteRows(count, nResults-1);
//loads and measures CD11c
open("File path and name"+zplane+".png");
run("Set Measurements...", "area mean median redirect=None decimal=3");
count=roiManager("count");
for (i=0; i<count; i++) {
        roiManager("select", i);
        run("Measure");
}
selectWindow("File name"+zplane+".png");
```

```
close();
for (m=count; m<nResults; m++) {
	newparameter=getResult("Mean", m);
	setResult("CD11c", m-count, newparameter);
}
IJ.deleteRows(count, nResults-1);
//loads and measures CD45
open("File path and name"+zplane+".png");
run("Set Measurements...", "area mean median redirect=None decimal=3");
count=roiManager("count");
for (i=0; i<count; i++) {
	roiManager("select", i);
	run("Measure");
}
selectWindow("File name "+zplane+".png");
close();
for (m=count; m<nResults; m++) {
	newparameter=getResult("Mean", m);
	setResult("CD45", m-count, newparameter);
}
IJ.deleteRows(count, nResults-1);
//loads and measures CD80 (if chosen)
//if (extractCD80==1) {
//open("File path and name"+zplane+".png");
//run("Set Measurements...", "area mean median redirect=None decimal=3");
//count=roiManager("count");
//for (i=0; i<count; i++) {
//	roiManager("select", i);
//	run("Measure");
//}
//selectWindow("File name "+zplane+".png");
//close();
//}
```

```
//for (m=count; m<nResults; m++) {
//	newparameter=getResult("Mean", m);
//	setResult("CD80", m-count, newparameter);
//}
//IJ.deleteRows(count, nResults-1);
//loads and measures CD86
open("File path and name"+zplane+".png");
run("Set Measurements...", "area mean median redirect=None decimal=3");
count=roiManager("count");
for (i=0; i<count; i++) {
	roiManager("select", i);
	run("Measure");
}
selectWindow("File name"+zplane+".png");
close();
for (m=count; m<nResults; m++) {
	newparameter=getResult("Mean", m);
	setResult("CD86", m-count, newparameter);
}
IJ.deleteRows(count, nResults-1);
//loads and measures F4/80
open("File path and name"+zplane+".png");
run("Set Measurements...", "area mean median redirect=None decimal=3");
count=roiManager("count");
for (i=0; i<count; i++) {
	roiManager("select", i);
	run("Measure");
}
selectWindow("File name"+zplane+".png");
close();
for (m=count; m<nResults; m++) {
	newparameter=getResult("Mean", m);
	setResult("F480", m-count, newparameter);
```

```
}
IJ.deleteRows(count, nResults-1);
//loads and measures MHCII
open("File path and name"+zplane+".png");
run("Set Measurements...", "area mean median redirect=None decimal=3");
count=roiManager("count");
for (i=0; i<count; i++) {
	roiManager("select", i);
	run("Measure");
}
selectWindow("File name"+zplane+".png");
close();
for (m=count; m<nResults; m++) {
	newparameter=getResult("Mean", m);
	setResult("MHCII", m-count, newparameter);
}
IJ.deleteRows(count, nResults-1);
saveAs("Results", " File path and name"+zplane+".xls");
run("Clear Results");
//clears ROIs and loads cytosol masks
roiManager("reset");
roiManager("Open", " File path and name"+zplane+".zip");
//loads and measures LeishRed
open("File path"+chnumberRed+" File name"+zplane+".png");
run("Set Measurements...", "area mean redirect=None decimal=3");
count=roiManager("count");
for (i=0; i<count; i++) {
	roiManager("select", i);
	run("Measure");
}
selectWindow("File name"+chnumberRed+"_001_0"+zplane+".png");
close();
//loads and measures LeishGreen
```

```
open("File path and name"+zplane+".png");
run("Set Measurements...", "area mean redirect=None decimal=3");
count=roiManager("count");
for (i=0; i<count; i++) {
	roiManager("select", i);
	run("Measure");
}
selectWindow("File name"+zplane+".png");
close();
for (m=count; m<nResults; m++) {
	newparameter=getResult("Mean", m);
	setResult("KikGreen", m-count, newparameter);

}
IJ.deleteRows(count, nResults-1);
saveAs("Results", " File path and name "+zplane+".xls");
run("Clear Results");
//draws a control image of kikRed and Green marker with Cell ROIs
roiManager("reset");
open("L:\\AG Müller\\MELC_SEGMENTATION\\"+folder+"\\g_PBS_2500_"+chnumberRed+"_001_0"+zplane+".png");
open("File path and name"+zplane+".png");
run("Merge Channels...", "c1= File path"+chnumberRed+" File name "+zplane+".png c2= File name "+zplane+".png");
roiManager("Open", " File path and name"+zplane+".zip");
roiManager("Select", 0);
count=roiManager("count");
for (i=0; i<count; i++) {
	roiManager("Select", i);
	setForegroundColor(255,255,255);
	 run("Draw");
}
saveAs("Tiff", " File path and name "+folder+"_"+zplane+".tif");
```

```
close();
//draws a control image of CD45 and CD11b marker with Marker ROIs
roiManager("reset");
open("File path and name"+zplane+".png");
open("File path"+folder File name"+zplane+".png");
run("Merge Channels...", "c1= File name"+zplane+".png c2= File name"+zplane+".png");
roiManager("Open", " File path and name"+folder+"\\Outlines_Plane"+zplane+".zip");
roiManager("Select", 0);
count=roiManager("count");
for (i=0; i<count; i++) {
        roiManager("Select", i);
        setForegroundColor(255,255,255);
        run("Draw");
}
saveAs("Tiff", " File path and name"+folder+"_"+zplane+".tif");
close();
roiManager("reset");
```

6.3 Supplementary macro 3: Heat-map generator for the analysis of APC-T cell interactions by 2-photon microscopy

Imaging data from intravital 2-photon microscopy analysis for APC-T cell interactions were analyzed via Imaris and Fiji software. Resting T cells were defined by running a heat-map generating macro script which was designed within Fiji.

```
Filename=getString("Enter Filename with extension")

Zsize=getString("Enter Z frame number")

Tsize=getString("Enter time frame number, USE ONLY MOVIES OF 28 to 32 FRAMES FOR CORRECT ANNOTATION")


rename("Bild");

run("Split Channels");

selectWindow("C2-Bild");

run("Close");

selectWindow("C3-Bild");

run("Close");

selectWindow("C1-Bild");

run("8-bit");

selectWindow("C4-Bild");

run("8-bit");

imageCalculator("Subtract create stack", "C1-Bild","C4-Bild");

selectWindow("C1-Bild");

run("Close");

selectWindow("C4-Bild");

run("Close");

selectWindow("Result of C1-Bild");

rename("TCells");
```

```
selectWindow("TCells");

run("Smooth", "stack");

setThreshold(30, 255);

run("Convert to Mask", "method=Default background=Dark black");

selectWindow("TCells");

run("Stack to Image5D", "3rd=t 4th=z 3rd_dimension_size="+Zsize+" 4th_dimension_size="+Tsize+" assign");

selectWindow("TCells");

run("Z Project", "start=1 stop="+Tsize+" projection=[Average Intensity] all copy");

run("8-bit");

setMinAndMax(0, 42);

run("Apply LUT", "stack");

rename(""+Filename+"");

run("Duplicate...", "title=Duplicate duplicate range=1-"+Zsize+"");

run("Stack to Image5D", "3rd=z 4th=ch 3rd_dimension_size="+Zsize+" 4th_dimension_size=1 assign");

selectWindow("Duplicate");

run("Z Project", "start=1 stop="+Tsize+" projection=[Max Intensity] all copy");

run("8-bit");

setMinAndMax(0, 41);

run("Apply LUT");

run("Fire");

rename(""+Filename+"Projection");

selectWindow("Duplicate");

close();

selectWindow("TCells");

close();
```